N · onal Library
of Canada

Acquisitions and
Bibliographic Services Branch

395 Wellington Street
Ottawa, Ontario
K1A 0N4

Bibliothèque nationale
du Canada

Direction des acquisitions et
des services bibliographiques

395 rue Wellington
Ottawa (Ontario)
K1A 0N4

Optical Fiber Networks: Wavelength Division and Code-Division Multiplexing

Fakher Ayadi

A Thesis

in

The Department

of

Electrical and Computer Engineering

Presented in Partial Fulfillment of the requirements
for the Degree of Doctor of Philosophy at
Concordia University
Montréal, Québec, Canada

November, 1994

ISBN 0-612-10821-X

Canada

Abstract

Optical Fiber Networks: Wavelength Division and Code-Division Multiplexing

Fakher Ayadi, Ph.D.
Concordia University, 1994

The general subject of our research is the use of optical fiber in Local Area Networks (LANs) and Metropolitan Area Networks (MANs). There are two basic topologies in these applications, single-hop networks and multihop networks. The latter operate in much the same fashion as well established store-and-forward packet-switched networks, but at a much higher rate. In both networks, Wave Division Multiplexing whereby separate channels are grouped around distinct wavelengths in the fiber passband is used. The data rate on each of the WDM channels may be as high as one gigabit/sec. Although this rate is high, it is still low enough to permit processing of control information by electronic means.

We first propose a new logical topology, the bilayered ShuffleNet, which is shown to achieve a higher efficiency compared to the conventional ShuffleNet. This network will be studied under uniform and nonuniform traffic. We also propose a method of using WDM cross-connect in the implementation of two different multihop networks, the ShuffleNet and the Manhattan Street Network. The WDM cross-connect is a device based on integrating a two-dimensional array of Bragg diffraction cells. This device can be used in various

wavelength routing networks application and overcomes the major problems related to the conventional star coupler. In the second part of the study, we introduce the optical CDMA for the case of noncoherent and coherent detection. Also, a new configuration is proposed in order to increase the number of users in optical networks at the same time using optical CDMA. This configuration uses a hybrid WDMA/CDMA system with the addition of allowing different users to use the same code. The throughput performance of this new configuration known as partial CDMA is analyzed and compared to the conventional configuration.

Acknowledgment

I would like to express my deep and gratitude to my thesis supervisors Dr. J.F. Hayes and Dr. M. Kavehrad for their invaluable assistance and constant guidance through this research, and for their advice and constructive criticism during the preparation of this thesis.

I am deeply grateful to my family for their support and patience, especially my parents who gave the best of themselves so that my brothers and I had the best of everything. I would also thank my wife for her encouragement and support throughout the preparation of this thesis.

I would also like to express my appreciation to the University Mission of Tunisia for its support through my studies.

I dedicate this work

to

my parents

and

my wife

Table of Contenents

List of Figures

List of Tables

List of Abreviations

APD : Avalanche Photodetector.

ASK : Amplitude-Shift Keying

DS/SSMA : Direct-Sequence Spread-Spectrum Multiple Access

Fox : Fiber Optic Crossconnect.

LAN : Local Area Network.

MAN : Metropolitan Area Network.

MSN : Manhattan Street Network.

NUI : Network Unit Interface.

WDM : Wave Division Multiplexing.

CDMA : Code Division Multiple Access.

LED : Light Emitting Diode.

TDM : Time Division Multiplexed.

SR_Net : Shuffle Ring Network.

OCC: optical orthogonal code

SIK : shift inversion keying

List of Principal Symbols

a : core radius

c : light velocity

f : frequency

k : the number of columns in the ShuffleNet

n : refractive index

$\hat{N}$: number of modes

$\bar{n}_D$: the expected queue length for the higher priority traffic

B : the total bandwidth used by one source

C : achievable capacity

C_w : bit rate per wavelength

$\overline{C}_K$:the average number of captured packets

D : is one pass through a link

D_1 : the higher priority delay

D_2 : the lower priority delay

D_p : the processing delay

D_T : the total delay

$E[L]$: the expected queue length for the lower priority traffic

$G_{(1)}(z)$: the higher priority generating function

$G_{(2)}(z)$:the lower priority generating function

$\overline{H}$: the expected number of hops

K_m :Maximum number of simultaneous users

L : the number of links in the ShuffleNet

M : the average number of i-to-j traffic pairs

N : the total number of stations

P : the number of arcs going out from each station

P_{def} : probability of deflection

P_{nc} : probability of a successfully transmitted packet

$P_T(k)$: input power at the input port

S : channel throughput

SIR : signal to interference ratio

T_c : pulse duration

W : the total number of physical channels

Y_W : the Wth-order statistic

λ : the amount of traffic destinated for each station

$\hat{\lambda}$: free-space optical wavelength

λ_{local} : the locally generated traffic per link

μ : mean

η : channel utilization efficiency

σ : standard deviation

Δ : the number of wavelengths covered by each optical amplifier

$\Delta\lambda^*$: spectral width of the source

Λ : the total amount of traffic on each link

Λ^* : the spectral bandwidth

Λ' : the traffic generated by one source

Λ_T : the through traffic

Chapter I

Introduction

1.1 Motivation

Optical fiber has become the preferred transmission medium for the terrestrial links of telecommunications systems. Single mode fiber, which has superior transmission quality because of absence of modal noise [1] and low loss, offers an enormous bandwidth: thousands of GHz. Various access techniques such as wavelength, time, space, and code division multiplexing have been proposed to tap this enormous bandwidth [2]. Using the available technology, multichannel-multihop lightwave networks are specially designed to achieve efficient use of the channel bandwidth.

Optical fiber networks consist of a physical distributed optical topology, and a logical connectivity graph among the nodes. The key property of the optical fiber networks in certain implementations is the relative independence between the logical interconnection pattern among nodes and the physical topology or fiber layout. There are two possible logical configurations for the interconnection pattern among nodes: the multihop configuration where a message may have to hop through several intermediate nodes before reaching the destination and a single-hop configuration where all nodes communicate with one another in one hop. Among all possible physical topologies, we mention the bus topology, the tree topology, the star topology, and all combinations of these topologies (example: tree-star-tree topology).

In multihop networks, messages traveling from a source to a destination are relayed via intermediate nodes when there is no direct connection. Several virtual structures can be used such as the ShuffleNet [3] and the Manhattan Street structure. One of the impor-

tant parameters related to this kind of network is the expected number of hops or the average number of hops required for a message to reach its destination. This expected number of hops can be reduced using bidirectional configurations such as the bidirectional MSN or by another configuration that duplicates the connectivity so as to achieve better performance without the modification of existing logical configurations.

When multihop networks are implemented using basic topologies, such as the bus, the star, the tree, or compound configurations, such as the tree-star-tree configuration [4], they introduce two major problems. First, the number of different wavelengths needed in the network is very large. Second, even with the use of optical amplifiers, network size is limited by inherent power splitting of the required passive couplers used to interconnect various nodes. To overcome this problem, wavelength division multiplexing cross-connect plays an important role in wavelength routing in multihop networks. One way to implement such a wavelength routing device is to use the WDM cross-connect star design based on the Bragg diffraction grating. In the sequel, the use of this device will be demonstrated for all different multihop network configurations.

In single-hop networks, all nodes must communicate with one another in one hop. This requires a significant amount of dynamic coordination among the nodes. All the users in the network share a common physical topology (one among those mentioned above). In this case, the bandwidth offered by the optical fiber can be effectively exploited by grouping several simultaneous transmissions on the same physical link. Several users may independently access a common communication channel using code division multiple access (CDMA) modulation. This multiaccess scheme does not use time or frequency allocation. Users may transmit without the delay inherent to some multiaccess protocols. In the direct-detection optical CDMA channel, interference immunity is achieved by the assignment of rapidly varying, on-off waveforms or signature sequences, which constitute a set of orthogonal codes. The use of a more efficient sequence such as the Gold sequences by using a coherent transmission scheme and a +1/-1 waveforms using PSK modulation, insure a larger number of simultaneous users in the network. Most of the research concen-

trates on the probability of bit error in fiber optic CDMA networks, and it is assumed that the communication links are being used to transmit messages continuously (or for a very long period of time). There is limited research on the performance of fiber optic packet CDMA networks and on throughput calculation. Hence, extending the result of a simple CDMA system for the case hybrid Wavelength CDMA networks and partial CDMA systems can considerably increase the number of users in such networks with the same network resources.

1.2 Contribution of Thesis

The main contributions of the work are summarized as follows:

1. A new logical topology, the bilayered ShuffleNet, has been proposed. A general form of the tree growth as a function of the number of hops is found. Using this result, the expected number of hops is found.

2. An analysis of performance under uniform and nonuniform traffic of this new configuration indicates a significant improvement for the case of the bilayered ShuffleNet compared to the conventional case. A similar comparison between this new configuration and the SR_Net is also carried out.

3. The signal flow graphs for path enumeration analysis in bilayered ShuffleNet and SR_Net show that the routing strategies in this case can provide alternative paths to reach a node in case of deflection routing due to congestion or link failure, with increased reliability, recoverability, and reduced delay. This results is an advantage for the bilayered ShuffleNet when the probability of deflection is higher than a certain threshold because the bilayered ShuffleNet offers shorter alternative paths than the SR_Net.

4. A new adaptive configuration which uses the combination of bilayered and SR_Net logical configuration. This configuration will minimize the average expected number of hops as a function of the probability of deflection.

5. The cross-connect technique is applied to different multihop Networks. Using this technique the total number of wavelengths used in the conventional NxN star coupler is reduced to only P or $2P$ wavelengths depending on the configuration used.

6. A new network architecture for CDMA optical networks is proposed. This configuration uses the combination of hybrid WDMA/CDMA system and partial CDMA system. The performance of this new configuration has been analyzed and compared to the conventional configuration. The number of users in this configuration can be increased considerably without a loss in performance compared to the conventional configuration.

1.3 Thesis Outline

The intention of this thesis is to offer a discussion of various aspects of optical network architecture such as the introduction of a new logical configuration for multihop networks, which is called the bilayered ShuffleNet, and another configuration for single-hop networks, which uses optical CDMA.

Chapter 2 gives an overview of various optical devices and detection methods that can be used in optical fiber networks. Then, we review the different physical configurations used to implement the various logical configurations.

Chapter 3 presents a new logical configuration for multihop lightwave networks. This configuration uses the same number of users and number of columns as the conventional ShuffleNet with the addition of a second layer of connectivity between stations. The study of this configuration under uniform and non-uniform traffic is a part of the performance analysis. We also present a comparison between this new configuration and other multihop configurations.

In chapter 4, the signal flow graphs for path enumeration analysis in bilayered ShuffleNet shows that the routing strategies in this case can provide alternative paths to reach a

node in case of congestion or link failure, with increased reliability and recoverability, and reduced delay. The performance of this network and the SR_Net in terms of the expected number of hops as a function of deflection probability is also evaluated.

In chapter 5, the cross-connect technique is applied to different multihop networks such as the conventional ShuffleNet, the Manhattan Street Network, the bilayered ShuffleNet and the SR_Net. Using this technique, the total number of wavelengths used in the conventional physical topologies is considerably decreased.

Chapter 6 presents the use of CDMA in optical networks and the new configuration proposed in order to accommodate a larger number of users in such a network. The performance of this configuration in terms of throughput is carried out. The results show that by a small reduction in the total throughput, we considerably increase the total number of users with the same complexity.

Finally, concluding remarks and directions for future research are given in chapter 7.

Chapter II

Overview of Optical Fiber Networks

In this chapter, we will discuss a number of fiber optic components that can be used in the implementation of an optical fiber network. In general, an optical network consists of a physically distributed optical topology, and a logical connectivity graph among the nodes. The logical configuration determines the means of connecting stations together. In the next section, we will discuss a number of optical network devices, then, we present each of the different physical topologies that can be used in the implementation of an optical fiber network. A simple classification of all these topologies is also included. Finally, we present each of the different classes of optical fiber networks: the multi-hop and the single-hop networks.

2.1 Optical Network Devices

In this section, we review some optical devices for networks such as optical fibers, light sources and light detectors.

2.1.1 Optical fibers

The transmission of optical signals via optical fibers was first proposed by Kao and Hocklam [5] in 1966. At the beginning, the losses or attenuation in fibers were in excess of 1000 dB/km. However, after a great deal of research, the current excess loss has been

reduced to 0.2 dB/km [6]. Further research show that an ultra-low-loss fiber with a loss less than 0.01 dB/km for non-silica-based fibers was theoretically possible [7]. This low loss together with the high bandwidth is the basis for the current interest in fiber as a transmission medium.

When an optical signal is launched into the fiber from the source, all rays having angles between 90^{0} and the critical angle are allowed to propagate. All the other rays exceeding the critical angle are evanescent waves, i.e., the waves are severely attenuated as they propagate along the fiber. The allowed direction corresponds to the modes of the optical waveguide. The mode is a complex mathematical and physical concept describing the propagation of electromagnetic waves. This concept can be summarized in the following points.

- Each mode corresponds to a specific direction of the ray travel and has a unique transverse field pattern.
- The modes are the resonances of the waveguide for ray directions that are inclined with respect to the boundary normal.
- The effective refractive index of a given mode can be found from a mode chart. The longitudinal propagation factor can also be obtained.
- Two orthogonal polarizations exist, denoted as transverse electric and transverse magnetic modes.
- The number of allowed modes increases with core thickness and with the difference in refractive indices between the core and the cladding of the fiber.
- For a sufficiently thin core, the optical fiber can support only a single mode. This corresponds to the single mode fiber.

There are two principal types of fibers that are used in optical fiber communications: step index fibers and graded index fibers. These fibers are fabricated by varying the material composition of the core [8]. In the case of step index fiber the refractive index of the core is uniform throughout the fiber cross-section except at the core-cladding boundary. At the boundary the refractive index undergoes an abrupt change (or step). In a graded index fiber the core refractive index varies as a function of the radial distance from the center of the fiber [8]. Step index and graded index fibers can be further classified into single mode and multimode fibers.

In the single mode fiber, only one mode is allowed to propagate. In multimode fibers the propagation of optical energy is allowed in many modes. The number of modes a fiber can support depends on the physical parameters of the fiber and the frequency of the signal to be transmitted. The relation between the number of modes in a fiber and physical parameters of the optical waveguide is given by [9]:

$$\hat{N} = \frac{2\pi^2 a^2}{\hat{\lambda}^2}(n_1^2 - n_2^2) \tag{2.1}$$

where

$\hat{N}$: is the number of modes (integer part)

a : is the core radius

$\hat{\lambda}$: is the free-space wavelength

n_1 : is the refractive index of the core

n_2: is the refractive index of the cladding

Essentially, there are three sets of standard fiber dimensions:

- For graded-index multimode fibers, a core diameter of 50 μm and a cladding diameter of 125 μm.

- For step-index fibers, a core diameter of 200 μm but an unspecified cladding diameter.
- For single mode fibers, a core diameter of 5 μm.

2.1.1.1 Transmission Characteristics

From a transmission performance point of view, single mode fibers have a clear advantage over any other transmission medium including the multimode fibers, as the distance becomes large.

First, the single mode fibers present a typical attenuation characteristic as shown in Figure 2.1, which gives the variation of attenuation with the wavelength of the optical signal. The attenuation in the case of single mode fibers is primarily caused by the intrinsic Rayleigh scattering of the doped fused silica, which is proportional to the inverse of the 4^{th} power of the wavelength. Beyond 1600 nm, a rapid increase in the attenuation is due to the intrinsic infrared tail of the material used in the fiber. Other sources of losses can be mentioned such as the Hydroxyl (OH) absorption losses and excess losses caused by waveguide imperfection and metallic impurities. These losses are negligible, and can be eliminated completely in certain cases. For example, the absorption loss of the Hydroxyl (OH) ion at 1380 nm is zero [10].

Multimode fiber losses have the same fundamental limitations as single mode fibers, however, they are generally higher than those of the single mode fibers because of the higher dopant concentrations and a higher sensitivity to microbending losses particularly of the higher-order modes.

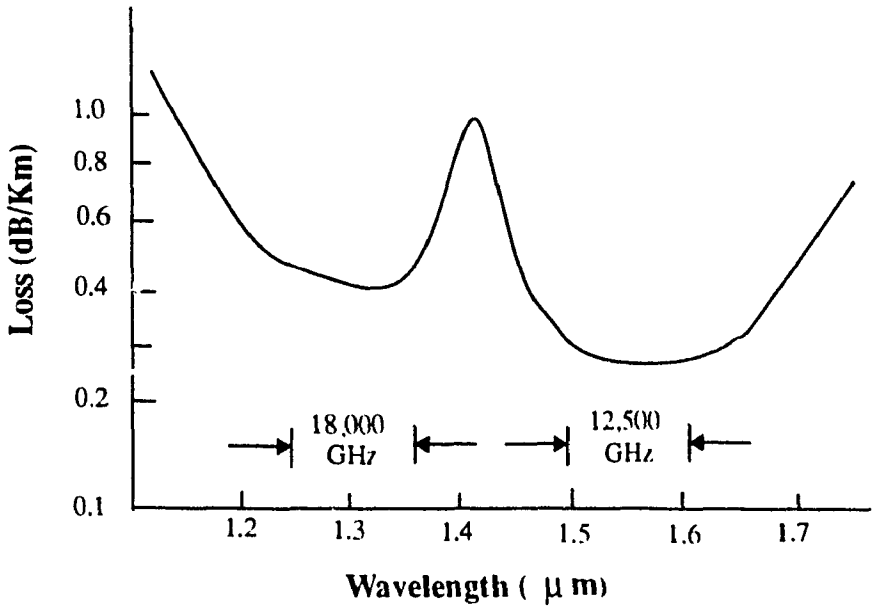

FIGURE 2.1 Single mode fiber bands

2.1.1.2 Properties and Impact of the Optical Fiber

Single mode fiber has become the preferred transmission medium for telecommunications, because of its practically unlimited transmission bandwidth over very long, unrepeatered distances. The single mode fiber propagation exhibits a low dispersion of the transmitted pulse [9], and this kind of fiber does not suffer from intermodal dispersion[1].

Furthermore, single mode fiber has two low-loss regions near 1300 nm and 1500 nm, and offers an enormous transmission bandwidth: thousands of GHz are available [10] as shown in Figure 2.1. These advantages make the use of single mode fibers very attractive for Metropolitan Area Networks (MAN).

Multimode fiber is preferred to single mode fiber for low bandwidth and low transmission distances such as local loops and telephony and Local Area Networks (LAN),

1. Intermodal dispersion, or pulse spreading, is caused by the difference in the propagation times of light rays that take different paths down a fiber.

which have less need for high performance because of the distance. Multimode fibers and LEDs have been used in LANs operating at rates ≤ 100 Mbps. Since multimode fibers have a larger core diameter than single mode fibers, it is easier to launch optic power from an LED into a multimode fiber than a single mode fiber.

The single mode fibers are always excited with Laser diodes because of their narrow core diameter. At the same time, single mode fiber presents certain limitations. The transmission rate on a single mode fiber can be limited by fundamental energy considerations. Consider the simple point-to-point optical link, consisting of a transmitter coupled to a receiver via a lossless fiber. To detect a transmitted bit, the receiver requires a minimum amount of optical energy, E. In the ideal case, E is independent of bit rate, so operation of the link at a rate B requires a power level of $E.B$ at the receiver. We conclude that for a transmitter with output power P, the maximum (power-limited) transmission rate is P/E. This power problem makes it difficult to translate many high-capacity networking concepts into practical photonic implementations. For example, the absence of amplification will place a limit on the splitting that can take place for a given physical topology due to the power problem.

Although photonic technology is capable of supporting many Tb/s of throughput, the digital electronic components at the nodes of the lightwave network, which typically operate at rate of 1 Gb/s or less, can drastically limit total throughput. This situation is the electronic bottleneck [11].

2.1.2 Optical Sources

The principal optical sources used in fiber optic communication systems are Laser diodes and Light Emitting Diodes (LEDs). The operation of these two sources are dealt with in the following sections.

2.1.2.1 Light Emitting Diodes (LED)

The LED is simply a P-N junction diode. It is usually made from a semiconductor material such as Aluminum Gallium Arsenide (AlGaAs) or Gallium Arsenide Phosphide (GaAsP). LEDs emit light by spontaneous emission; light is emitted as a result of the recombination of electrons and holes.

2.1.2.2 Lasers

Laser is the abbreviation for Light Amplification by Stimulated Emission of Radiation. The medium for lasing can be a gas, a liquid, a crystal or a semiconductor [8]. For optical communications the Laser sources employed are semiconductors. The Laser is similar to LED. In fact, below a certain threshold current a Laser acts the same as an LED.

The major difference between LEDs and Lasers is that the power emitted from an LED is incoherent, whereas that from a Laser is coherent. In a coherent source, the optical power is generated in an optical resonant cavity. The optical power radiated from this cavity is highly chromatic and the output beam is very directional. In an incoherent source such as an LED no optical cavity exists for wavelength selectivity, consequently the output radiation has a broad spectral width. The coherent optic power from Laser can be coupled into single mode or multimode fibers. However, the optical power output from an LED because of its incoherency can only be coupled into a multimode fiber [8].

In selecting an LED or a Laser diode as a source there are certain advantages and disadvantages for each type of device. Some of the advantages of a Laser over an LED are [5], [8]:

- A faster response time. This implies faster data transmission rates are possible.
- The spectral width of a Laser is narrow, which implies less distortion due to dispersion.

- The optic power that can be coupled from a Laser is greater, consequently, greater transmission distance is possible.

Some of the disadvantages of Lasers are:

- Fabrication of Lasers is more complicated.
- The optical output is strongly dependent on temperature. As a result, the transmitter circuitry is more complicated than for the LED transmitter.

The choice of a particular optical source depends on many factors. As an aid in selecting a particular diode for fiber optic communication, the characteristics of optical sources are summarized in Table 2.1.

TABLE 2.1 Typical characteristics of diode light sources

Property	LED	Laser Diode	Single Mode Laser Diode
Spectral width (nm)	20-50	1-5	<0.2
Rise time (ns)	2-250	0.1-1	0.1-1
Modulation bandwidth (MHz)	< 300	< 2000	2000
Coupling efficiency	very low	moderate	moderate
Temperature sensitivity	low	high	high
Circuit complexity	simple	complex	complex

2.1.3 Light Detectors

The purpose of the light detector is to convert an optical signal to an electrical signal. The signal is then amplified and processed further. If the chosen detector has good characteristics, such as linearity and responsivity, the requirements on the rest of the signal processing circuitry are less stringent. The two main photodetectors used in optical fiber communications are silicon positive-intrinsic-negative (PIN or p-i-n) photodiodes and Avalanche photodiodes (APD).

2.1.3.1 PIN Photodetectors

PIN photodetectors are the most common type of detectors employed in optical fiber systems. Basically, a PIN photodiode operates in a fashion which is just the reverse of an LED. Most of the photons are absorbed by electrons in the valence band of the intrinsic material. When photons are absorbed, they add sufficient energy to generate carriers and allow current to flow out of the device.

2.1.3.2 Avalanche Photodetectors (APD)

In the ideal situation, for a PIN diode, if every incident photon produces a hole-electron pair, then at wavelength of 1μm, the responsivity is about 0.8 A/w [12]. Most of the receivers operate with input power levels as low as few nano watts. Thus, with PIN detectors, the photocurrent generated would be very small; in the order of few nano amperes. Such a small current would be severely corrupted by the amplifier noise. To increase the number of electron-hole pairs generated for each incident photon an avalanche photodiode is used.

An avalanche photodiode has a high electric field region (avalanche region). In the avalanche region, carriers move randomly and occasionally collide with ions, thereby producing new carriers. The newly created carriers gain sufficient velocity, thus producing some more carriers. This phenomenon is called the avalanche effect [8].

The avalanche effect multiplies the primary photo current by a random gain factor, thereby increasing the effective responsivity of an APD by a random gain factor G. As a result, the receiver sensitivity is also increased.

The carrier multiplication achieved by this method causes noise, since the gain factor is random [12]. This randomness in the avalanche process produces an effective noise, which limits the receiver sensitivity of the APD devices. However, for a certain range of gain factor, the effective noise of the APD is less than that produced by amplifier noise;

consequently, the APD offers significant benefits over a PIN detector [12]. The typical characteristics of PIN and APD's are shown in Table 2.2.

TABLE 2.2 Typical characteristics of junction photodetector.

Material	Structure	Rise Time ns	Wavelength nm	Gain
Silicon	PIN	0.5	300-1100	1
Germanium	PIN	0.1	500-1800	1
InGaAs	PIN	0.3	1000-1700	1
Silicon	APD	0.5	400-1000	150
Germanium	APD	1	1000-1600	150

2.2 Detection Methods in Optical Communication

In optical communication two detection schemes are available, direct detection, and coherent (heterodyne or homodyne) detection.

2.2.1 Principle of Direct Detection

Direct detection of light pulses implies a photo detection that converts light energy into electrical signals. The detection mechanism is based on photon counting. In the case of binary transmission, a *one* or a *zero* is translated into the presence or absence of optical energy. This mechanism is illustrated in Figure 2.2. This single pulse description can be extended to an entire data wave by assuming that superposition holds for optical fiber transmission. When an Avalanche detector is used to gain optical amplification, fluctuations get larger as the average value gets large; consequently, losses cannot be neglected. Thus, one of the chief motivations for turning to coherent techniques is to minimize this loss in detector sensitivity [13].

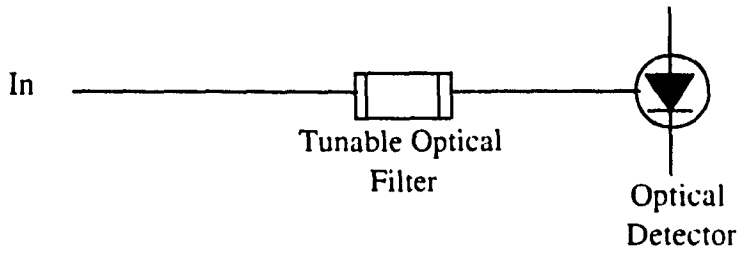

FIGURE 2.2 Direct detection

2.2.2 Principle of Coherent Detection

Figure 2.3 shows the principle of coherent detection. The optical process is similar to radio heterodyning using an average power detector. A weak signal is first combined using a partially silvered mirror or an optical fiber coupler with a locally generated wave or Local Oscillator (LO) signal. The combined wave is then detected using a photodiode, which can be viewed as an ideal square-law device since its output current is proportional to the optical intensity [14]. The result of this mixing process is a modulation of the average detector photo-current at a frequency equal to the difference between the frequencies of the signal, $A_s \cos(\omega_s t + \rho_s)$, and the LO, $A_{lo} \cos(\omega_{lo} t + \rho_{lo})$.

$$I_{photo} = \frac{1}{2}A_s^2 + \frac{1}{2}A_{lo}^2 + A_s A_{lo} \cos[(\omega_s - \omega_{lo})t + (\rho_s - \rho_{lo})] \tag{2.2}$$

The new optical signal is called the Intermediate Frequency (IF) signal. When the signal and LO frequencies are identical, the process is called homodyne detection and the information appears directly at baseband frequencies (i.e., near zero frequency), otherwise the process is called heterodyne detection. Figure 2.4 shows the basic elements of heterodyne and homodyne optical receivers. Notice that for heterodyne and homodyne reception, respectively, frequency and phase tracking are required. The term *coherent* is used in optical communications literature to refer to any heterodyne or homodyne process.

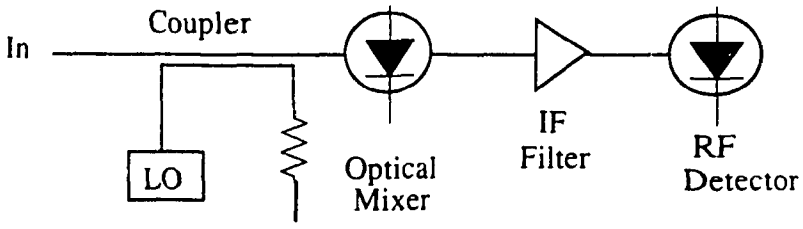

FIGURE 2.3 Coherent detection

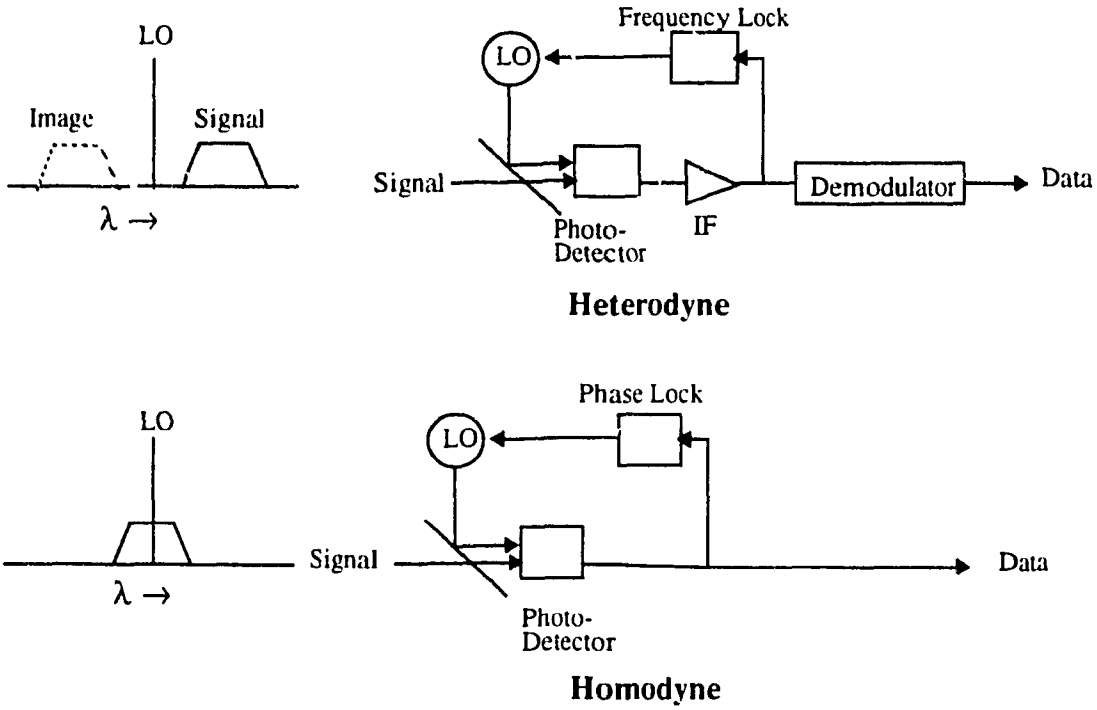

FIGURE 2.4 Coherent receivers

Since the amplitude of the IF signal is proportional to the product of the input signal and the LO amplitudes, the IF power can be made arbitrarily large compared with amplifier noise by increasing the LO power. This means that a weak signal mixed with a strong local oscillator wave results in an effective signal gain proportional to the local oscillator amplitude, which can be substantial. This optical gain is extremely valuable since it

increases the signal strength before the signal reaches the detection stage and becomes subject to the inevitable noise from components after detection [15]. Compared to direct-detection receivers, the heterodyne receivers are about 10 dB more sensitive but require the added cost and complexity of a high-power, optical LO, as well as polarization diversity or control of the signal to assure efficient mixing with the LO. For direct detection, this 10 dB difference can be made up by using an optical amplifier so there is little difference and both detection methods will have a similar performance.

2.3 Physical Configurations

There are many physical configurations that can be used to implement an optical fiber network. The configurations considered here can be grouped into two classes: basic and compound, based on the topology of their data networks. We also take into consideration the WDM cross-connect star topology, which replaces the passive star coupler and can be used to implement different multihop networks with the advantage of reducing the total number of wavelengths and increasing the number of users in the network.

2.3.1 Basic Configurations

There are three basic configurations; the bus, the tree and the star. The classification of these three configurations is based on the maximum number of users that the configuration can accommodate.

2.3.1.1 Bus Configuration

The bus configuration differs from the others by the virtue of the fact that the network is based on a linear bus topology. Traffic from each station is first injected into the "talk side" of the bus, via directional couplers, then broadcast to the receivers on the "listen side", via a second set of couplers as shown in Figure 2.5. Although attractive for use with coaxial cable-based networks such as Ethernet, the architecture has a drawback with fiber because it wastes signal power. In a N-station network only P/N^2 useful power is delivered

to each receiver. For any linear arrangement of N taps, the end-to-end loss in dB is given by [16]:

$$L = -10N\log(1-\alpha) - 10N\log(\beta) \tag{2.3}$$

where α correspond to the coupler power splitting ratio and β the coupler excess loss. For typical values $\alpha = 0.1$ and $\beta = 0.8$, and for a power margin in the order of 40 dB, the maximum number of users for a bus configuration is limited to 8 users. Optical amplifiers can be used to ameliorate this difficulty to make the bus more viable by increasing the power efficiency by up to *P/N*. However, due to many time-overlapped transmissions that occur in the bus, the maximum number of users in this case cannot exceed 482 with the appropriate choice of α, β and the amplifier gain [16].

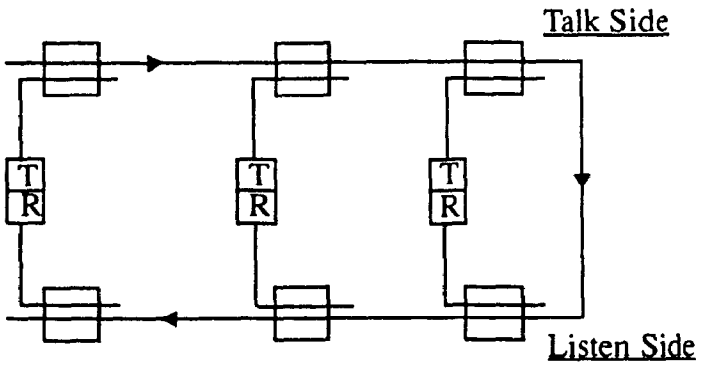

FIGURE 2.5 Bus configuration

2.3.1.2 Tree Configuration

The number of stations in a tree configuration (Figure 2.6) is a power of 2. Because of the power splitting, the maximum number of stations supported by this kind of configuration is equal to 16 for the same power margin as in the case of the bus; by using amplification at the root of the tree this number can reach a total of 512 [17].

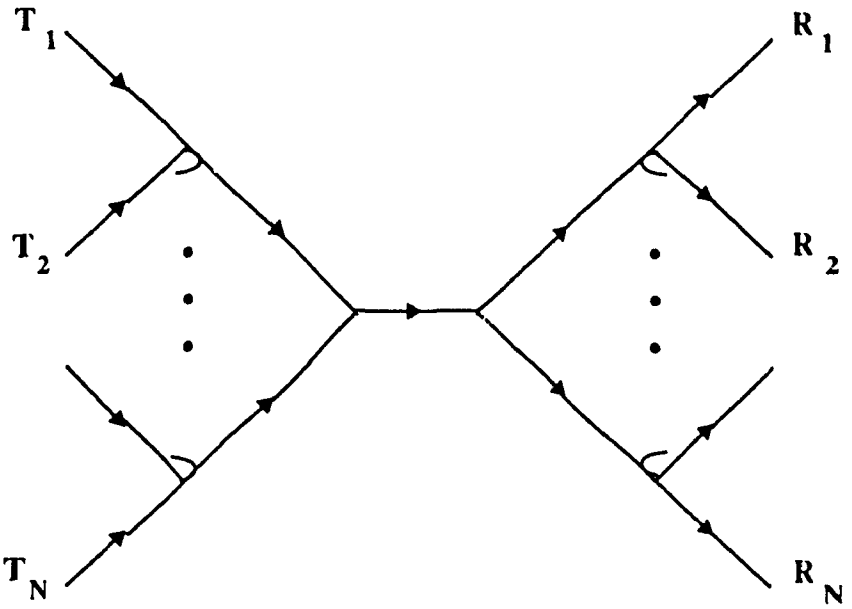

FIGURE 2.6 Tree configuration

2.3.1.3 Star Configuration

The third basic configuration to implement a photonic network is the star topology. In this configuration, we use an *N*x*N* star coupler (where *N* is the number of stations) where the transmitters and the receivers are connected to the star coupler via a set of fibers as shown in Figure 2.7. The main advantage of the star architecture over other LAN architectures such as bus where various stations are coupled in succession to a single fiber, is its small excess loss such as the dividing losses in the star coupler or in the splitters, taps, filters and line losses. For example, the excess loss for an *N*-station star increases only logarithmically with *N*, while that of an *N*-station bus increases linearly with *N* [18]. The difference in loss can be quite significant, especially for large values of *N*. The maximum number of users that can be accommodated in such a configuration can reach up to 1000 users, which is much larger than the case of bus and tree configurations [18].

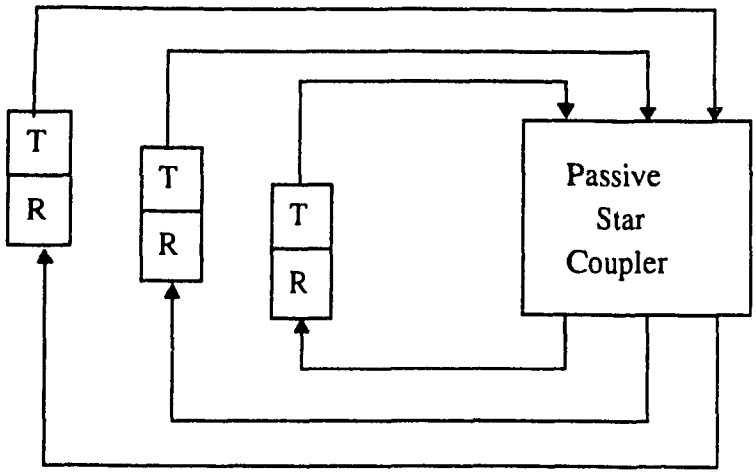

FIGURE 2.7 Star configuration

2.3.2 Compound Configurations

The basic configurations described in the previous section can support a limited number of network stations. The technique of interconnecting several trees with a passive modular star, as shown in Figure 2.8, is an effective way of increasing the total number of stations. The number of stages in a modular star is $\log_2 S$ where S is the number of ports [18]. Each stage introduces a 4 dB attenuation. Using the assumptions in the previous section, a system with a four-stage star ($S = 16$) and with a three-level tree can support $8 \times 16 = 128$ stations without requiring amplification. This is a major improvement with respect to the 16 stations in a tree. If amplification is used, the modular star permits a dramatic increase in the total number of stations. Assuming that amplifiers are used at the inputs and the outputs of the star, a configuration with a 10-stage star (1024 inputs and outputs) or the equivalent star that uses the Free-Space planar guide, and a 3-level tree becomes feasible (from a power budget standpoint). This configuration supports up to 16384 stations [19].

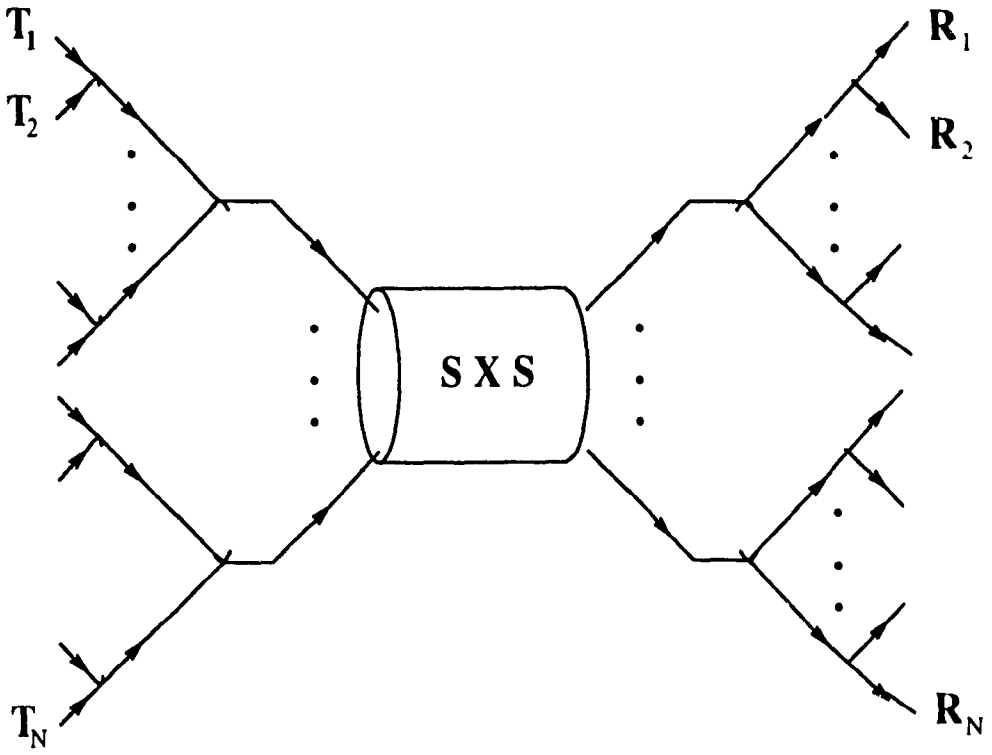

FIGURE 2.8 The Tree-Star-Tree configuration.

2.3.2.1 WDM cross-connected star topology

The wavelength division multiplexed (WDM) cross-connect [21] is used to replace the conventional NxN passive star coupler. This device plays an important role in wavelength routing networks, where the path that the signal takes is uniquely determined by the wavelength and the port through which it enters the network. The fabric of the network consists of an array of wavelength-selective devices connected in a specific pattern in order to obtain the required interconnection between the nodes of the network. The implementation and the use of this device will be discussed in more detail in Chapter 4. In summary, classification of different physical configurations is presented in Figure 2.9. These physical configurations can be used for both single-hop or multi-hop networks. The choice of one configuration over the other depends on the number of users in the network.

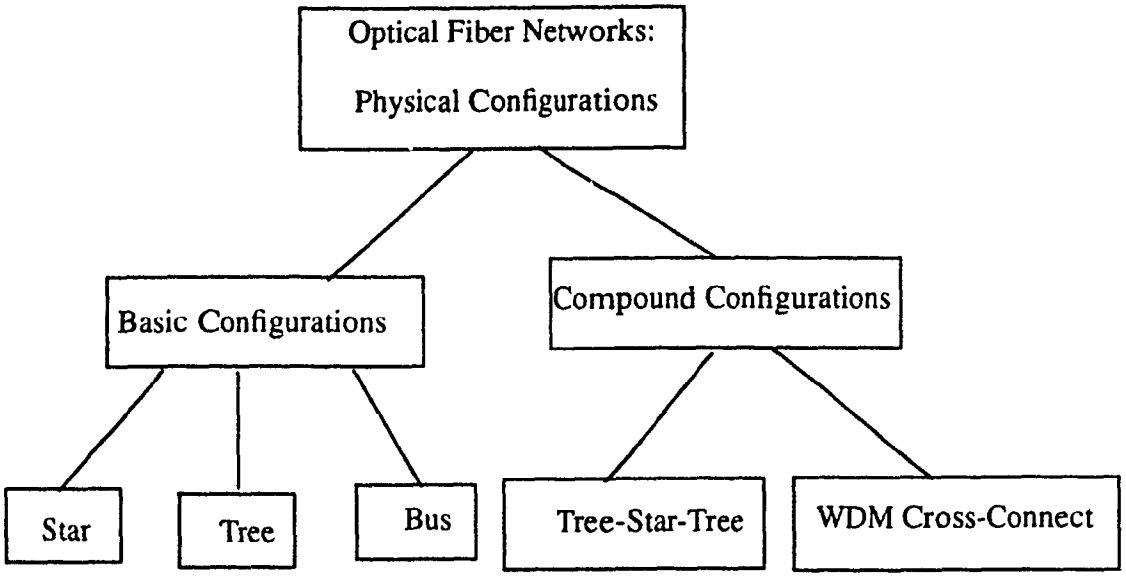

FIGURE 2.9 Different physical configurations used for the implementation of an optical fiber network.

2.4 Optical Networks: Logical Configuration

For a given source-destination pair a message may have to hop through several intermediate nodes before reaching the destination, this corresponds to the multihop case. Otherwise, if all nodes communicate with one another in one hop, this corresponds to the single-hop case.

2.4.1 Multihop Networks

In multihop networks, the connectivity between any arbitrary pair of nodes is achieved by having all the nodes also acting as intermediate routing nodes. The intermediate nodes are responsible for routing data among lightwave channels such that a message on the transmitting side has to go through one or several nodes to reach its destination. A number of different multihop architectures is possible. An example of these, we have the ShuffleNet, the Manhattan Street Network and the SR_Net [26]. All of these architectures will be discussed in the next chapter.

2.4.2 Single-Hop Networks

Single-hop networks refer to networks where a message, once transmitted, reaches its destination directly without being routed through different nodes in the network or being converted to electronic form on the way. In single-hop networks, all users share the same transmission medium (same physical configuration). Generally, in a WDM single-hop network each user transmits on a unique wavelength different from others. All transmissions are broadcast to all stations and at each station, a tunable optical filter selects one of the wavelengths for reception. This requires rapidly tunable lasers and/or filters over a wide wavelength range with a high-selectivity. It also requires a significant amount of dynamic coordination between the nodes. Given that the tuning ranges of current optical components are limited, and that their current tuning times are significantly long, the total number of wavelengths used in single-hop networks and consequently the maximum number

of users is limited. Another alternative for the single-hop networks is the use of optical CDMA which apparently can accommodate more users without using sophisticated protocols [27].

2.4.2.1 WDM Single-Hop Networks

The system considered here can be configured as a broadcast network in which all of the inputs from different nodes are combined in a WDM passive star coupler or any other physical configuration, and the combined optical information is broadcast to all users in the network. In this system, there are no intermediate nodes; consequently, a significant amount of dynamic coordination is required among the nodes. The transmitting node and the receiving node must be tuned to the same wavelength during the transmission time of a packet in order for the packet to be received [28], [29].

For an effective WDM network to be developed, each user should be able to transmit into multiple WDM channels, or receive from multiple WDM channels, or both. Accordingly, a great amount of effort is being devoted to design of tunable transmitters (lasers) and tunable receivers (filters), which can operate over a wide range of WDM channels and the channel tuning (switching) operations of which can also be performed very quickly (ideally in a few nanoseconds or less) [30]. In the case of tunable lasers, a tuning range of 100 nm and a switching time of 1.8 ns can be achieved depending mainly on the technology adopted. There are thermally tuned lasers, mechanical lasers and lasers with an acousto-optic tunable filter within the cavity [28], [31].

For WDM single-hop systems several different classifications are listed in [31]. Among these, there is a classification depending on whether the transmitter of each node is tunable or not. The other classification is based on whether pretransmission coordination is required or not. Based on the first classification, each node can have one of four possible configurations, the first set of these configurations employs fixed transmitters and fixed

receivers. This limits the number of users in the network but there is no requirement for having a control channel. The LAMBDANET is an example of the networks that use this configuration [32]. Due to the restriction on the number of users, this configuration is mainly used in multihop networks where each user has access to a limited number of users in the network. The second configuration employs tunable transmitters and fixed receivers. This configuration may not require coordination via a control channel. The Fiber Optic Crossconnect (FOX) [33] is an example of networks that use this configuration. The third configuration employs fixed transmitters and tunable receivers. In this configuration, if each node is assigned a different channel, a simple access protocol can be used. An experimental version of this configuration falls under the RAINBOW project of IBM [33].The last configuration employs tunable transmitters and tunable receivers. This configuration is the most flexible in accommodating a scalable user population but it also has to deal with the channel-switching overhead of the transceivers [30].

The second consideration based on whether or not pretransmission coordination is needed leads to two different classes. If pretransmission coordination is required, the network uses a single or several shared control channels through which nodes that have a packet to transmit coordinate their transmission requirements and then transmission can occur through a number of data channels [1], [30]. In the absence of pretransmission coordination, the control channel is not required and the coordination is performed either in a preassigned fashion or through contention-based data transmission on the regular data channels (e.g., requiring nodes to either transmit on or receive from pre-determined channels) [28], [32], [36], [37]. As a result, for a large user population whose size may be time-varying, pretransmission coordination may be the preferred choice, although most experimental demonstrations and prototype WDM systems belong to the non-pretransmission-coordination category.

2.4.2.2 CDMA Single-Hop Networks

Optical code division multiple access (CDMA) has been proposed as a second alternative to take advantage of the large bandwidth of single-mode fiber. It maps low-information-rate electrical or optical signals into high-rate optical sequences to achieve random, asynchronous multi-access [39]. In optical CDMA, many nodes transmit simultaneously in the same frequency band. Accordingly, signals must be designed to reduce interference. In order for the signal waveforms not to interfere, their bandwidth would be several orders of magnitude greater than the information bandwidth $1/T$ of the digital modulation; T being a bit duration. In order to do this, each bit is sub-divided into a number of binary "chips". The chip sequence constitutes a code that permits a bit stream broadcast on a network to be selected by means of a correlation process at the receiver destination. A large number of chip codes can be assigned to different users. The set of optical sequences essentially becomes a set of address codes or signature sequences for the network.

The advantage of CDMA is that, it is a true tell-and-go protocol. When one node wants to send traffic to another node, prior coordination is required only with that node. Multiple users can simultaneously access the channel with no waiting time, in contrast to other asynchronous protocols like CSMA or CSMA/CD where each user must wait for the channel to become idle before gaining access [27]. A CDMA network is also highly scalable and modular.

A typical fiber-optic CDMA system is shown in Figure 2.10, the network is supported by a physical configuration, which is the star topology. A total of N users share a NxN star coupler. For each user, the transmitting side consists of an information data source followed by a laser and an optical encoder. This encoder maps each bit of the output information into a very-high-rate optical sequence. The output of the encoder is then coupled into the star coupler. At the receiving side, the sequence would be compared to a stored replica of itself (correlation process) and to a threshold level at the comparator for data recovery

[40]. Each user can use different sets of optical sequences depending on the destination of the message. These optical sequences essentially become a set of address codes or signature sequences for the network. A CDMA receiver has the ability to extract the data with the desired optical pulse sequence in the presence of all other users' optical pulse sequences.

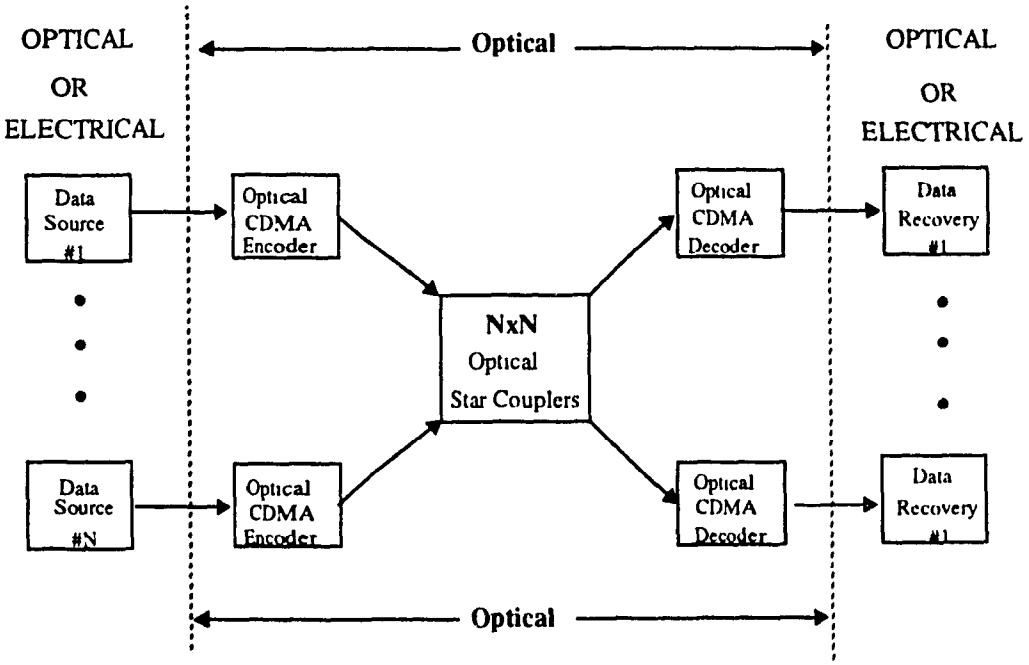

FIGURE 2.10 Optical CDMA communication systems.

2.5 Discussion

The use of the optical technology in the implementation of networks leads to the design of several network architectures in order to exploit the 30 THz bandwidth of a single mode fiber. Two general classes of optical networks can be identified: the single hop network and the multihop network. In the single-hop network each message once transmitted, reaches its destination directly without being routed through different nodes in the

network or being converted to its electronic form on the way. The huge bandwidth can be exploited in this case either by using WDM or by using CDM. In multihop networks, each message has to go through one or multihop in order to reach its destination, for this case, WDM is used mainly. Different architectures are presented such as the ShuffleNet, the MSN and so on. The choice of architecture is mainly related to the application of the network.

In the next chapter, we introduce a new logical configuration for multihop networks. This configuration will add another set of connections to the existing configuration of the ShuffleNet.

Chapter III

Bilayered ShuffleNet: A New Logical Configuration for Multihop Lightwave Networks

Multichannel-multihop lightwave networks are designed to achieve efficient use of the channel bandwidth using the available optical technology. As examples of multihop lightwave networks, we have the ShuffleNet and the Manhattan Street Network. In this chapter, we present an overview of different multihop networks; then, we present a new logical configuration for multihop networks, which will improve the performance of such networks in a certain respect. The study of this configuration under uniform and non-uniform traffic is a part of the performance analysis. We also present a comparison between this new configuration and other multihop configurations.

3.1 Multihop Networks: Logical Configuration

In multihop networks, the connectivity between any arbitrary pair of nodes is achieved by requiring all the nodes also to act as intermediate routing nodes. The intermediate nodes are responsible for routing data among lightwave channels such that a message on the transmitting side has to go through one or several nodes to reach its destination. A number of different multihop architectures are possible. In order to make a comparison, we shall consider the expected required number of hops for a packet to reach its destination in each of these networks.

3.1.1 The General Perfect ShuffleNet

In this section, we introduce the ShuffleNet connectivity graph in which stations are arranged in k columns, each consisting of P^k stations [3]. Each of the P^k stations in a column has P arcs directed to P different stations in the next column. If the stations in a column are numbered from 0 to P^k-1, station j has arcs directed to stations i, i+1,..., and i+P-1 in the adjacent column; where $i = (j \bmod P^{k-1})\, P$. There are a total of P^{k+1} directed arcs to connect 2 successive columns. All the columns are arranged in a fixed shuffle pattern, with the last column connected to the first to form a cylindrical pattern. The total number of stations is given by

$$N = kP^k; \qquad k = 1, 2, \ldots \qquad P = 1, 2, \ldots \tag{3.4}$$

Figure 3.1 shows the connectivity of an 18-station (P=3, k=2) ShuffleNet, where the first column is repeated on the right to show the cylindrical nature of the connectivity graph. Let h be the number of hops, and $n(h)$ be the number of stations h hops from the source.

$$n(h) = \begin{cases} P^h; & 1 \le h \le k-1 \\ P^k - P^{h-k}; & k \le h \le 2k-1 \end{cases} \tag{3.5}$$

Hence, the expected number of hops between two randomly selected stations is given by

$$\overline{H} = E[hops] = \frac{kp^k (P-1)(3k-1) - 2k(P^k-1)}{2(P-1)(kP^k-1)} \tag{3.6}$$

3.1.2 Manhattan Street Network

An NxM Manhattan Street Network (MSN) is a regular mesh structure of degree 2 with an even number of rows and columns and is not defined for an arbitrary number of nodes [42]. There are two links arriving at and leaving each node. Logically, the links form a grid on the surface of a torus. Unidirectional communication links connect its

nodes into N rows and M columns, with adjacent row links and column links alternating in direction. An example of a 4x4 Manhattan Street network is shown in Figure 3.2. This structure was originally proposed as a metropolitan area network in [42], [43], but it can be considered as a virtual topology for multihop lightwave networks. The maximum length of the shortest path between any pair of nodes is given by [47]

$$d_{max} = \begin{cases} \dfrac{N+M}{2} + 1, & \text{if } \dfrac{N}{2} \text{ and } \dfrac{M}{2} \text{ are even} \\ \dfrac{N+M}{2}, & \text{otherwise} \end{cases} \tag{3.7}$$

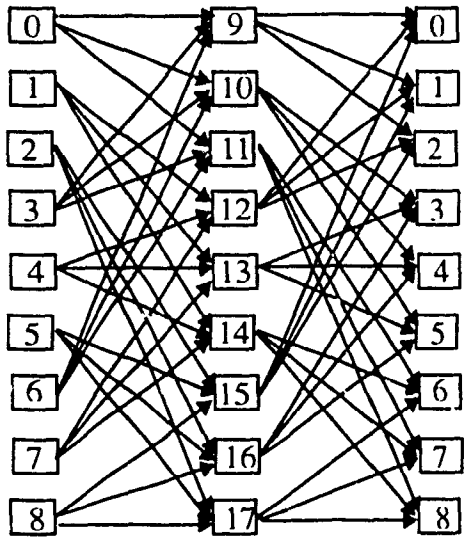

FIGURE 3.1 An 18-user (P=3, k=2) ShuffleNet

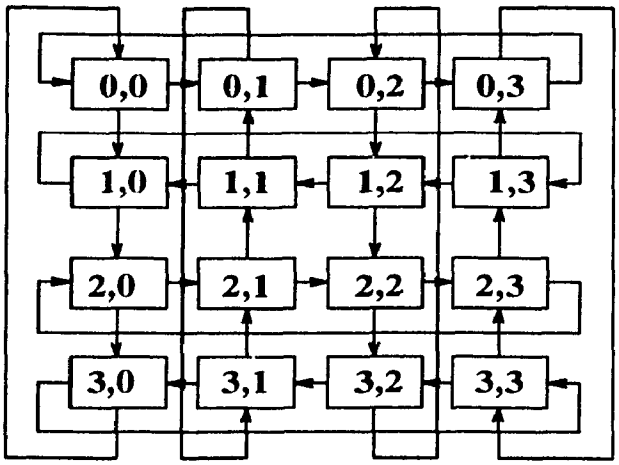

FIGURE 3.2 The logical configuration for a 16-user Manhattan Street Network.

The expected number of hops between two randomly selected stations is given by:

$$E[hops] = \begin{cases} \dfrac{\frac{NM}{4}(N+M+4)-4}{NM-1}, & \text{if both } \frac{N}{2} \text{ and } \frac{M}{2} \text{ are even} \\ \dfrac{\frac{NM}{4}(N+M+4)-M-4}{NM-1}, & \text{if } \frac{N}{2} = \text{even and } \frac{M}{2} = \text{odd} \\ \dfrac{\frac{NM}{4}(N+M+4)-M-4}{NM-1}, & \text{if } \frac{M}{2} = \text{even and } \frac{N}{2} = \text{odd} \\ \dfrac{\frac{NM}{4}(N+M+4)-N-M-2}{NM-1}, & \text{if } \frac{N}{2} = \text{odd and } \frac{M}{2} = \text{odd} \end{cases} \tag{3.8}$$

3.1.3 Shuffle Ring Network

In this section, we consider the Shuffle Ring Network or SR_Net in the general case where P can be equal to 2,3,.... and not limited to the case of P=2 as shown in [48]. An (n, k, P) SR_Net has a total of kP^n nodes; the connectivity graph consists of k columns of P^n nodes each, arranged with shuffle interconnections between the consecutive columns. An important special case of the (n, k, P) SR_Net is the ShuffleNet when n=k and the same connectivity is used (same P). There are a total of kP^{n+1} links in the SR_Net in order to

interconnect all the stations. In the SR_Net, the address of each node can be denoted by a two-tuple (c, r) where $0 \le c \le k$ and $0 \le r \le P^n$. Let $(r_{n-1}, r_{n-2}, \ldots, r_0)$ be the row index r expressed in the base P notation, i.e., $r_i \in \{0, 1, \ldots, P\}$, $0 \le i < n$. In an (n, k, P) SR_Net, each node $(c, r_{n-1}, \ldots, r_0)$ has P output links connecting to the nodes $(c \oplus 1, r_{n-2}, \ldots, r_0, 0)$, $(c \oplus 1, r_{n-2}, \ldots, r_0, 1)$, ... and $(c \oplus 1, r_{n-2}, \ldots, r_0, P-1)$ where $c \oplus 1 \equiv (c+1) \bmod k$. Similar to the ShuffleNet and the bilayered ShuffleNet, the SR_Net has a cylindrical pattern where the last column is connected back to the first column.

Let h be the number of hops, and $n(h)$ be the number of stations h hops from the source.

$$n(h) = \begin{cases} P^h; & 1 \le h \le n-1 \\ P^n; & n \le h \le k-1 \\ P^n - P^{h-k}; & k \le h \le k+n-1 \end{cases} \tag{3.9}$$

the expected number of hops between two randomly selected stations is given by:

$$E[hop] = \frac{kP^n[(P-1)(2n+k-1) - 2k(P^n-1)]}{2(P-1)(kP^k-1)} \tag{3.10}$$

The results obtained above for a general case of the SR_Net can be used for the case of the ShuffleNet. By letting $k=n$ in (3.9) and (3.10), we obtain the same results found in (3.5) and (3.6). Given that the ShuffleNet is only a particular case of the SR_Net, we choose the SR_Net in order to have more flexibility in the choice of the network configuration. As an example, a network with size 64 can be presented in different ways; among these, we have the (4, 4, 2) SR_Net which corresponds to a (2, 4) ShuffleNet and a (4, 2, 4) SR_Net where the connectivity is doubled and the number of columns is kept the same, this case is shown in Figure 3.3.

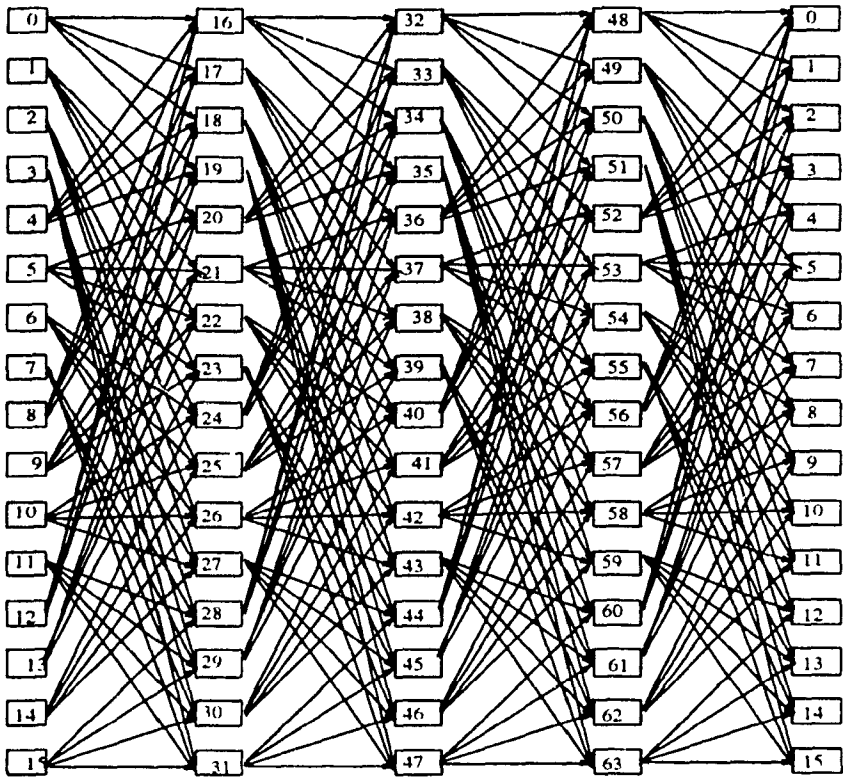

FIGURE 3.3 A 64-node SR_Net

3.2 Bilayered ShuffleNet: Logical Configuration

The bilayered ShuffleNet connectivity graphs use the same connectivity graph as the conventional ShuffleNet twice, once in each direction around a cylinder. For a (P, k) bilayered ShuffleNet, the number of stations is equal to $N = kP^k$ arranged in k columns of P^k stations each. Instead of only connecting each station in the network to P different stations in the next column, now we let each station be connected to a "mirror" image of stations from the previous column; thereby, doubling the connectivity between stations [23]. In this case, the connectivity graph of the ShuffleNet will look as though all stations are wrapped around the same cylinder twice, one from left to right and one from right to left (see Figure 3.4). The same set of connections is used in both directions. This will increase the connectivity in the network and the total number of links will be double that of the conventional ShuffleNet, i.e., equal to $2k\,P^{k+1}$.

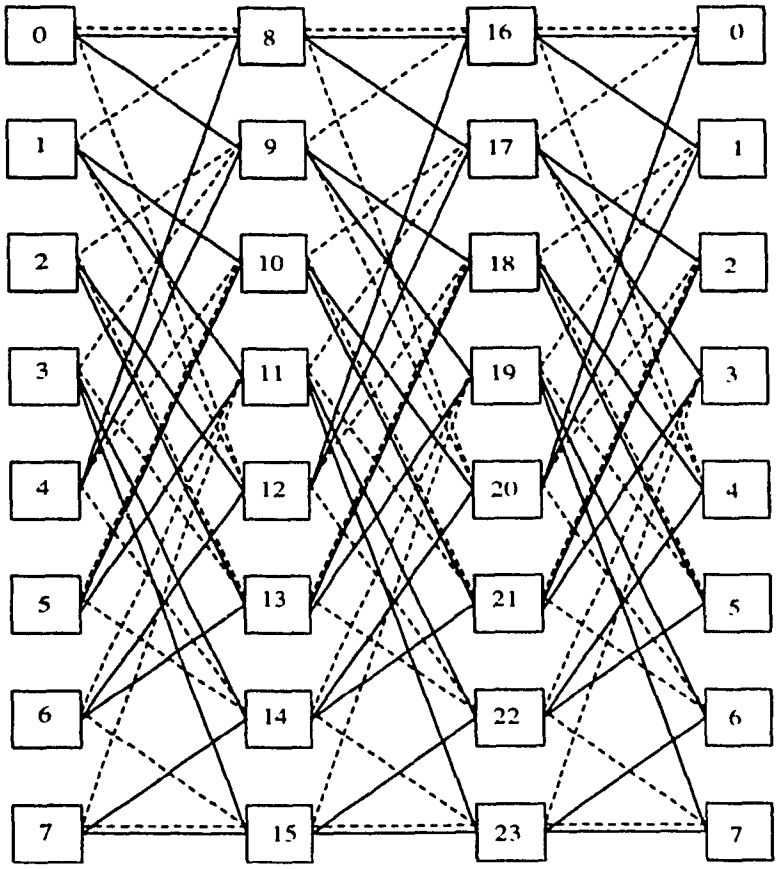

FIGURE 3.4 A (2, 3) bilayered ShuffleNet N=24.

As an example, we take the case of (2, 3) ShuffleNet (N = 24), the new bilayered connectivity between stations is shown in Figure 3.4. If any station is allowed to transmit in both directions, starting from station number 0 we can reach $2P$=4 stations in the first hop. In the second hop, we can reach 7 other stations and finally in the last hop we reach all the remaining stations (12 stations) in the network. The tree-growth for this case is shown in Figure 3.5. The maximum number of hops required in this case is equal to k=3 compared to $2k$-1=5 in the conventional case.

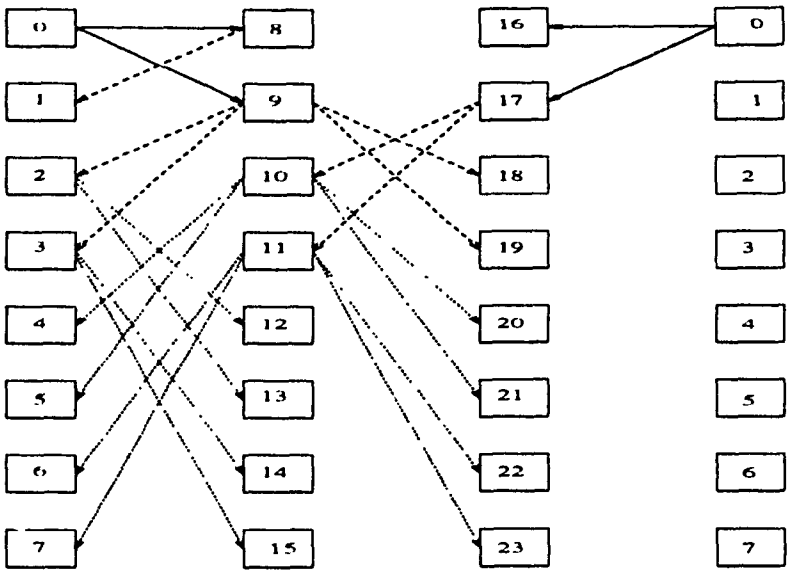

FIGURE 3.5 A tree growth of a (2, 3) bilayered ShuffleNet N=24.

We consider the case of k=4, which is slightly different from the previous example, taking P=2 (N=64) and allowing each station to transmit in both directions. In this case, if we start from the first station we can reach four stations in the first hop, seven stations in the second hop, 12 stations in the third hop, 24 stations in the fourth hop, and finally 16 stations in the fifth (last) hop. For the case of k=4 the maximum number of hops is equal to k+1=5 compared to only k for the case of k=3. The tree-growth for this case is shown in Figure 3.6. In the next section, we compute the maximum number of hops required to reach all stations in the network. As we shall see, it is necessary to distinguish between the cases k being even and k odd.

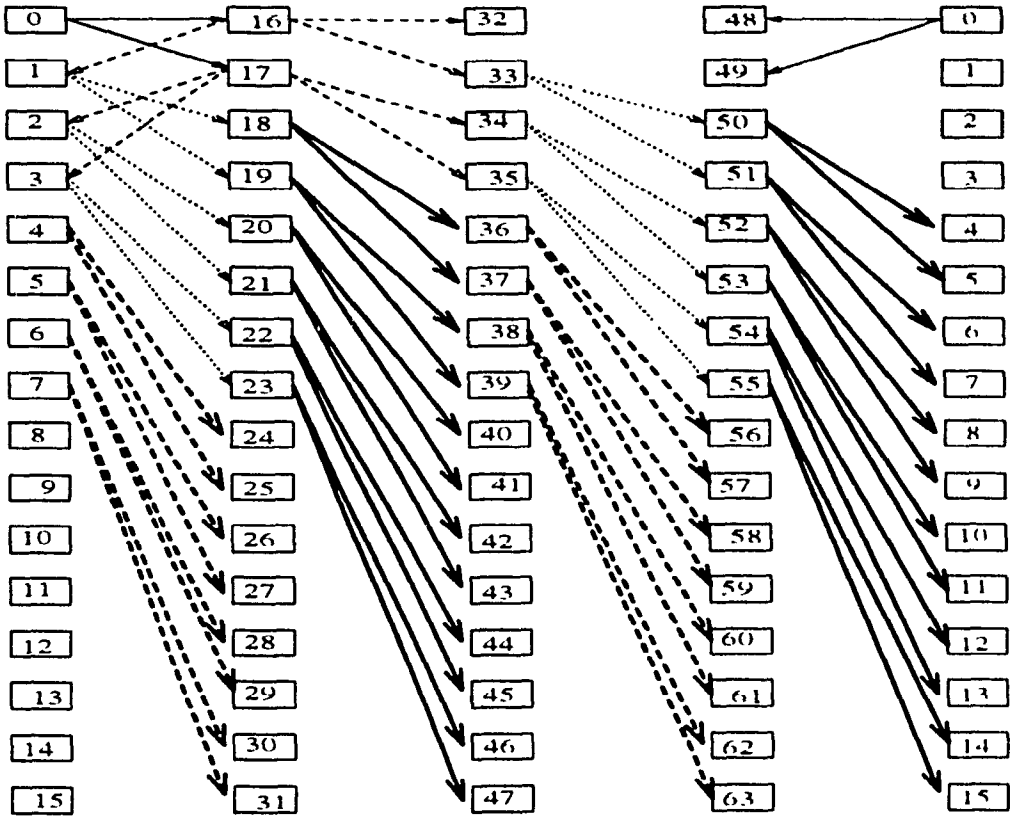

FIGURE 3.6 A tree growth of a (2, 4) bilayered ShuffleNet N=64.

3.2.1 Bilayered ShuffleNet: General Form

In this section, we evaluate the general form of the number of stations as a function of the number of hops, the expected number of hops, and the channel efficiency in the case of the bilayered ShuffleNet.

3.2.1.1 Number of Stations as a Function of the Number of Hops

The general form of the number of stations reached as a function of the number of hops for a given P and k is given by the following relations:

For k odd (k=3,5,7,....) we have $h_{max} = k$ and

$$n(h) = \begin{cases} (h+1)P^h - (h-1)P^{h-2} & ;h = 1, 2, \ldots, \frac{k-1}{2} \\ (h+1)P^h - (2h+1-k)P^{h-1} - (k-h)P^{h-2} & ;h = \frac{k+1}{2}, \ldots, k-1 \\ k[P^h - P^{h-1}] & ;h = k \end{cases} \quad (3.11)$$

For k even (k=2,4,6,.....) we have $h_{max} = k+1$ and

$$n(h) = \begin{cases} (h+1)P^h - (h-1)P^{h-2} & ;h = 1, 2, \ldots, \frac{k}{2} - 1 \\ hP^h - (h-1)P^{h-2} & ;h = \frac{k}{2} \\ \frac{k}{2}[P^h - P^{h-2}] & ;h = \frac{k}{2} + 1, \ldots, k \\ \frac{k}{2}[P^{h-1} - P^{h-2}] & ;h = k+1 \end{cases} \quad (3.12)$$

In the new configuration we decrease the maximum number of hops from ($2k$-1) to only (k) hop (k odd). In the case of k even, the maximum number of hops will be (k+1) instead of ($2k$-1). For the case of k=2 we have $2k$-1=k+1=3; hence, there is no decrease in the maximum number of hops.

3.2.1.2 Expected Number of Hops

After we have found the general form of the tree growth in the case of the bilayered ShuffleNet, we evaluate the expected value of the number of hops required for a message to reach its destination.

$$E[hops] = \sum_{h=1}^{h_{max}} \frac{hn(h)}{N-1} \quad (3.13)$$

for the case of k odd we have:

$$E[hops] = \frac{(1-P)^2 kN + (1-P)N - (1-P)P^k - (1-P)^2 P^{k-1} - 2\left(1 - P^{\frac{k-1}{2}}\right)}{(1-P)^2 (N-1)} \quad (3.14)$$

and for the case of k even we have

$$E[hops] = \frac{-\frac{2}{p} - 2 + P^{\frac{k}{2}-2}[k + (2-k)P + 2P^2] + N\left[k + \frac{3}{2} - 2kP - 2P + kP^2 + \frac{P^2}{2}\right]}{(1-P)^2(N-1)} \quad (3.15)$$

3.2.1.3 Channel Efficiency

For the symmetric case and uniformly distributed traffic, the channel efficiency, η, for the bilayered ShuffleNet is given by

$$\eta = \frac{1}{E[hops]} \quad (3.16)$$

In Figure 3.7, we plot the channel efficiency as a function of k, for large P, for the case of bilayered ShuffleNet and the case of the conventional ShuffleNet. From this figure, we observe how the bilayered ShuffleNet achieves a better channel efficiency than the conventional case due to the addition of a second set of connections, which decrease in the maximum number of hops required to reach a station in the network. From the same figure, we also observe that this improvement applies for both cases k odd and k even with a certain advantage to the case of k odd compared to the case ok k even (peaks in Figure 3.7 when k is odd) and this due to the decrease of the maximum number of hops in this case from $2k$ - 1 to only k compared to the other case where the maximum number of hops decrease is from $2k$ - 1 to k + 1. The efficiency in both cases decreases as a function of k, since increasing the number of columns, k, in the bilayered or conventional ShuffleNet connectivity graph increases the expected number of hops required for a message to reach its destination.

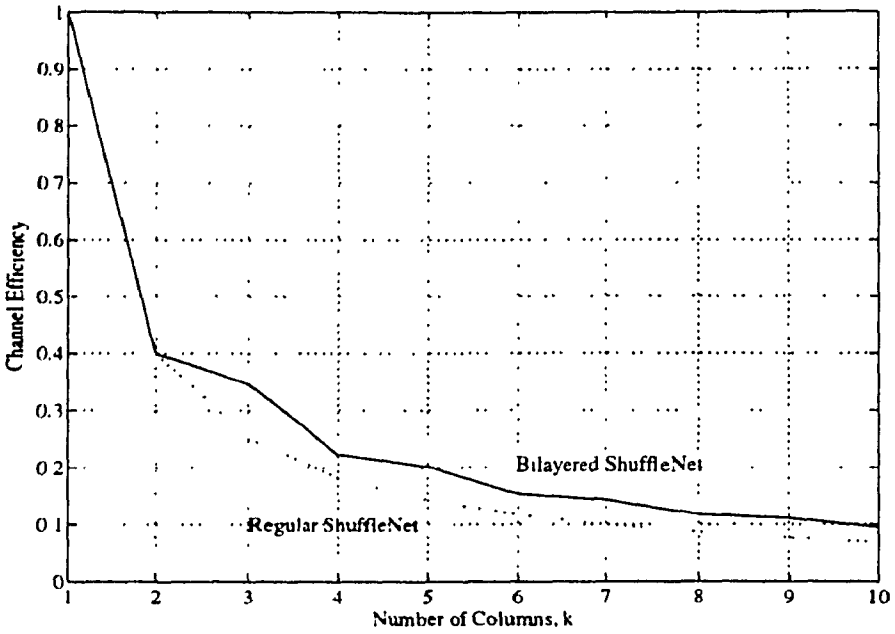

FIGURE 3.7 Bilayered ShuffleNet channel efficiency for a large P

Using the same method described in the previous section, this network will use only two wavelengths that can be reused in different links; this corresponds to the case of dedicated channel where each user is equipped with multiple transmitters and receivers. In this case, for a given N-user (P, k) bilayered ShuffleNet connectivity graph, the number of transmitters T and receivers R will be equal to $2P$ for each case, and the number of channels is given by

$$W = N \times T = 2kP^{k+1} \tag{3.17}$$

The total throughput and user throughput are given by $\eta.W$ and $\frac{\eta.W}{N}$ where η is the channel efficiency given by (3.16). Table 3.1 compares these two parameters in the case of bilayered ShuffleNet and the conventional ShuffleNet [3] for the case of (P=2, k=3) a 24-user ShuffleNet and a 1Gb/s user transmission rate.

TABLE 3.1 A 24-user ShuffleNet, 1Gb/s user transmission rate

	η	Total traffic rate	User traffic rate
Conventional ShuffleNet	0.3067	14.722 Gb/s	613 Mb/s
Bilayered Shuffle-Net	0.426	40.896 Gb/s	1.704 Mb/s

The results presented in this table confirm the improvement already predicted by passing from the conventional to the bilayered ShuffleNet because we not only double the connection between stations, but we also improve the total end user throughput by more than twice, which justifies the fact of doubling the connectivity for the case of the bilayered ShuffleNet.

3.3 Comparison

The expected number of hops from a source to a randomly selected destination is also defined to be the average distance, d_{avg}, between nodes [43]. The larger the average distance between the nodes in a network, the longer the packets will have to remain within the network on the average, thereby consuming network resources; this directly translates into a smaller throughput. Due to the importance of this parameter, we find it is important to compare our results to the existing ones.

First, we compare our results to the case of the conventional ShuffleNet since we are using the same N and same k. Then, we compare our results to other networks with the same connectivity P. In this case, due to the fact that for the ShuffleNet N is always equal to kP^k, it is difficult to pass from one ShuffleNet to another one while keeping the number of stations the same while doubling the connectivity ($P'=2P$). For example, for $P=4$, the minimum number of stations is 32 and there is inefficiency for smaller systems. To identify the better one of these two ways of comparison, the results are shown in Figure 3.8. As predicted, the bilayered ShuffleNet achieves a better performance in terms of average distance compared to the conventional ShuffleNet with the same N and same k, but this result is not as good as that of the conventional ShuffleNet with the same connectivity P as

the bilayered ShuffleNet. From the same figure, we see that the curve obtained for the bilayered ShuffleNet is closer to the conventional ShuffleNet with a connectivity equal to 4 paths than to the conventional ShuffleNet with connectivity equal to 2. In this case, we can confirm that the bilayered ShuffleNet has a performance comparable to a conventional ShuffleNet with a doubled connectivity. We argue that the slight loss in the performance is compensated for by the increased number of possible configurations (notice that in Table 3.2 and for a network size of up to 10,000, we have more N's than $N1$'s).

TABLE 3.2 Network size for the case of P=2 and P'=4 as a function of k.

(P,k)	N	(P',k)	$N1$
(2,2)	8		
(2,3)	24	(4,2)	32
(2,4)	64		
(2,5)	160	(4,3)	192
(2,6)	384		
(2,7)	896	(4,4)	1024
(2,8)	2048		
(2,9)	4608	(4,5)	5120
(2,10)	10240		

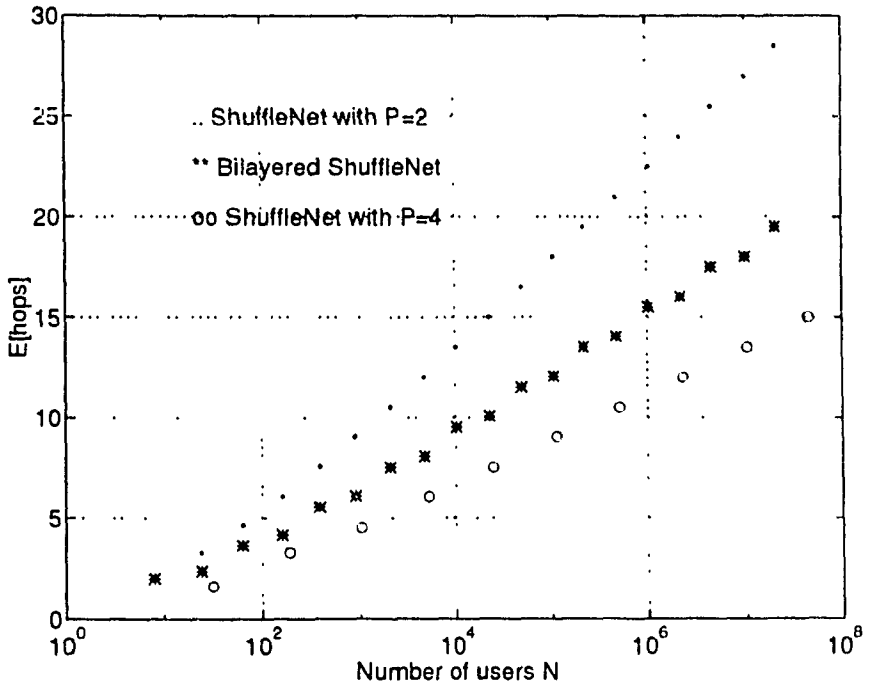

FIGURE 3.8 Comparison of the $E[hops]$ of the ShuffleNet with P=2, bilayered ShuffleNet and the ShuffleNet with P=4.

3.4 Performance Calculation

We turn now to consider the performance of the bilayered ShuffleNet as measured by delay as a function of throughput traffic. The delay of a message is defined as the time interval between its arrival at the system and its exit from the system. This delay encompasses queuing, transmission, propagation, and processing delay. We shall carry through an analysis of the delay under the assumption that circulating traffic has priority over newly generated traffic. We also assume that the traffic is time division multiplexed (TDM) and the message length is equal to the slot duration.

3.4.1 Presentation of the Node in the Bilayered ShuffleNet

The model of the node may be as shown in Figure 3.9, where the $2P$ input lines enter through a processor that distributes the traffic to the output lines. The processor is just a commutator since the traffic is TDM on the output lines. The output line queues are where congestion would occur. The model used for each output line is shown in Figure 3.10. A

discrete time statistical multiplexer is used for modeling our output line. Several assumptions are made:

1. Arrivals in the through traffic are governed by a binomial process.
2. Poisson arrival of the local traffic.
3. A priority discipline is used, where the local traffic has a lower priority than the through traffic coming from a distant station.

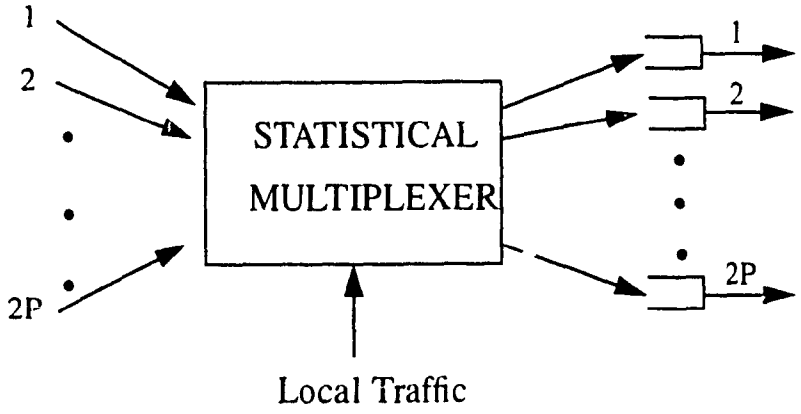

FIGURE 3.9 The node model.

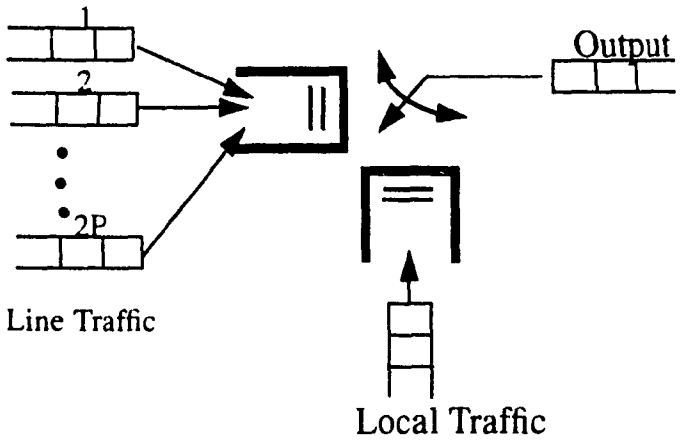

FIGURE 3.10 The output line.

3.4.2 Traffic Evaluation

In our evaluation of performance, we assume each station transmits the same level of traffic to every other station. If station i generates λ messages per second for station $j \neq i$ then the total level of traffic generated by station i can be represented as:

$$\Lambda' = \sum_{h=1}^{h_{max}} \lambda(h)\, n(h) \tag{3.18}$$

where $\lambda(h)$ is the amount of traffic that is destined for each station at distance h and $n(h)$ is the number of stations at distance h.

The more hops a message takes to reach its destination, the more network resources it uses. This is reflected in the amount of bandwidth required by a single source, which may be defined as

$$B = \lambda \sum_{h=1}^{h_{max}} hn(h) \tag{3.19}$$

From this equation, we notice that B is directly related to the expected value of h, in the sense that B is equal to

$$B = \lambda (N-1) \overline{H} \tag{3.20}$$

$\overline{H} = E[hops]$ in the above equation, h_{max} is equal to k if k is odd or $k+1$ if k is even. The total bandwidth used by all sources is equal to B multiplied by N the total number of users. Since there is a total of $2kP^{k+1}$ links in the network; accordingly, each link must carry

$$\Lambda = \frac{kP^k B}{2kP^{k+1}} = \frac{B}{2P} \qquad \text{messages / s} \tag{3.21}$$

This is the total amount of traffic on each link. Of this, $\Lambda'/2P$ is newly generated. If we follow the usual priority, the locally generated traffic $\lambda(N-1)$ is split $2P$ ways for each output trunk:

$$\lambda_{local} = \frac{\lambda(kP^k - 1)}{2P} = \frac{\lambda(N-1)}{2P} \tag{3.22}$$

and the through traffic on a line is equal to

$$\Lambda_T = \Lambda - \lambda_{local} \tag{3.23}$$

This amount of traffic has priority over the newly generated traffic (λ_{local}) as we mentioned before, and will be held in consideration for the remaining part of our performance evaluation.

3.4.3 Delay Components

The sources of delay are queuing, propagation, and processing delay at each node. Further, given that the transmission speed may be so much faster than the processing, there could be no traffic dependent delay within the nodes; consequently, one is required only to consider the processing delay as the main source for additional delay within a node.

Let $G_{(c)}(z)$ be the generating function of the distribution of the number of class c packets arriving in a slot, c=1,2. The generating function for the through packets has a binomial distribution

$$G_{(1)}(z) = (1 - q + qz)^{2P} \tag{3.24}$$

where $q = \frac{\Lambda_T T_F}{2P}$, and T_F is the frame duration, which is equal to slot duration since there is no channel multiplexing. For the locally generated traffic we assume that we have a Poisson distribution

$$G_{(2)}(z) = e^{\frac{\lambda(N-1)}{2P}T_F(1-z)} \tag{3.25}$$

For each message we have two kinds of queuing delay, the first queuing delay encountered by a message is when it enters the system [44] and is given by:

$$D_1 = T_F(E[L] - \rho_2) + \frac{\rho_2 T_F}{2} \tag{3.26}$$

where $E[L]$ is the expected queue length of the low priority packets [45], which is equal to

$$\begin{aligned} E[L] &= G_{(2)}'(1)\,[1 - G_{(1)}'(1)] \\ &\quad + \frac{G_{(2)}''(1) + 4G_{(1)}'(1)\,[G_{(1)}'(1)]^2}{2\,[1 - G_{(1)}'(1) - G_{(2)}'(1)]} \\ &\quad + \frac{G_{(1)}''(1)\,G_{(2)}'(1)}{2\,[1 - G_{(1)}'(1)]\,[1 - G_{(1)}'(1) - G_{(2)}'(1)]} \end{aligned} \tag{3.27}$$

and ρ_2 is equal to $\dfrac{\lambda(N-1)T_F}{2P}$.

At each of the subsequent hops an additional delay component is encountered. This delay [46] is equal to

$$D_2 = \frac{\Lambda_T T_F}{2} + \frac{(\Lambda_T T_F)^2 (1 - \frac{1}{P})}{2(1 - \Lambda_T T_F)} \tag{3.28}$$

If we add the processing and propagation delay (D_P), and transmission delay T, which is equal to the slot duration at each hop, the total delay is given by

$$D_T = D_2 + D_1 \times (\bar{H} - 1) + (D_P + T) \times \bar{H} \tag{3.29}$$

Concerning the processing delay, we assume that it is proportional to the connectivity P because the more connectivity is used, the more the processing delay becomes.

3.4.4 Numerical Results

The numerical results involve a comparison of the performance, in terms of the message delay, for two cases. First, we try to compare between the conventional ShuffleNet and the bidirectional ShuffleNet for the same configuration (same P and k). Second, we compare between the bilayered ShuffleNet and the SR_Net with the same configuration (N=64) when optimum routing is used and when deflection routing is used. The result shown in Figure 3.11 gives the total delay as a function of the traffic generated by each station. The bit rate per user is equal to 1 Gbit/s. It is observed that the traffic load increases as we pass from the conventional ShuffleNet to the bilayered ShuffleNet. At the same time, we have a decrease in the total delay due to a decrease in the expected number of hops compared to the conventional case.

In order to make a fair comparison between the two different networks with the same connectivity, we compare the bilayered ShuffleNet with the SR_Net for N=64 and the results are shown in Figure 3.12 and Figure 3.13. In the first case, the results are obtained under the optimal routing case where a message reaches its destination in the minimum number of hops. In this case, the SR_Net performs better than the bilayered ShuffleNet due to the fact that the average number of hops in the case of the SR_Net is lower than the bilayered ShuffleNet (3.24 compared to 3.65). In the second case, the results are obtained under the non-optimum case where a message is supposed to be deflected with a certain probability p. This case will be discussed in more detail in Chapter 4. A particular case of this is to assume that a message will be deflected with a probability 1/2. This will increase the expected number of hops for the case of the bilayered ShuffleNet and the SR_Net with one hop and two hops, respectively. In this case, the bilayered ShuffleNet will perform better than the SR_Net because the alternative paths when deflection routing is used are shorter in the case of the bilayered ShuffleNet than for the SR_Net.

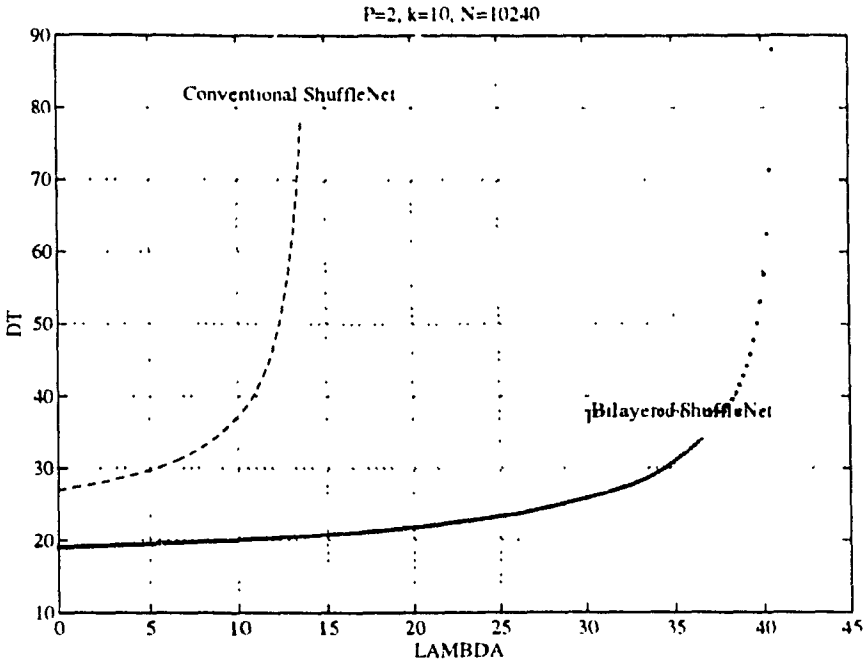

FIGURE 3.11 Performance results for the case of P=2, k=10.

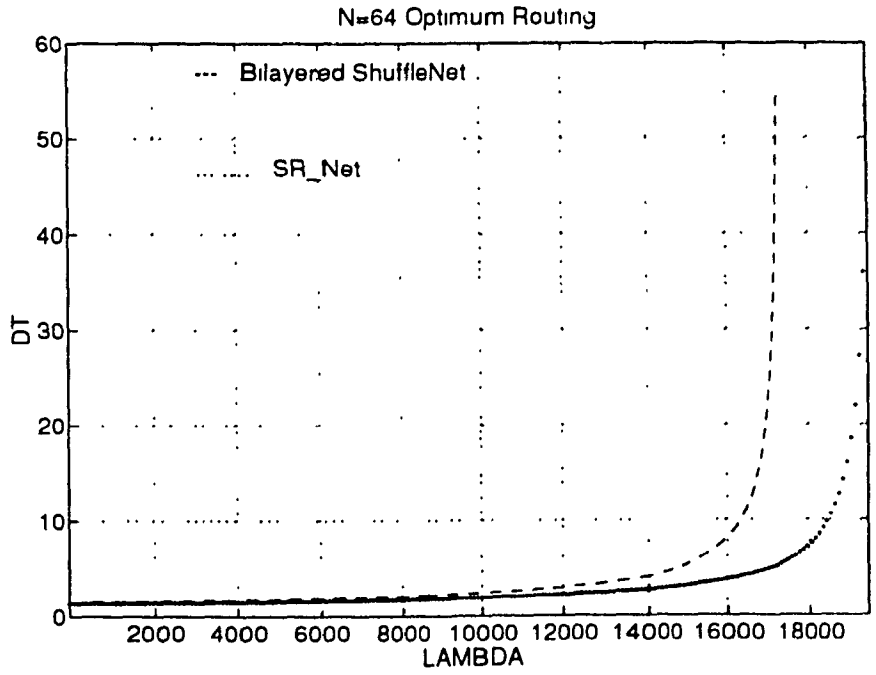

FIGURE 3.12 Performance results for the case of the bilayered ShuffleNet and the SR_Net with optimum routing

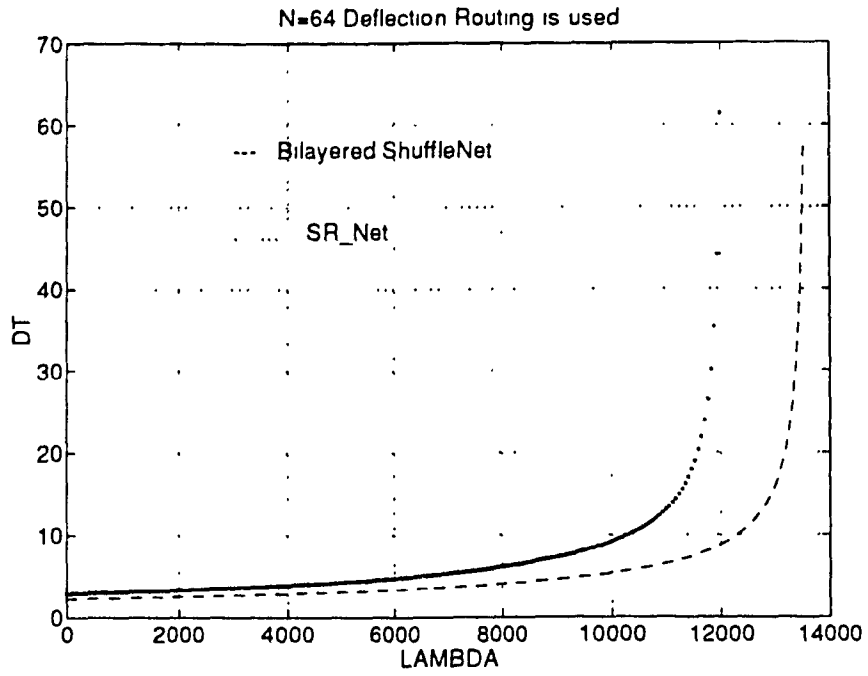

FIGURE 3.13 Performance results for the case of the bilayered ShuffleNet and the SR_Net with deflection routing

3.5 Performance of the Bilayered ShuffleNet Under Nonuniform Traffic

The bilayered ShuffleNet has been studied under the uniform traffic case. In the following, we consider the case of a nonuniform traffic distribution. Because unbalanced loads can occur in a multitude of ways, our study is limited to the case of "extreme-value analysis". This case is an approximate analytical technique that assumes the distribution of the loads is unique, but the intensity of traffic from individual users has a normal distribution [50]. The probability that a given channel is overloaded can be evaluated given the overall average and variance of the load intensity. Our results will also include a comparison of our new results to the results already found in [50] for the case of the conventional ShuffleNet under the same conditions.

3.5.1 Network Parameters

In the bilayered ShuffleNet network, the number of users grows according to the same formula, $N = kP^k, k = 2, 3, 4, \ldots, P = 2, 3, 4, \ldots$ as in the case of the conventional ShuffleNet, but the number of channels needed grows as $W = 2kP^{k+1}$ where each user has $2P$ transmitters and $2P$ receivers, and k is the number of stages in the bilayered ShuffleNet interconnection pattern. Notice that, the number of channels is equal to 2 times the number of channels used in the case of the perfect ShuffleNet (kP^{k+1}).

Different parameters are used to measure the performance of the network. These parameters are based on the fact that each channel is operating at a 1Gbit/s. We start with the total bandwidth offered by the entire network, which is equal to $W \times \eta \times 1\text{Gbit/s}$. η is the "channel utilization efficiency" under the assumption of a load-balancing routing algorithm, and it is given by

$$\eta = \frac{1}{E[hops]} \tag{3.30}$$

This parameter uses a capacity measure associated with an individual user, rather than one for the network as a whole. The "achievable capacity" is equal to the total bandwidth offered by the entire network normalized to the bandwidth of a single fiber channel which is equal to 1Gbit/s.

$$C = \frac{W}{E[hops]} \tag{3.31}$$

This quantity is also equal to the total number of channels divided by the expected number of hops due to the fact that there are a total of W channels where each one has a channel efficiency of $\frac{1}{E[hops]}$.

Finally, we define the normalized quantity "throughput per user", T, which is equal to the number of channels each user has access to, multiplied by the channel utilization efficiency

$$T = \frac{2P}{E[hops]} \tag{3.32}$$

These network parameters for the case of the bilayered ShuffleNet can be compared to the same parameters for the case of the SR_Net. From the above equations and for the same network size, the only difference between the bilayered ShuffleNet and the SR_Net is the average number of hops $E[hops]$, which is lower for the case of the SR_Net. Then, the "channel utilization efficiency", the "achievable capacity" and the "throughput per user" will be higher for the case of the SR_Net than for the bilayered ShuffleNet. This gives an advantage to the SR_net compared to the bilayered ShuffleNet.

3.5.2 Fixed load patterns with random load intensity variation: an extreme-value-type analysis

In this section, we evaluate the effects of the statistical variations of the users' mean traffic intensity on the worst channel for the case of the bilayered ShuffleNet [24] in a way similar to the case of conventional ShuffleNet as described in [50].

Assume that every user's traffic intensity is a normally distributed random variable with a mean μ and a standard deviation σ. This probability distribution is denoted by $N(\mu, \sigma)$. Assume a uniform traffic pattern (i.e., each user's traffic is uniformly destined to all other users) and a uniform routing pattern (i.e., the routing is such that each channel is used equally to carry the total traffic).

Let $\lambda_{i,j} (1 \le i \le N, \ 1 \le j \le N)$ and $\gamma_m (1 \le m \le W)$ be the intensity from user i to user j and the traffic intensity on channel m, respectively. Under the same assumptions as in the case of conventional ShuffleNet [50], we assume independence between $\lambda_{i,j}$'s and independence between γ_m's. These two assumptions lead to the following approximate analysis of the traffic intensity on the worst channel.

Since each user's traffic is uniformly destined to all other users, $\lambda_{i,j}$ is distributed according to $N(\mu/N, \sigma/\sqrt{N})$. Due to multi-hopping, the total traffic on each channel is the

sum of a number of traffic streams generated by different users. Let M be the average number of i-to-j traffic pairs that use a particular channel. Under the uniform traffic patterns, M is given by

$$M = \frac{N^2 E[hops]}{W} = \frac{NE[hops]}{2P} \tag{3.33}$$

Therefore, γ_m is distributed according to $N(M\mu/N, \sqrt{M}\,\sigma/\sqrt{N})$. Notice that for the same network size M is larger for the case of the bilayered ShuffleNet than the SR_Net due to the expected number of hops which is larger for the case of the bilayered ShuffleNet.

We are interested in looking at the performance of the worst of these W channels. Let Y_W be the Wth-order statistic of the sequence of random variables γ_m; that is, Y_W is the maximum of W normally distributed random variables with mean $M\mu/N$ and standard deviation $\sqrt{M}\,\sigma/\sqrt{N}$. This probability distribution is denoted by $N(M\mu/N, \sqrt{M}\,\sigma/\sqrt{N})$. The distribution of Y_W is the Wth power of the probability distribution $N(M\mu/N, \sqrt{M}\,\sigma/\sqrt{N})$.

Different parameters can be determined in order to characterize the traffic on the worst link. Among these, we can evaluate 1) the mean traffic intensity on the worst link, 2) the probability that the traffic intensity on the worst link exceeds the link capacity, 3) the value of μ for which such probabilities are small, and how these parameters can change as the number of users in the network increases.

3.5.2.1 Order Statistics

The order statistics of the random variables x_i are n random variables Y_k defined as follows [51]: For a specific outcome ζ, the random variables x_i take the values $x_i(\zeta)$. Ordering these numbers, we obtain the sequence

$$x_{r_1}(\zeta) \le \ldots \le x_{r_k}(\zeta) \le \ldots \le x_{r_n}(\zeta)$$

and we define the random variable Y_k such that

$$Y_1 = x_{r_1}(\zeta) \leq \ldots \leq Y_k = x_{r_k}(\zeta) \leq \ldots \leq Y_n = x_{r_n}(\zeta) \tag{3.34}$$

We note that for a specific i, the value $x_i(\zeta)$ of x_i occupies different locations in the above ordering as ζ changes. We maintain that the density $f_k(Y)$ of the kth statistic Y_k is given by

$$f_k(Y) = \frac{n!}{(k-1)!\,(n-k)!} F^{k-1}(Y)\,[1 - F(Y)]^{n-k} f(Y) \tag{3.35}$$

where $F(x)$ is the distribution of the independent, identically distributed random variables x_i, and $f(x)$ is the associated probability density function.

In our study, we are interested in the maximum order statistic which corresponds to Y_n. To derive the distribution function of Y_n, we note that the probability that exactly j of the x_i's lie in $(-\infty, y)$ and $(n\text{-}j)$ lie in (y, ∞) is:

$$\binom{n}{j} F^j(y)\,[1 - F(y)]^{n-j},$$

since the binomial distribution with parameters n and $p = F(y)$ is applicable. Then:

$$\begin{aligned} F_{Y_n}(y) &= P(Y_k \leq y) \qquad \text{for } k = n \\ &= \sum_{j=n}^{n} \binom{n}{j} F^j(y)\,[1 - F(y)]^{n-j}, \qquad -\infty < y < \infty \\ &= [F(y)]^n, \qquad -\infty < y < \infty \end{aligned} \tag{3.36}$$

3.5.2.2 Expected value and variances of order statistics from a standard normal population

If a sample of n observations $x_1, x_2, \ldots\ldots, x_n$ is drawn from a standard normal distribution, and the observations are arranged in an ascending order of magnitude $x_{(1)}, x_{(2)}, \ldots\ldots, x_{(n)}$, the ith value of the set $\{x_{(i)}\}$ is called the ith normal order. For the case of $i = n$, the expectation and the variance of the maximum order statistic are given by

$$E[x_{(n)}] = n \int_{-\infty}^{\infty} x f(x)\, F^{n-1}(x)\, dx \tag{3.37}$$

$$E[x^2_{(n)}] = n \int_{-\infty}^{\infty} x^2 f(x) F^{n-1}(x)\, dx \tag{3.38}$$

where $f(x) = \frac{1}{\sqrt{2\pi}} e^{-\frac{1}{2}x^2}$,

and $F(x) = \int_{-\infty}^{x} \frac{1}{\sqrt{2\pi}} e^{-\frac{t^2}{2}} dt$

If all the $Y_{(i)}$ are drawn from a normal distribution with mean μ and a variance σ, then every $x_{(i)} = \frac{Y_{(i)} - \mu}{\sigma}$ will have a normal distribution with mean equal to zero and a variance equal to one ($N(0, 1)$). In this case, the expected value of $Y(n)$ will be given by

$$E[Y_{(n)}] = \sigma E[x_{(n)}] + \mu \tag{3.39}$$

$$Var[Y_{(n)}] = \sigma^2 Var(x_{(n)}) \tag{3.40}$$

Certain values of $E[x_{(n)}]$ and $E[x^2_{(n)}]$ can be evaluated using some numerical integration methods. In this case the result can be found for any value of n with any desired accuracy we want.

3.5.3 Numerical results

In the following, we present the numerical values of different performance measures related to the random variable Y_W, the traffic intensity on the worst channel. The distribution of Y_W is the Wth power of $N(M\mu/N, \sqrt{M}\sigma/\sqrt{N})$. The expected value of Y_W is given by:

$$\begin{aligned} E[Y_W] &= E\left[\sqrt{\frac{M}{N}}\sigma x_{(W)} + \frac{M}{N}\mu\right] \\ &= \sqrt{\frac{M}{N}}\sigma E[x_{(W)}] + \frac{M}{N}\mu \end{aligned} \tag{3.41}$$

where $E[x_{(W)}]$ corresponds to $E[x_{(n)}]$ when $W = n$.

In order to show the sensitivity of different performance measures to the variation of μ and σ for fixed network sizes, in Figure 3.14 a)-c) we show the mean traffic on the worst channel as a function of μ and σ for networks of size 8, 18, and 24, respectively. As shown in (3.41), the mean traffic intensity on the worst channel increases with μ and σ. The same results can be obtained for the case of the SR_Net, the only difference is that the mean traffic intensity on the worst channel for the SR_Net is less than the case of the bilayered ShuffleNet because of the direct relation with the value of M in the equation (3.41).

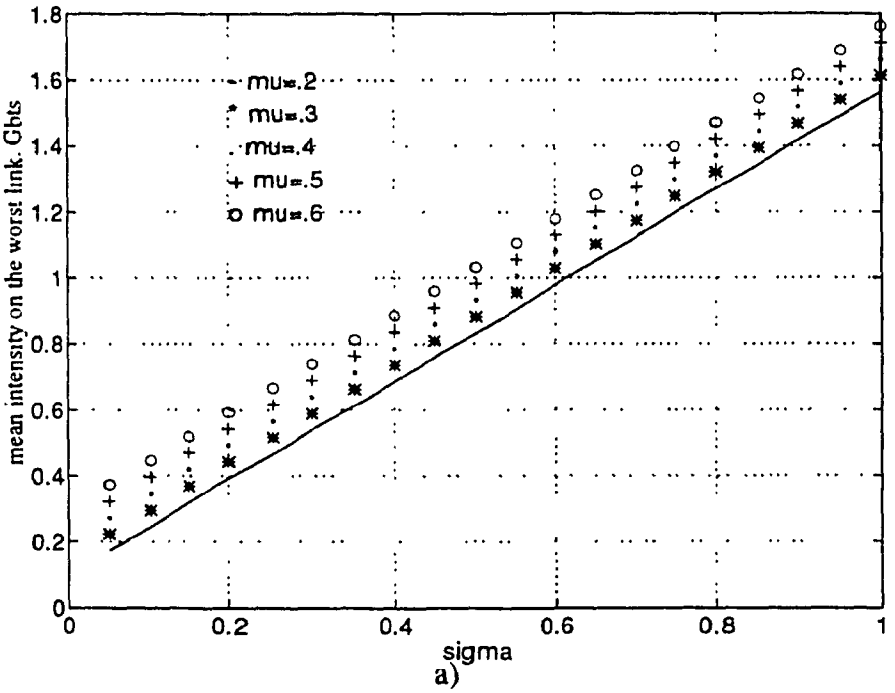

a)

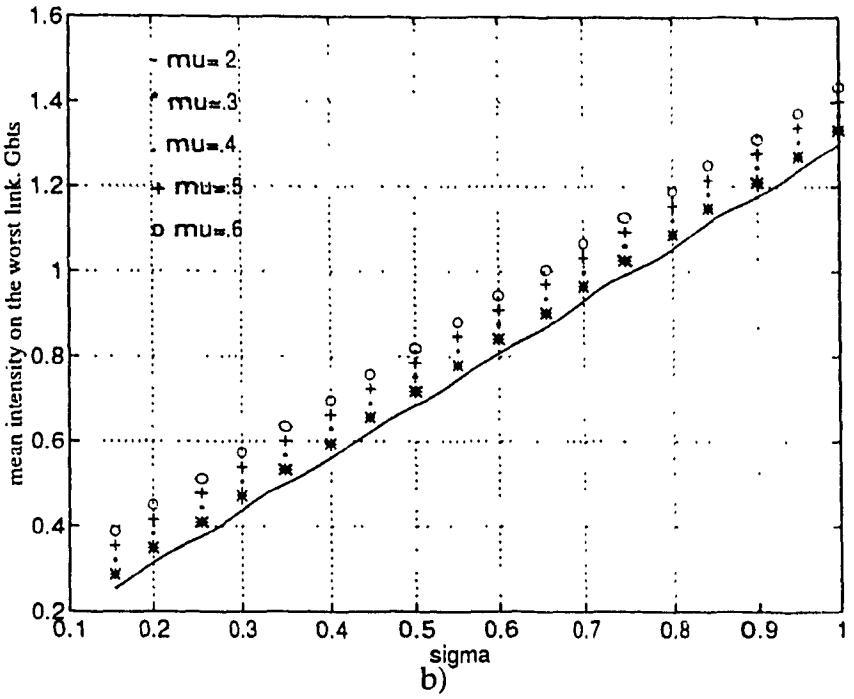

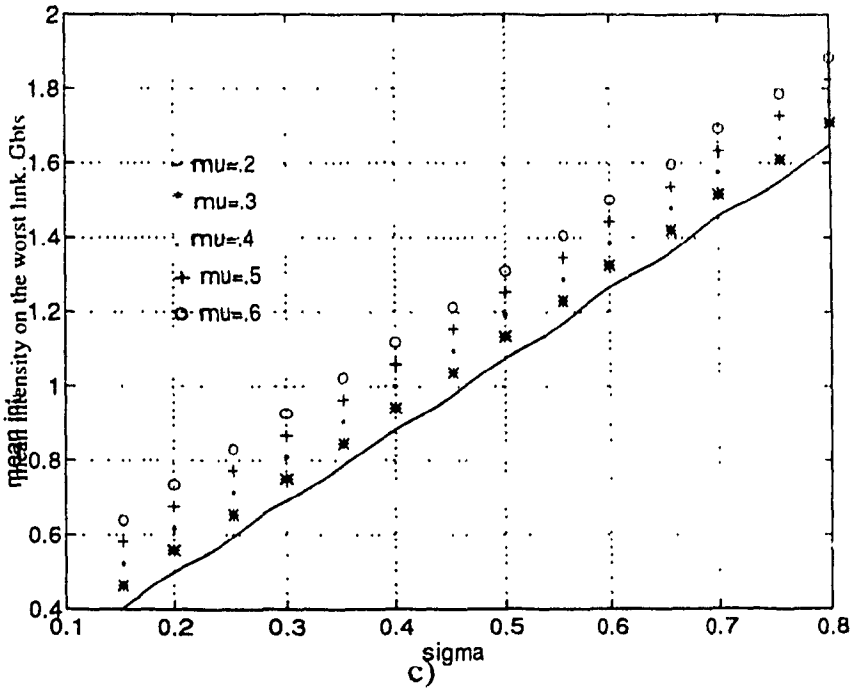

FIGURE 3.14 Mean traffic intensity on the worst channel for a)N=8 b)N=18 and c)N=24.

In the next step, we define P_{Ext} as the probability that the traffic intensity on the worst channel is greater than the capacity of the channel, which is assumed to be 1 Gbits/s. The result obtained is based on the following steps:

$$\begin{aligned} Prob(Y_W > \alpha) &= 1 - Prob(Y_W \leq \alpha) \\ &= 1 - Prob\left(\frac{Y_W - a\mu}{b\sigma} \leq \frac{\alpha - a\mu}{b\sigma}\right) \\ &= 1 - Prob\left(Z_{(W)} \leq \frac{\alpha - a\mu}{b\sigma}\right) \\ &= 1 - \left[Prob\left(Z \leq \frac{\alpha - a\mu}{b\sigma}\right)\right]^W \end{aligned} \tag{3.42}$$

where $Z = N(0, 1)$, and by using the above equation P_{Ext} can be evaluated. Figure 3.15 a)-c) shows the results for different network size as a function of μ and σ. We can see that the probability that the traffic intensity on the worst channel is greater than the channel capacity will increase as a function of μ for all values of N. This result can be evaluated for any other channel capacity by using the same principle compared with the results obtained in [50]. For the same network size and for the same value of μ and σ, we see the probability that the traffic intensity on the worst channel is greater than the capacity of the channel is much lower for the case of the bilayered ShuffleNet than the case of conventional ShuffleNet due to the fact that the channel efficiency in the case of bilayered ShuffleNet is larger than the conventional case. This implies that a much higher traffic level is required before the traffic on the worst channel exceeds the channel capacity. By comparing the same results for the case of the SR_Net and the bilayered ShuffleNet under the same conditions, we can show an advantage for the case of the SR_Net because of the channel efficiency which is larger for the case of the SR_Net.

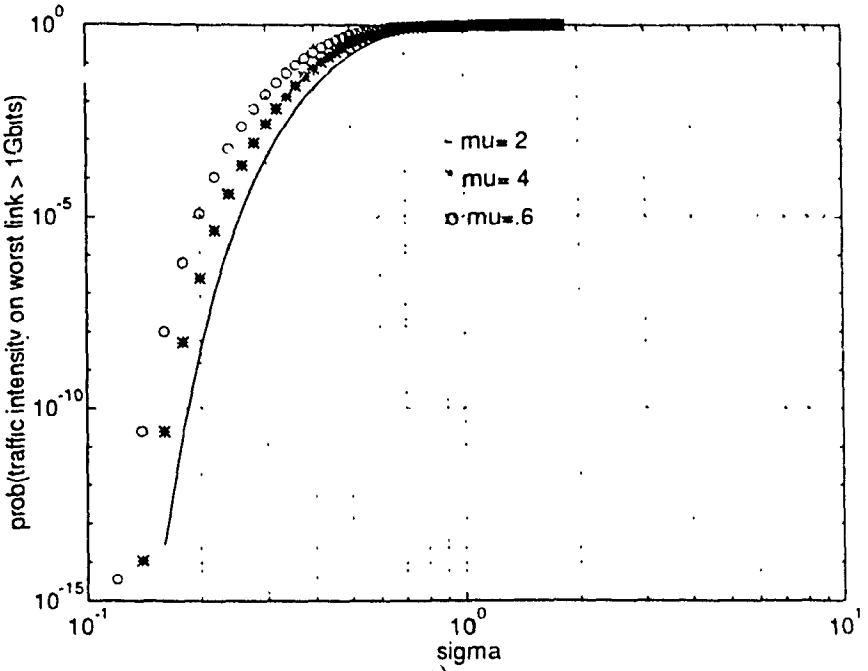
prob(traffic intensity on worst link > 1Gbits)
sigma
- mu= 2
* mu= 4
o mu=.6

a)

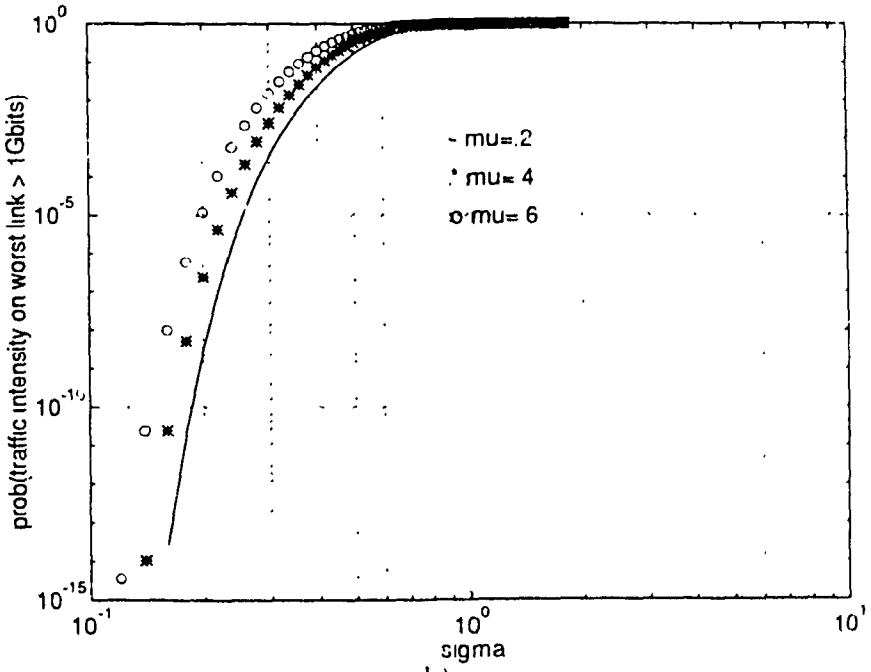
prob(traffic intensity on worst link > 1Gbits)
sigma
- mu=.2
* mu= 4
o mu= 6

b)

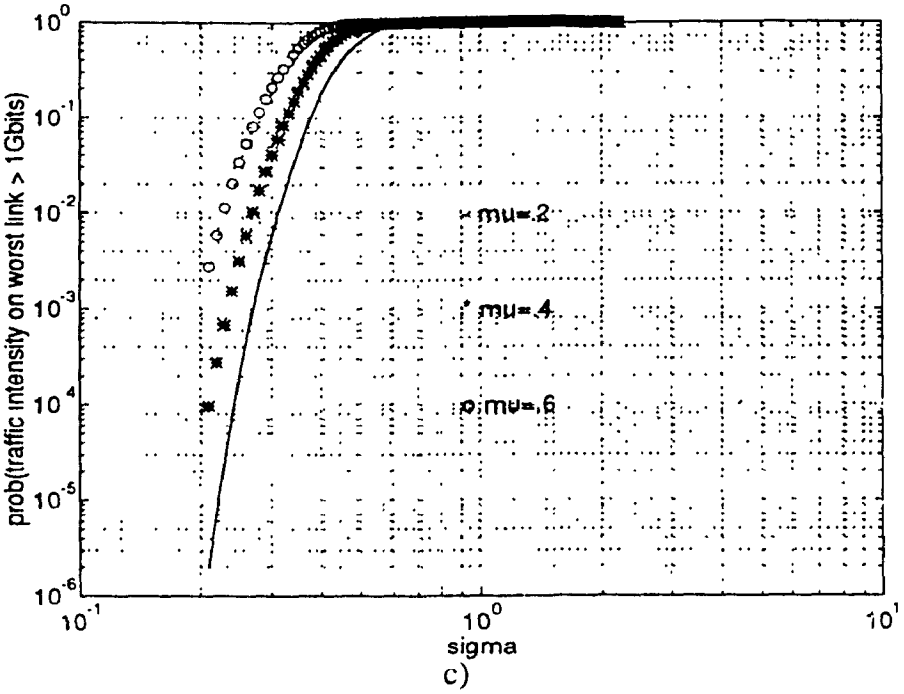

FIGURE 3.15 Probability that the traffic intensity on the worst channel is greater than the channel capacity a) N=8 b) N=18 and c) N=24

The same results obtained in Figure 3.15 can be redrawn in a way to show the maximum individual user traffic intensity μ, for which P_{Ext} is no greater than 10^{-L} as a function of L and σ for networks of size 8, 18, and 24, respectively. The results shown in Figure 3.16 a)-c) are based on the following:

$$10^{-L} = P_{Ext} = 1 - \left[Prob\left(Z \leq \frac{\alpha - a\mu}{b\sigma}\right) \right]^{W} \tag{3.43}$$

$$Prob\left(Z \leq \frac{\alpha - a\mu}{b\sigma}\right) = \left[1 - 10^{-L}\right]^{\frac{1}{W}} \tag{3.44}$$

Given that $Z = N(0, 1)$, the value of μ can be found using the ErfInv (inverse function of Erf).

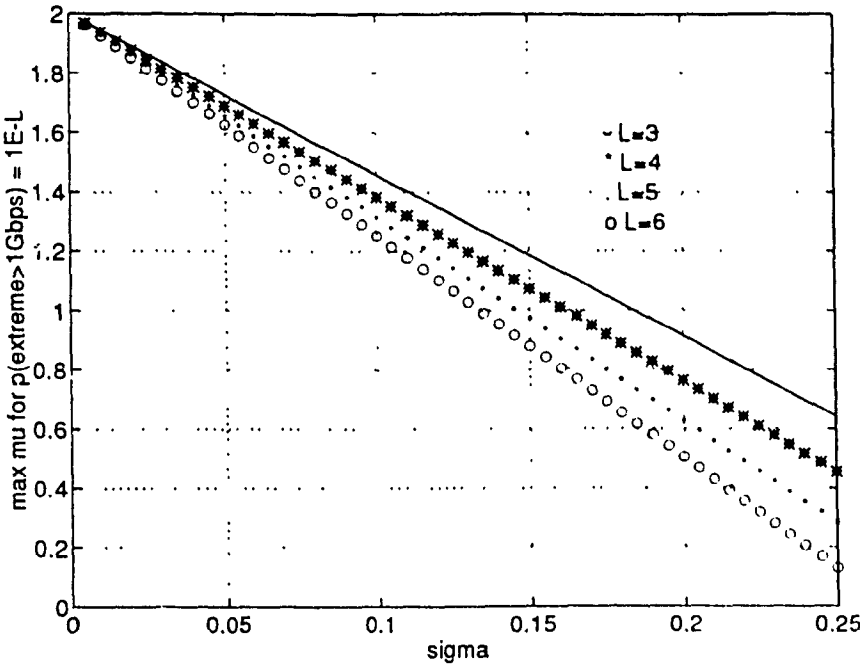
max mu for p(extreme>1Gbps) = 1E-L
sigma
L=3
L=4
L=5
L=6
0
0.2
0.4
0.6
0.8
1
1.2
1.4
1.6
1.8
2
0.05
0.1
0.15
0.2
0.25

a)

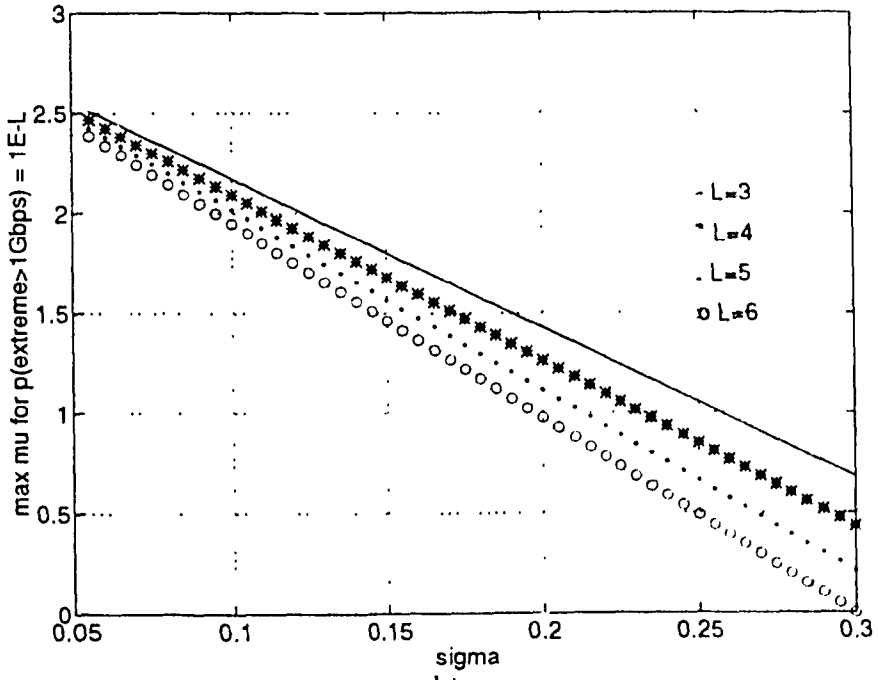
max mu for p(extreme>1Gbps) = 1E-L
sigma
L=3
L=4
L=5
L=6
0
0.5
1
1.5
2
2.5
3
0.05
0.1
0.15
0.2
0.25
0.3

b)

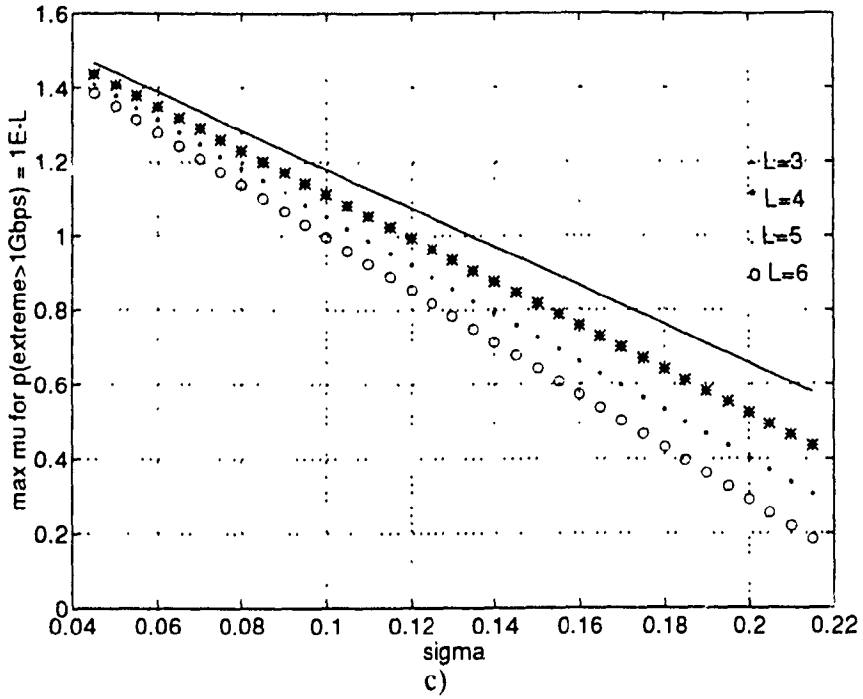

c)

FIGURE 3.16 Largest μ for which P_{Ext} is no greater than 10^{-L} a) N=8 b) N=18 and c) N=24.

In the following, we try to make a fair comparison that takes into consideration the fact that the maximum throughput per user decreases as the size of the network increases for the same value of P (for N=8, N=24 and N=64). However, this is not true for the case when the size of the network increases by increasing P and keeping k the same as for the case of N=8, N=18 and N=32. In this case, the maximum throughput per user increases as the network size increases. For example, in the case of N=18 we achieve a higher user throughput than in the case of N=8 due to the fact that P in this case is equal to 3 compared to P=2 for the case of N=8. This leads to larger user throughput (see Table 3.3) due to the fact that the increase in P compensates for the decrease in the channel efficiency in order to have a larger user throughput which is equal to $2P \times \eta$. The results of this comparison are shown in Figure 3.17 (for the case when P=2 and different values of N: N=8, N=24 and N=64), in Figure 3.18 (for the case when k=2 and for different values of N: N=8, N=18 and N=32), and in Figure 3.19 (for the case when k=3 and for different values of N: N=24,

N=81 and N=192). The values of different performance measures are shown for μ set to a fixed percentage of the maximum throughput of an individual user. Figure 3.17 shows the mean traffic intensity on the worst link as a function of σ and N for μ equal to 30, 50, and 70 percent of the maximum throughput of an individual user, respectively. We can observe from this figure that for a fixed value of σ, the mean traffic intensity on the worst channel increases with N if the same connectivity degree is used (same P and different k), but if the connectivity degree increases (same k but different P Figure 3.18 and Figure 3.19), the mean traffic intensity on the worst channel is kept the same for different N given that we keep k the same. The first case gives a more interesting result, and from these results we can find the corresponding performance for any other N by only checking the value of k. For example, the performance for the case of N=192 is the same as the case of N=24.

TABLE 3.3 Numerical parameters for the bilayered ShuffleNet

k	P	N	W	E[hops]	η	T	CE	E[XW]
2	2	8	32	2	.5	2	16	2.0697
3	2	24	96	2.3478	.4259	1.7037	40.8864	2.4930
4	2	64	256	3.3810	.2958	1.1831	75.7183	2.8269
2	3	18	108	2.1765	.4595	2.757	49.626	2.5350
3	3	81	486	2.6000	.3846	2.3076	186.9156	3.0281
2	4	32	256	2.2581	.4429	3.5432	113.3824	2.8269
3	4	192	1536	2.7120	.3687	2.9496	566.3232	3.3627

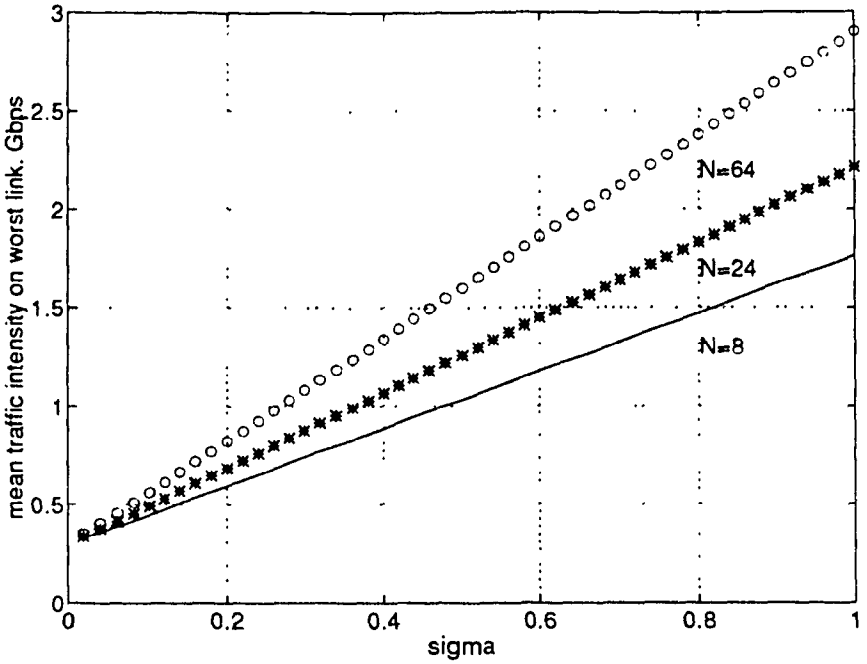
mean traffic intensity on worst link. Gbps
sigma
N=64
N=24
N=8
0
0.5
1
1.5
2
2.5
3
0.2
0.4
0.6
0.8

a)

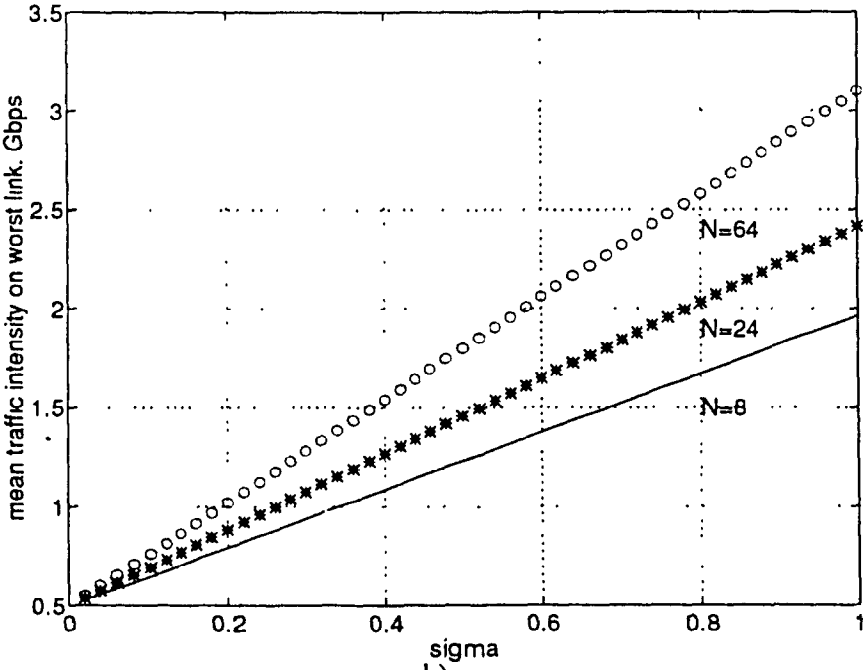
mean traffic intensity on worst link. Gbps
sigma
N=64
N=24
N=8
0.5
1
1.5
2
2.5
3
3.5
0.2
0.4
0.6
0.8

b)

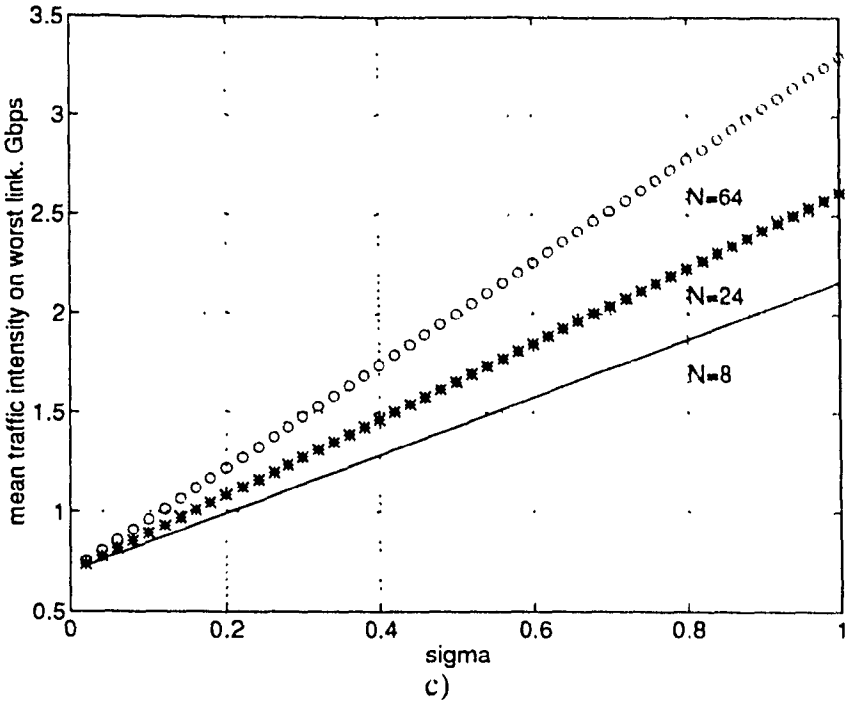

FIGURE 3.17 Mean traffic intensity on the worst link for μ equal to a)30% b)50% and c)70% of the maximum throughput of an individual user for different N but with equal P=2.

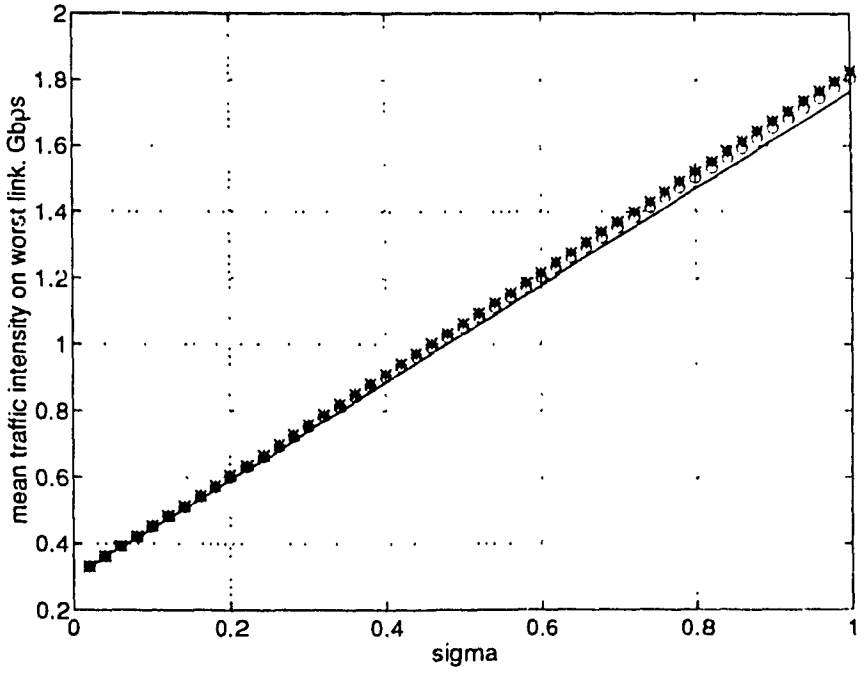

FIGURE 3.18 Mean traffic intensity on the worst link for μ equal to 30% for different N (N=8, N=18 and N=32) and same k equal to 2.

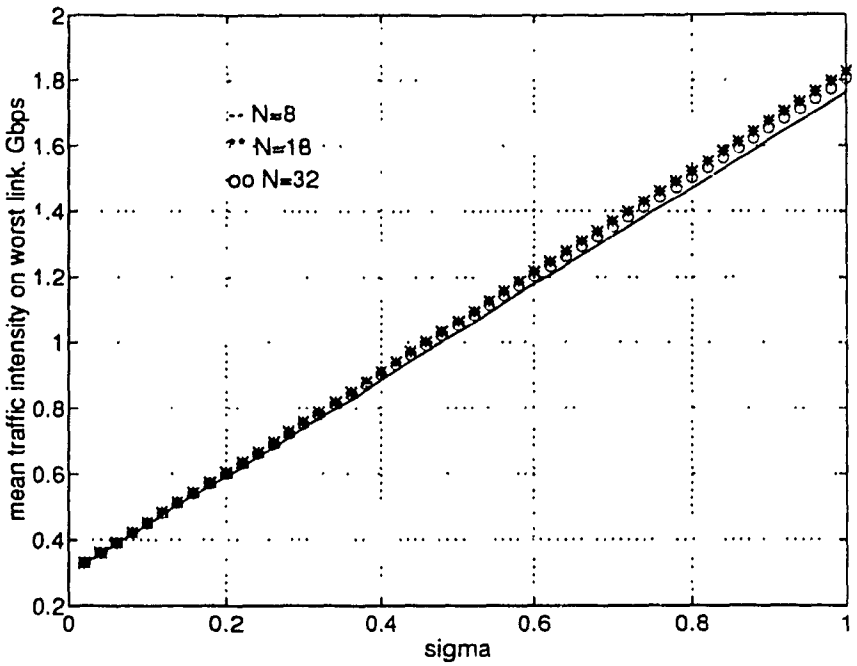

FIGURE 3.19 Mean traffic intensity on the worst link for μ equal to 30% for different *N* (*N*=24, *N*=81 and *N*=192) and same *k* equal to 3.

Based on the results obtained in Figure 3.17 and in order to counteract this degradation, the maximum offered load by each user must be reduced. It remains to characterize the amount by which the load must be reduced. Such characterization is shown in Figure 3.20 a)-c).

Let $\mu_{extreme}$ be defined as the maximum individual user traffic intensity μ for which $P_{extreme}$ is no greater than 10^{-L}. The results in Figure 3.20 a)-c) show $\mu_{extreme}$ as a function of the coefficient of variation, $\eta 1 = \sigma/\mu$, and *N* for L=3, 4, and 5, respectively. Parameter, $\mu_{extreme}$ corresponds to the value of μ when $\eta 1=0$ and is the maximum individual user throughput.

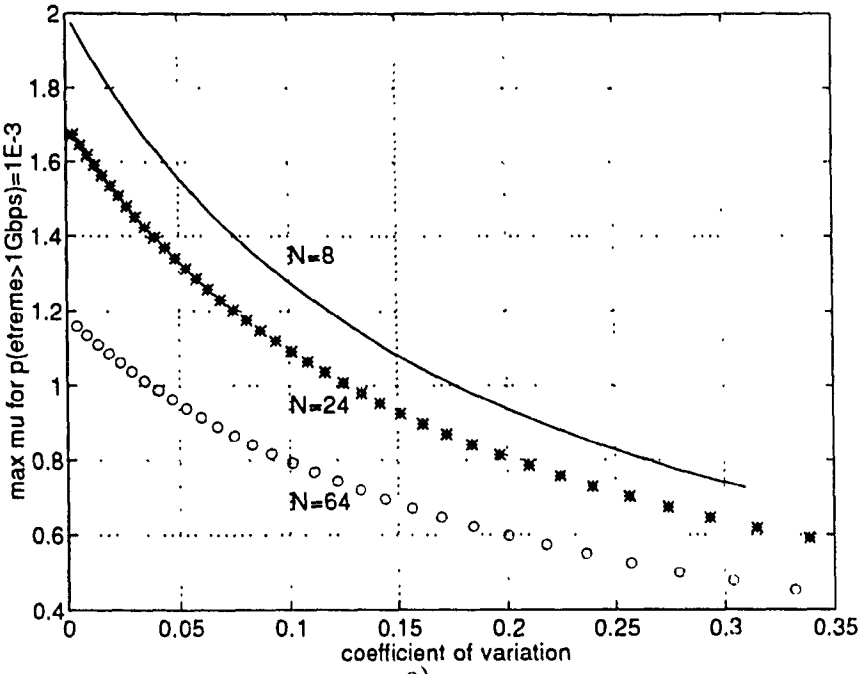
max mu for p(etreme>1Gbps)=1E-3
coefficient of variation
N=8
N=24
N=64
2
1.8
1.6
1.4
1.2
1
0.8
0.6
0.4
0
0.05
0.1
0.15
0.2
0.25
0.3
0.35

a)

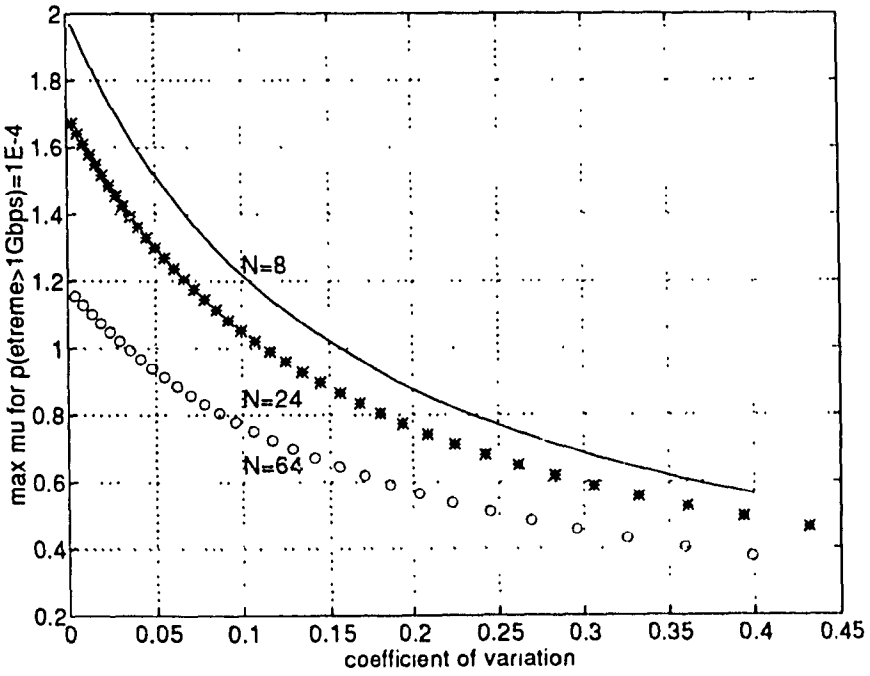
max mu for p(etreme>1Gbps)=1E-4
coefficient of variation
N=8
N=24
N=64
2
1.8
1.6
1.4
1.2
1
0.8
0.6
0.4
0.2
0
0.05
0.1
0.15
0.2
0.25
0.3
0.35
0.4
0.45

b)

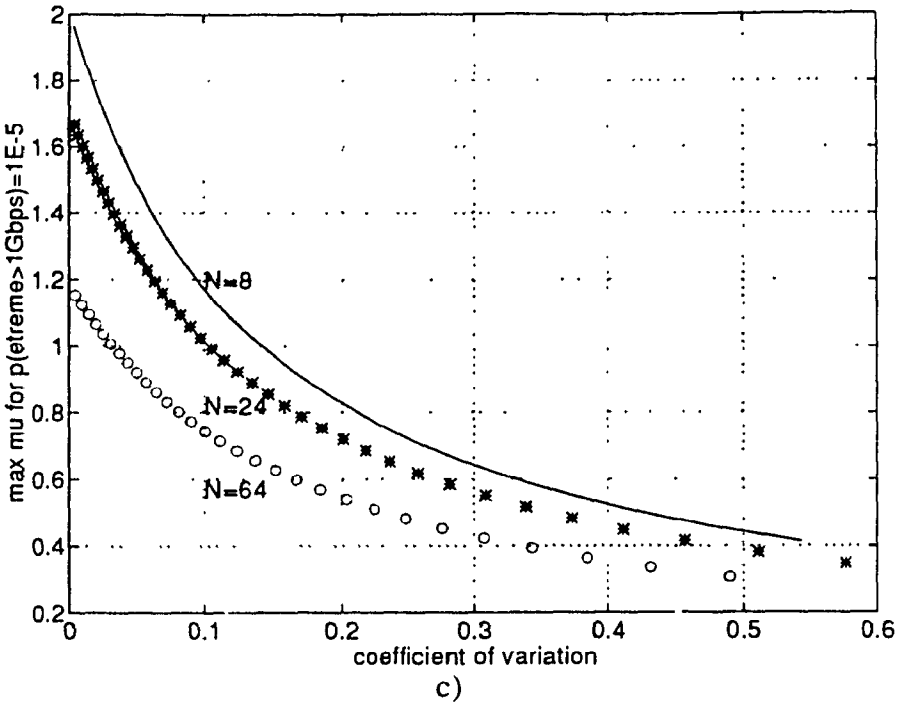

c)

FIGURE 3.20 Largest μ for which $P_{extreme}$ is no greater than 10^{-L} a) L=3 b) L=4 and c) L=5

In order to better illustrate the information in Figure 7a), we compare the ratio of the $\mu_{extreme}$ and the maximum user throughput for a fixed value of the coefficient of variation, $\eta 1 = \sigma/\mu$, for different values of N. This ratio corresponds to the deloading factor, and it is the fraction by which the offered load from each user must be reduced relative to the balanced-load case. The results are shown in Tables 3.4 and 3.5.

TABLE 3.4 Deloading Factor Computed from data in Figure 3.20 (a) when $\eta 1 = .05$

N	T	$\mu_{extreme}$	Deloading Factor
8	2	1.56	.78
24	1.7036	1.34	.7866
64	1.1831	0.96	.8114

TABLE 3.5 Deloading Factor computed from data in Figure 3.20 (a) when $\eta 1 = .2$

N	T	$\mu_{extreme}$	Deloading Factor
8	2	.95	.47
24	1.7036	.81	.4755
64	1.1831	.6	.5071

Note that the deloading factor increases as the user throughput decreases by going from N=8 to N=24 to N=64 for two different values of the coefficient of variation (η=.05 and η=.2). This indicates that the necessary load reduction slowly decreases with network size.

By comparing these results to the results obtained in [50] for the case of conventional ShuffleNet for the same N and the same η=.2, we see that the deloading factor for N=8, 24 and 64 is equal to 0.47, 0.4755 and 0.5071, respectively, compared to 0.57, 0.62 and 0.65, respectively for the conventional case. The deloading factor is smaller for the case of the bilayered ShuffleNet. Since the deloading factor is the fraction by which the offered load from each user must be reduced relative to the balanced-load case, we can say that the case of the bilayered ShuffleNet is closer to the balanced-load case than the conventional ShuffleNet indicating that the bilayered ShuffleNet offers a better performance under the case of nonuniform traffic than the conventional ShuffleNet.

The same conclusion still holds by comparing bilayered ShuffleNet and the SR_Net with an advantage to the SR_Net, which achieves a higher channel efficiency and a lower expected number of hops for the same network size.

3.6 Discussion

The bilayered ShuffleNet is a multihop network which has been proposed as a means of using the enormous capacity of the optical fiber in the local environment. Using this new configuration, information bearing packets are switched from source to destination through a uniform logical configuration of nodes. Transmission through the fiber is over Wavelength Division Multiplexed (WDM) channels. This configuration uses the same

number of stations and columns as the conventional ShuffleNet. By adding a new set of connections, we improve the network performance in terms of expected number of hops.

Through this chapter, we have studied this new configuration under uniform and non-uniform traffic. This configuration offers a large number of shorter alternative paths in case of deflection routing. This feature is very important and will be discussed in the next chapter.

Chapter IV

Signal Flow Graphs for Path Enumeration and Deflection Routing Analysis in Bilayered ShuffleNet

In this chapter, we first apply the method of signal flow graphs to path enumeration analysis in the case of the bilayered ShuffleNet and the SR_Net. This is another way to evaluate the performance of the bilayered ShuffleNet compared to the conventional case, and to the Shuffle Ring Network (SR_Net) [52]. The virtue of this approach is that it identifies the alternative paths between source destination pairs. We carry out the necessary computations for the bilayered ShuffleNet and the SR_Net and compare to the conventional case as shown in [53]. The signal flow graph is a weighted directed graph, which has a one-to-one correspondence with a set of linear equations [54]. This method is similar to the one used for calculation of the distance properties and error performance of convolutional codes. It uses a labeling of the edges of the network graph, and the subsequent solution for the transfer function of the resulting signal flow graph. A Taylor series expansion of the transfer function yields the number of paths of a given length between the source and destination.

Second, we evaluate the performance analysis of the bilayered ShuffleNet and the SR_Net with deflection routing in terms of the expected number of hops as a function of

deflection probability. The analysis makes use of the connectivity properties of such networks to characterize the probabilistic behavior of a typical packet in the network in terms of a simple discrete-time Markov chain with a specific number of states, one of which is an absorbing state. A comparative study between the bilayered ShuffleNet, the SR Net and the conventional ShuffleNet using this approach is also shown.

4.1 Path Enumeration

In the following, we illustrate some of the discussed concepts by means of an example. Consider the simple network shown in Figure 4.1. We are interested in finding the number of paths from node a to node b at a distance h in the network, where the unit of distance is one pass over one link. To do this, we remove the paths outgoing from the output node b under consideration, making it a true sink, and add an auxiliary node a', which will serve as a source, providing a directed edge from this node to node a. Associating weight 1 to this edge, and weight D to all other edges to obtain the directed graph in Figure 4.2. D is a dummy variable representing one pass through a link. In a signal flow graph, the contributions of the traversed edges are multiplicative, therefore this formulation enables one to represent the number of passes in terms of powers of D.

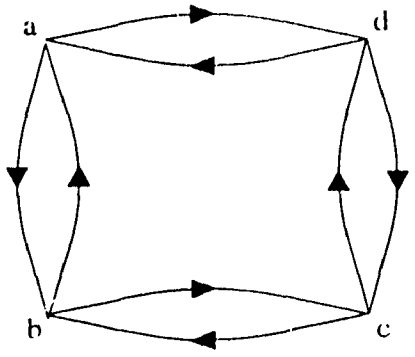

FIGURE 4.1 Example network

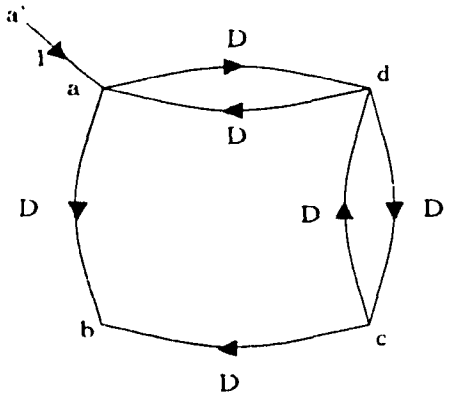

FIGURE 4.2 Modified example network

For each node, we write the node equations (i.e., the weighted paths that terminate at the node), we obtain:

$$\begin{aligned} a &= a' + Dd \\ b &= Da + Dc \\ c &= Dd \\ d &= Da + Dc \end{aligned} \tag{4.45}$$

Solving this set of linear equations, b in terms of a' is given by:

$$b = \frac{Da'}{1 - 2D^2} \tag{4.46}$$

from which the transfer function $T_{ba}(D) = b/a'$ can be obtained. By expanding the rational function into a geometric series, one obtains

$$T_{ba}(D) = \frac{D}{1 - 2D^2} = D + 2D^3 + 4D^5 + \ldots \tag{4.47}$$

This series yields significant information on path length properties of the graph in Figure 4.2. It states that there is one path from node a to node b of length 1, two paths of length 3, four paths of length 5, and so on. However, for more complicated graphs, the signal flow graph method described above can be automated by using a symbolic evaluation package like **Maple**[1], or by using Mason's rule. By using this software we solve this set of equations, from which the transfer function of the output node b to the input node a can be

obtained. By expanding the rational function into a geometric series, this series yields the same results obtained in (4.47).

In the following, we will show the results obtained for the case of the conventional ShuffleNet and apply the same study for the case of the bilayered ShuffleNet and the SR_Net. The number of users in the network is equal to 64. For the case of conventional ShuffleNet and the bilayered ShuffleNet, this can be obtained by choosing P=2 and k=4. For the (n, k) SR_Net, this can be obtained by choosing P=4, k=3 and n=2.

4.1.1 Path Enumeration for the case of the conventional ShuffleNet

Let us consider the case of a conventional ShuffleNet with 64 nodes as shown in Figure 4.4. The result of this study is already contained in [53] and shows the number of paths from node 0 to any other node at distance h in the network. We present these results in order to make a comparison between the case of the conventional ShuffleNet and other network architectures that we will study.

Seven distinct transfer functions are found and due to the symmetry in the network different nodes have the same transfer function. We have:

for nodes 16 and 17

$$T_1(D) = D + D^5 + 15D^9 + 225D^{13} + \ldots \quad (4.48.a)$$

for nodes 32, 33, 34, and 35

$$T_2(D) = D^2 + 3D^6 + 45D^{10} + 675D^{14} + \ldots \quad (4.48.b)$$

for nodes 48, 49, 50, 51, 52, 53, 54, and 55

$$T_3(D) = D^3 + 7D^7 + 105D^{11} + 1575D^{15} + \ldots \quad (4.48.c)$$

1. Registered Trademark of University of Waterloo

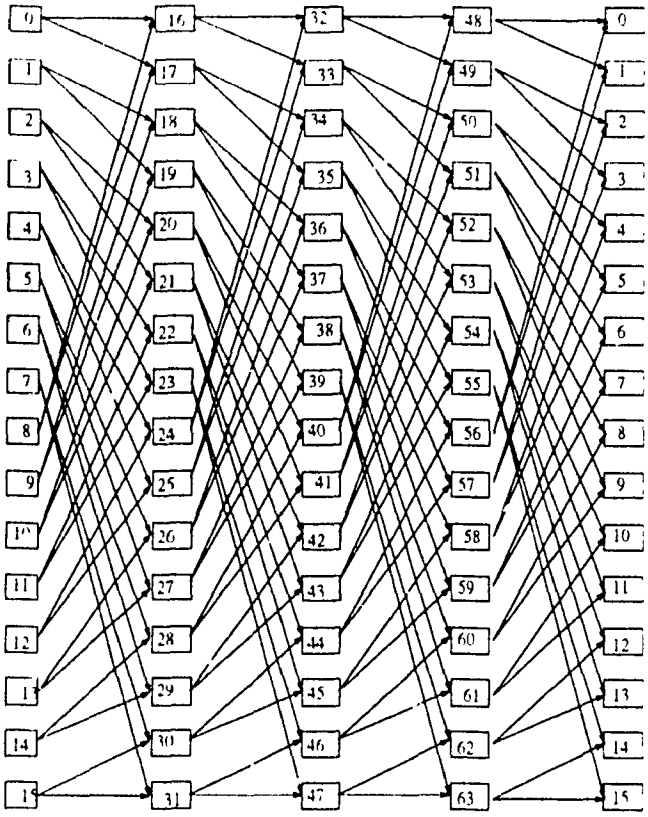

FIGURE 4.3 A 64-user conventional ShuffleNet.

for node 1 to node 15

$$T_4(D) = D^4 + 15D^8 + 225D^{12} + 3375D^{16} + \ldots \tag{4.48.d}$$

for node 18 to node 31

$$T_5(D) = 2D^5 + 30D^9 + 450D^{13} + \ldots \tag{4.48.e}$$

for node 36 to node 47

$$T_6(D) = 4D^6 + 60D^{10} + 900D^{14} + \ldots \tag{4.48.f}$$

Finally, for node 56 to node 63

$$T_7(D) = 8D^7 + 120D^{11} + 1800D^{15} + \ldots \tag{4.48.g}$$

We show these results in Table 4.1. The h^{th} entry in the upper row of the table represents the superscript of D or the length of a path in the series, the number inside the table represents the nonzero coefficient or the number of paths for that term, and the numbers of the leftmost column represent the number of nodes with that transfer function.

TABLE 4.1 First 10 Terms of the transfer functions of the 64-user conventional ShuffleNet. Upper row: power of D, table entries: coefficient for that term (number of paths), leftmost column: number of nodes with that transfer function

	1	2	3	4	5	6	7	8	9	10
2	1				1				15	
4		1				3				45
8			1				7			
15				1				15		
14					2				30	
12						4				60
8							8			

Another step is to calculate the *total* series for this network by multiplying each series in Table 4.1 by the number of times they appear, and adding the resulting series. This gives:

$$T_T(D) = 2D + 4D^2 + 8D^3 + 15D^4 + 30D^5 + 60D^6 + 120D^7 + 120D^7 + 225D^8 + \ldots \quad (4.49)$$

These series give the number of paths of length h from node 0 to any other node regardless of whether the nodes that are reached are distinct or not. A better approach is to have an idea of the number of distinct nodes that can be reached at h hops, indicating that one network can be considered superior to another. This information is obtained by adding the leftmost column entries for the nonzero entries in the table for a particular power of D. The series is equal to:

$$T'_D(D) = 2D + 4D^2 + 8D^3 + 15D^4 + 16D^5 + 16D^6 + 16D^7 + 15D^8 + \ldots \quad (4.50)$$

4.1.2 Path Enumeration for the case of the Bilayered ShuffleNet

Consider the bilayered ShuffleNet with 64 nodes as shown in Figure 4.4. Seven distinct transfer functions are found, and due to the symmetry in the network different nodes have the same transfer function. We have:

for nodes 16 and 48

$$T_1(D) = D + 2D^3 + 20D^5 + 328D^7 + 5072D^9 + \ldots \quad (4.51.a)$$

for nodes 17 and 49

$$T_2(D) = D + 4D^3 + 24D^5 + 352D^7 + 5440D^9 + \ldots \quad (4.51.b)$$

for nodes 21 and 53

$$T_3(D) = 4D^3 + 24D^5 + 432D^7 + 6629D^9 + \ldots \quad (4.51.c)$$

for nodes 18, 19, 20, 22, 23, 50, 51, 52, 54 and 55

$$T_4(D) = 4D^3 + 32D^5 + 480D^7 + 7424D^9 + \ldots \quad (4.51.d)$$

for nodes 26, 31, 58 and 63

$$T_5(D) = 32D^5 + 448D^7 + 7040D^9 + \ldots \quad (4.51.e)$$

for nodes 24, 25, 27, 28, 29, 30, 56, 57, 59, 60, 61 and 62

$$T_6(D) = 32D^5 + 512D^7 + 7936D^9 + \ldots \quad (4.51.f)$$

for nodes 1, 2, 3, 32, 33, 34 and 35

$$T_7(D) = 2D^2 + 8D^4 + 112D^6 + 1728D^8 + \ldots \quad (4.51.g)$$

for nodes 5, 10, 15, 37, 42 and 47

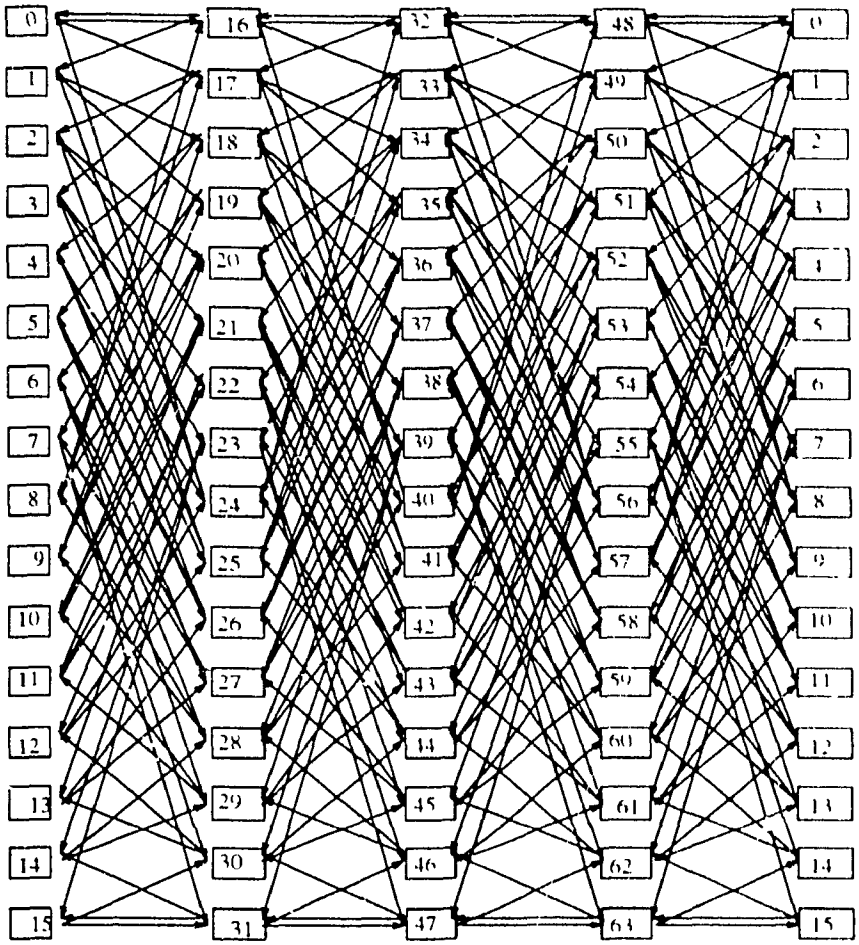

FIGURE 4.4 A 64-user bilayered ShuffleNet

$$T_8(D) = 8D^4 + 112D^6 + 1760D^8 + \ldots \tag{4.51.h}$$

Finally, for nodes 4, 6, 7, 8, 9, 11, 12, 13, 14, 36, 38, 39, 40, 41, 43, 44, 45 and 46

$$T_9(D) = 8D^4 + 128D^6 + 1884D^8 + \ldots \tag{4.51.i}$$

These results are summarized in Table 4.2 the h^{th} entry in the upper row of the table represents the superscript of D or the length of a path in the series. The number inside the table represents the nonzero coefficient or the number of paths for that term, and the numbers of the leftmost column represent the number of nodes with that transfer function

TABLE 4.2 First 10 Terms of the transfer functions of the 64-user bilayered ShuffleNet. Upper row: power of D, table entries: coefficient for that term (number of paths), leftmost column: number of nodes with that transfer function.

	1	2	3	4	5	6	7	8	9	10
2	1		2		20		328		5072	
2	1		4		24		352		5440	
2			4		24		432		6629	
10			4		32		480		7424	
4					32		448		7040	
12					32		512		7936	
7		2		8		112		1728		26752
6				8		112		1760		27328
18				8		128		1884		30720

Another step is to calculate the *total* series for this network by multiplying each series in Table 4.2 by the number of times they appear, and adding the resulting series. This gives

$$T_I(D) = 4D + 14D^2 + 60D^3 + 248^4 + 860D^5 + 3760D^6 + 14960D^7 + \ldots \quad (4.52)$$

Compared to the conventional ShuffleNet [53], the result is

$$T'_T(D) = 2D + 4D^2 + 8D^3 + 15D^4 + 30D^5 + 60D^6 + 120D^7 + 120D^7 + 225D^8 + \ldots (4.53)$$

These series give the number of paths of length h from node 0 to any other node regardless of whether the nodes that are reached are distinct or not. A better approach is to have an idea of the number of distinct nodes that can be reached at h hops, indicating that one network can be considered superior to another. This information is obtained by adding the leftmost column entries for the nonzero entries in the table for a particular power of D. For the bilayered ShuffleNet and the standard ShuffleNet respectively, this series is equal to:

$$T_D(D) = 4D + 7D^2 + 16D^3 + 31D^4 + 32D^5 + 31D^6 + 32D^7 + 31D^8 + \ldots \quad (4.54)$$

$$T'_D(D) = 2D + 4D^2 + 8D^3 + 15D^4 + 16D^5 + 16D^6 + 16D^7 + 15D^8 + \ldots \quad (4.55)$$

The above results show that the number of paths of a given length between source and destination is larger for the case of bilayered ShuffleNet than for the case of conventional ShuffleNet. This implies that the routing strategies in the case of the bilayered ShuffleNet

can provide alternate paths to reach a node in case of a congestion or link failure, with increased reliability, recoverability, and reduced delay. Table 4.2 also reveals distance information about the network. The distance between two nodes is the power of the first nonzero entry in the transfer function. The maximum distance is the column index for the row whose first nonzero index is the largest in Table 4.2, which is equal to 5 for our case compared to 7 in the conventional ShuffleNet. On the other hand, the weighted distance (sum of distance of all nodes) of bilayered ShuffleNet is 230 and that of the conventional ShuffleNet is 292. This makes the average distance of BSN 3.65 whereas that of SN is 4.63.

A more interesting way of comparison is to compare this 64 node bilayered ShuffleNet to a similar network which is a 64 node SR_Net where the connectivity is the same or equal to 4 and the number of columns is also the same. The connectivity graph of this SR_Net is shown in Figure 4.5. This connectivity is similar to the case of a ShuffleNet with P=4. From this point we can say that the SR_Net will perform better than the bilayered ShuffleNet. By using the method of flow graph for path enumeration, we make the comparison between the bilayered ShuffleNet and the SR_Net.

4.1.3 Path Enumeration for the case of the SR_Net

The same method applied for the case of the bilayered ShuffleNet is also used for the case of the SR_Net shown in Figure 4.5, and the following results are obtained:

From nodes 16 to node 19

$$T_1(D) = D + 48D^5 + 11520D^9 + \ldots \tag{4.56}$$

From nodes 20 to node 31

$$T_2(D) = 64D^5 + 15360D^9 + \ldots \tag{4.56.a}$$

From nodes 32 to node 47

$$T_3(D) = D^2 + 192D^6 + \ldots \tag{4.56.b}$$

From nodes 48 to node 63

$$T_4(D) = 4D^3 + 960D^7 + \ldots \quad (4.56.c)$$

From node 1 to node 15

$$T_5(D) = 16D^4 + 3840D^8 + \ldots \quad (4.56.d)$$

The calculation of the total series for this network provides the following results:

$$T_T(D) = 4D + 16D^2 + 64D^3 + 240D^4 + 960D^5 + 3072D^6 + \ldots \quad (4.57)$$

A comparison of (4.54) and (4.57) indicates an advantage for the SR_Net since paths seem to be shorter in general. For example, for the bilayered ShuffleNet, there are seven direct paths of length two between source and destination pairs while for the SR_Net there are 16 such paths. However, if one considers alternate paths between source destination pairs, the assessment of relative performance is somewhat different. Consider equations (4.51)a-h for the bilayered ShuffleNet and (4.56)a-d for the SR_Net. For the bilayered ShuffleNet, the length of secondary paths increases incrementally by two hops over the shortest path while for the SR_Net the incremental increase is four. For example, for node 16, we have:

$$T_1(D) = D + 2D^3 + 20D^5 + 328D^7 + 5072D^9 + \ldots$$

for the bilayered ShuffleNet and

$$T_1(D) = D + 48D^5 + 11520D^9 + \ldots$$

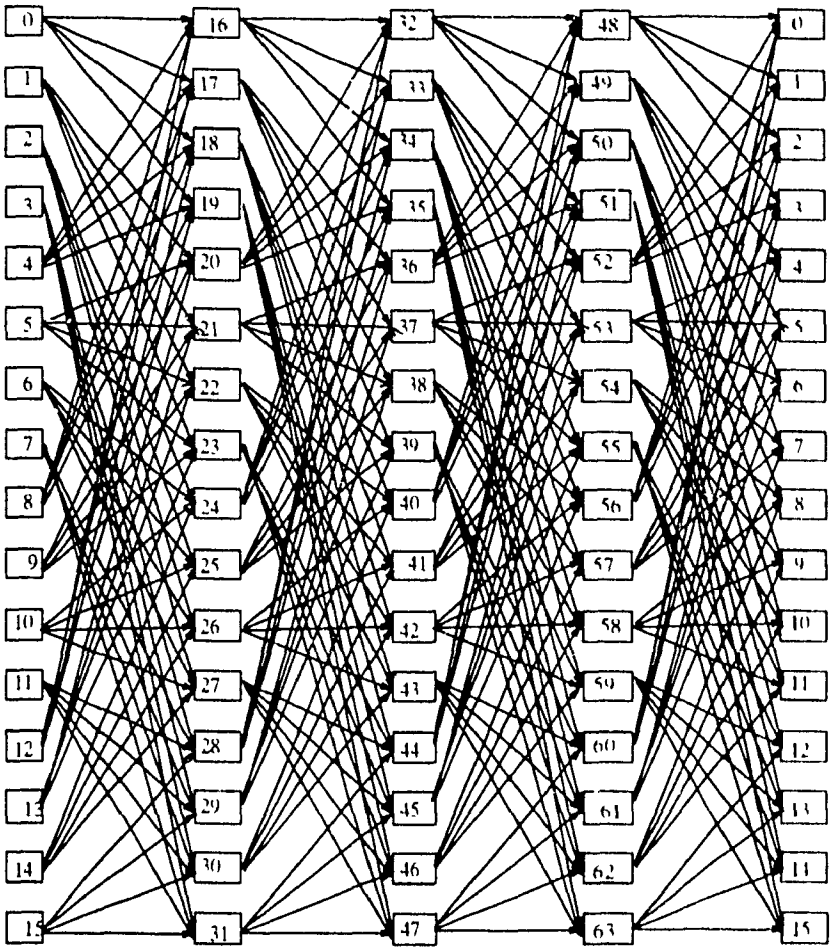

FIGURE 4.5 A 64-node SR_Net

for the SR_Net. For the bilayered ShuffleNet, the alternative paths are of lengths, 3, 5, 7, ...; whereas, for the SR_Net they are of length 5, 9, 13, ... These results indicate that a packet that is deflected from a path is more likely to find a shorter alternative path in the bilayered ShuffleNet than in the SR_Net. Such deflections can be the result of traffic or a breakdown of components. In the next section, when we consider performance under traffic load, these observations will be quantified.

4.2 Study of the Bilayered ShuffleNet and the SR_Net under deflection Routing.

In this section, we evaluate the expected number of hops for the case of the conventional ShuffleNet, the bilayered ShuffleNet and the SR_Net as a function of the probability of deflection, which occurs when there is a collision between different packets contending for the same output channel during the process of routing. We are interested in this parameter because the larger the average distance between the nodes in the network, the longer the packets will have to remain within the network on the average, thereby consuming network resources; this directly translates into smaller throughput. If there is any deflection in the network, several packets will be routed through a much longer path, which cause an increase in the average number of hops and start consuming network resources.

For a 64-node network using the logical configuration of the bilayered ShuffleNet and the SR_Net, the average number of hops is equal to 3.65 and 3.24 respectively and with no deflection in the network (the minimum path is used). In this case, the SR_Net has the advantage compared to the bilayered ShuffleNet. If there is a deflection routing in the network, the results found in the previous section can be applied. In this case, we take into account the fact that for the bilayered ShuffleNet, the deflection index (the number of extra hops taking by a message when is deflected) is equal to two; whereas, for the SR_Net it is equal to four. These results indicate that a packet when is deflected from a path is more likely to find a shorter alternative path in the bilayered ShuffleNet than in the SR_Net. In the following, we try to summarize these results in order to evaluate the expected number of hops as a function of the probability of deflection. The model used in this calculation is based on the results obtained for the case of the conventional ShuffleNet [56] and is described in the following section.

4.2.1 Performance analysis of the conventional ShuffleNet with deflection routing.

In this section, we present the analytical relationships between P_{def} and $E[hops]$ for the case of the conventional ShuffleNet. In any (P, k) ShuffleNet, for each deflection it suf-

fers, a packet simply takes k more hops to reach its destination. In this case, the "critical" nodes for a packet are the nodes within diameter k from its destination. All other nodes are "non-critical" nodes where the packet will not suffer deflection.

Let us select a packet arbitrarily and observe the behavior of the "tagged" packet. Let our state space $S = \{0, 1, ..., 2k\text{-}1\}$ be a collection of possible distances between the current position of the tagged packet and its destination. Here, the distance is defined as the minimum number of hops that the packet must make to travel to its destination in the absence of deflection. Let

$$D_i = \text{E[number of hops when the tagged packet is at distance } i \text{ from its destination | probability of deflection} = P_{def}\text{]}, \quad \forall i \in S \tag{4.58}$$

The ShuffleNet is modeled as an absorbing Markov chain with space S, and state 0 is the absorbing state and each deflection increases the packet's hops by k. Then, we will have:

$$D_i = P_{def} D_{i-1+k} + (1 - P_{def}) D_{i-1} + 1, \quad 1 \le i \le k \tag{4.59}$$

When the packet is at a distance more than k hops from its destination, it is at its "non-critical" node and therefore will not suffer deflection (i.e. $P_{def} = 0$) until it is k hops from its destination. Hence,

$$D_i = D_k + (i - k), \quad k + 1 \le i \le 2k - 1 \tag{4.60}$$

Since state 0 is the destination of the tagged packet, we have $D_0 = 0$. Solving equation (4.59) and (4.60), we get

$$D_j = \begin{cases} j + \dfrac{k}{(1 - P_{def})^k}\left[1 - (1 - P_{def})^j\right], & 1 \le j \le k \\ D_k + (j - k), & k + 1 \le j \le 2k - 1 \end{cases} \tag{4.61}$$

In order to evaluate the expected number of hops, we note that for $1 \le j \le k-1$, there are P^j nodes at j hops away from a given node, and for $0 \le j \le k-1$, there are $(P^k - P^j)$ nodes at $k+j$ hops away, the expected value is then given by:

$$E[hops] = \frac{1}{kP^k - 1}\left[\sum_{j=1}^{k-1} P^j D_j + \sum_{j=0}^{k-1} (P^k - P^j) D_{k+j}\right]$$

$$= -\frac{kP\,(1 - P^{k-1}(1 - P_{def})^{k-1})}{(kP^k - 1)\,(1 - P_{def})^{k-1}(1 - P + PP_{def})}$$

$$+ \frac{kP^k}{kP^k - 1}\left(\frac{k-1}{2}\right) + \frac{k}{(1 - P_{def})^k} \tag{4.62}$$

As an example, we take the case of a (2, 4) conventional ShuffleNet for a total of 64 users. For this case, the transition diagram is shown in Figure 4.6. The state number represents distance i, $0 \le i \le 2k-1$, i.e., the number of hops that a packet must take from the current node to its destination without deflection.

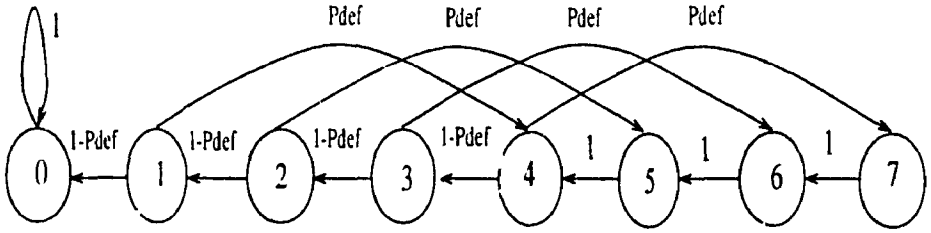

FIGURE 4.6 State transition diagram for a 64-node ShuffleNet

From this diagram equations (4.59) to (4.62) can be derived. The $E[hops]$ as a function of the deflection for this case is given by:

$$E[hops] = \frac{4}{63} \times \frac{73 - 62P_{def} + 116P_{def}^2 - 88P_{def}^3 + 24P_{def}^4}{(1 - P_{def})^4} \tag{4.63}$$

and the results of this are shown in Figure 4.7. We note that for the case of no deflection the $E[hops]$ is equal to:

$$\lim_{P_{def} \to 0} E[hops] = 4.6349. \tag{4.64}$$

which corresponds to the result originally obtained for the conventional ShuffleNet [3].

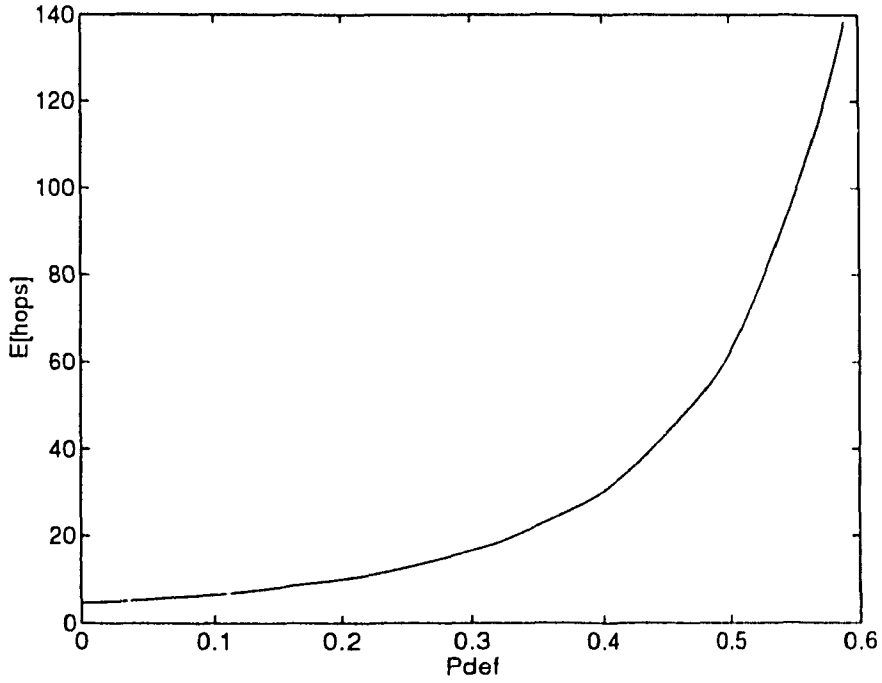

FIGURE 4.7 The average number of hops versus probability of deflection for the case of ShuffleNet

4.2.2 Performance analysis of the Bilayered ShuffleNet with deflection routing.

In the case of the bilayered ShuffleNet, the same network architecture is used. The only difference is the use of a second set of connections which allows a packet to reach its destination in fewer hops. At the same time, a packet can find a shorter path; which cost an extra 2 or four hops in the case of deflection as we mentioned in our study in the first part of this chapter. For the case of a 64 nodes bilayered ShuffleNet the maximum number of hops is equal to 5; which means that state 5 is a "non-critical" state and all the other states are "critical" states. Since any deflection will cost an extra two or four hops for a packet to

reach its destination this means that the maximum number of states in the transition diagram is equal to 6 or 8. In the first case, we assume that the only path chosen in the case of deflection is the shortest path thereby obtaining the lower bound model. For the second case, we consider a more realistic model in which both deflection paths are allowed. This leads to a maximum of 8 transition states. Those two models will be studied in the following sections.

4.2.2.1 The lower bound model

In the case of the bilayered ShuffleNet, four output links are available. Two of these are "non-critical links" for nodes at a distance two, three and four. For nodes at a distance five, all four links are "non-critical links". From our study in the first part (path enumeration) we assume that the deflected packet will take the second optimum link or an extra two hops to reach its destination with a probability of 1/2. The state transition diagram for this case is shown in Figure 4.8.

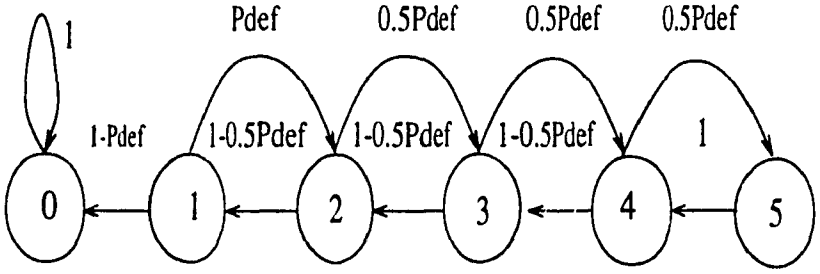

FIGURE 4.8 State transition diagram for a 64-node bilayered ShuffleNet under the first assumption.

From this diagram, the following equations are obtained:

$$D_1 = P_{def}D_2 + (1 - P_{def})D_0 + 1 \tag{4.65}$$

$$D_2 = 0.5P_{def}D_3 + (1 - 0.5P_{def})D_1 + 1 \tag{4.66}$$

$$D_3 = 0.5P_{def}D_4 + (1 - 0.5P_{def})D_2 + 1 \tag{4.67}$$

$$D_4 = 0.5P_{def}D_5 + (1 - 0.5P_{def})D_3 + 1 \tag{4.68}$$

$$D_5 = D_4 + 1 \tag{4.69}$$

where D_0 is equal to 0, and by solving those equations all D_i's can be evaluated as a function of P_{def} only. In this case, the expected number of hops as functions of the deflection probability is equal to:

$$E[hops] = \frac{8}{63} \times \frac{4P_{def}^4 - 18P_{def}^3 + 145P_{def}^2 - 298P_{def} + 230}{P_{def}^4 - 7P_{def}^3 + 18P_{def}^2 - 20P_{def} + 8} \tag{4.70}$$

Figure 4.9 shows the expected number of hops as a function of the deflection probability.

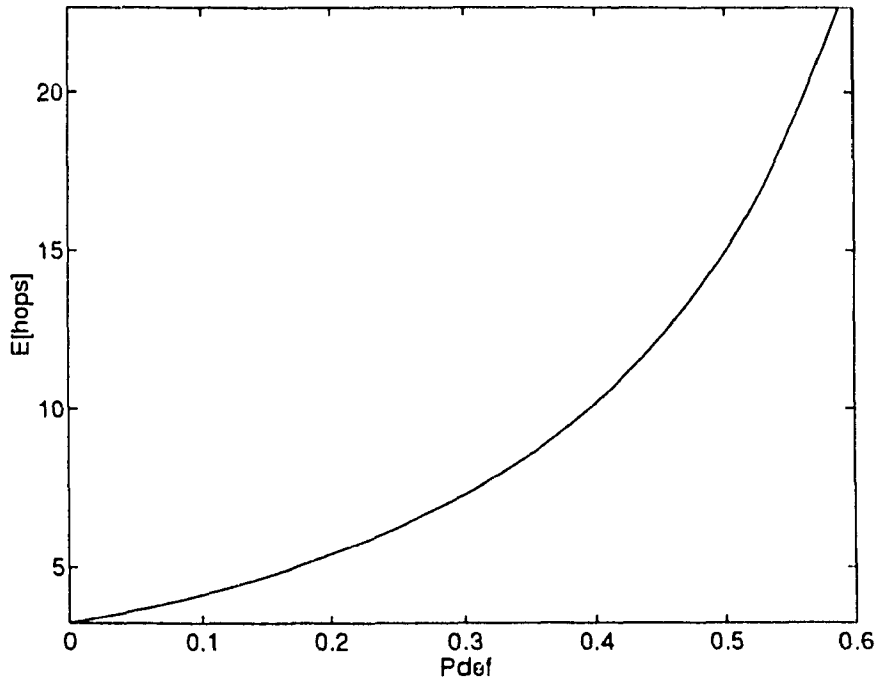

FIGURE 4.9 Average number of hops versus probability of deflection for the case of bilayered ShuffleNet for the first case.

4.2.2.2 The more realistic model

This model is based on the assumption that when a message is deflected, it will take an extra two hops with a probability 1/2 or an extra four hops with a probability 1/2. This model is the combination of the model for the case of the conventional ShuffleNet and the lower bound model used for the bilayered ShuffleNet. The state transition diagram for this case will have a total of 8 states and it is shown in Figure 4.10.

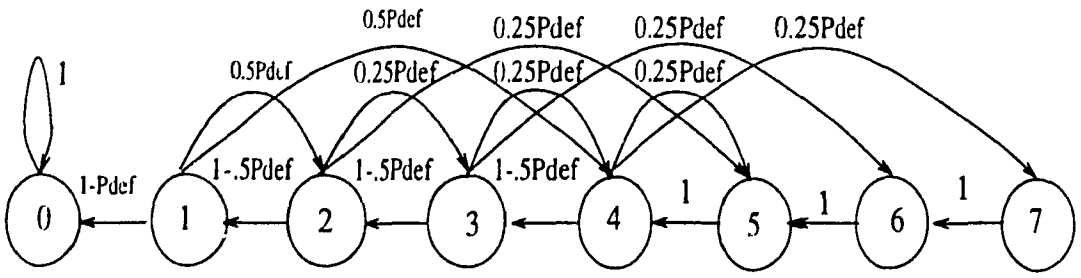

FIGURE 4.10 State transition diagram for a 64-node bilayered ShuffleNet under the second assumption.

From this diagram, the following equations are obtained:

$$D_1 = 0.5P_{def}(D_2 + D_4) + (1 - P_{def})D_0 + 1 \tag{4.71}$$

$$D_2 = 0.25P_{def}(D_3 + D_5) + (1 - 0.5P_{def})D_1 + 1 \tag{4.72}$$

$$D_3 = 0.25P_{def}(D_4 + D_6) + (1 - 0.5P_{def})D_2 + 1 \tag{4.73}$$

$$D_4 = 0.25P_{def}(D_5 + D_7) + (1 - 0.5P_{def})D_3 + 1 \tag{4.74}$$

$$D_5 = D_4 + 1 \tag{4.75}$$

$$D_6 = D_4 + 2 \tag{4.76}$$

$$D_7 = D_4 + 3 \tag{4.77}$$

$$E[hops] = \frac{1}{126} \times \frac{43P_{def}^4 - 109P_{def}^3 + 1206P_{def}^2 - 2552P_{def} + 3680}{P_{def}^4 - 7P_{def}^3 + 18P_{def}^2 - 20P_{def} + 8} \tag{4.78}$$

Figure 4.7 shows the expected number of hops as a function of the deflection probability.

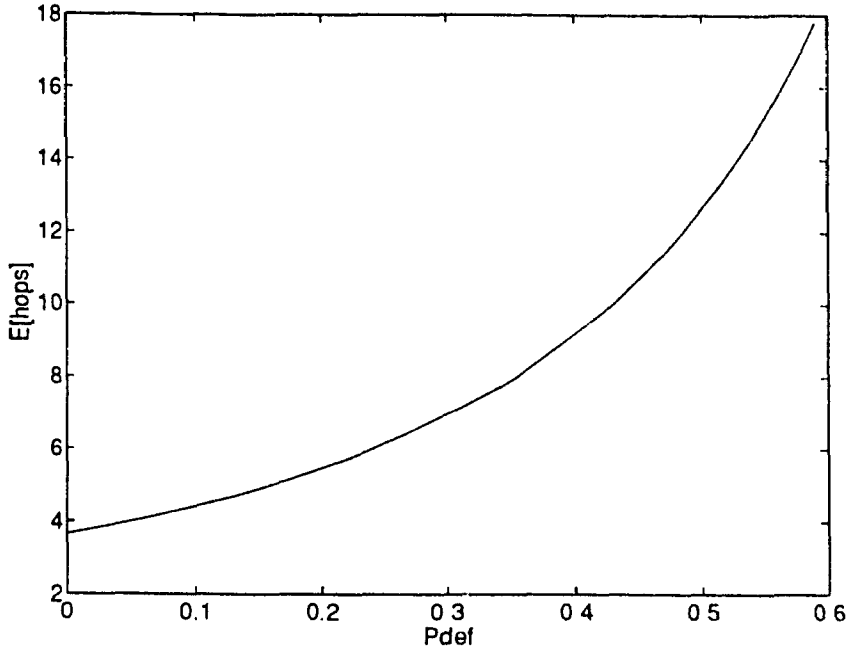

FIGURE 4.11 Average number of hops versus probability of deflection for the case of bilayered shuffling in the second case

4.2.3 Performance analysis of the SR_Net with deflection routing.

In the case of the SR_Net, which is a more general case of the conventional ShuffleNet, the maximum number of hops is equal to 5 for the case of a 64-node network. Any deflection in the network will cause a packet to take four more hops to reach its destination. Figure 4.12 shows the state transition diagram, which has 6 states.

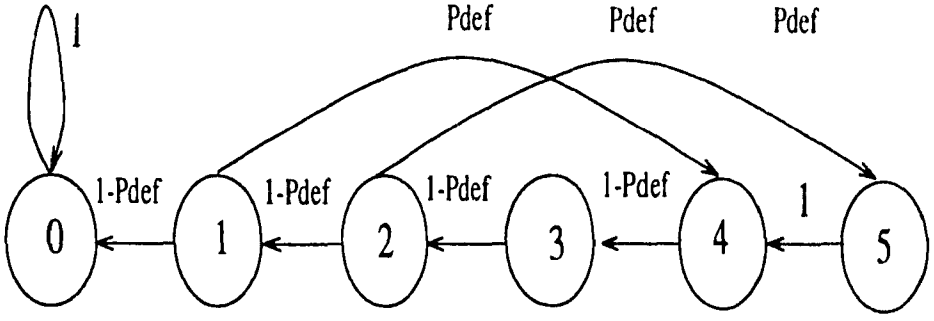

FIGURE 4.12 State transition diagram for a 64-node SR_Net.

From this diagram, the following equations are obtained:

$$D_1 = P_{def}D_4 + (1 - P_{def})D_o + 1 \tag{4.79}$$

$$D_2 = P_{def}D_5 + (1 - P_{def})D_1 + 1 \tag{4.80}$$

$$D_3 = D_2 + 1 \tag{4.81}$$

$$D_4 = D_2 + 2 \tag{4.82}$$

$$D_5 = D_2 + 3 \tag{4.83}$$

where D_0 is equal to 0, and by solving those equations all D_i values can be evaluated as function of P_{def} only. In this case, the expected number of hops as a function of the deflection probability is equal to:

$$E[hops] = \frac{4}{63} \times \frac{51 + 20P_{def} - 8P_{def}^2}{(1 - P_{def})^2} \tag{4.84}$$

Figure 4.13 shows the expected number of hops as a function of the deflection probability.

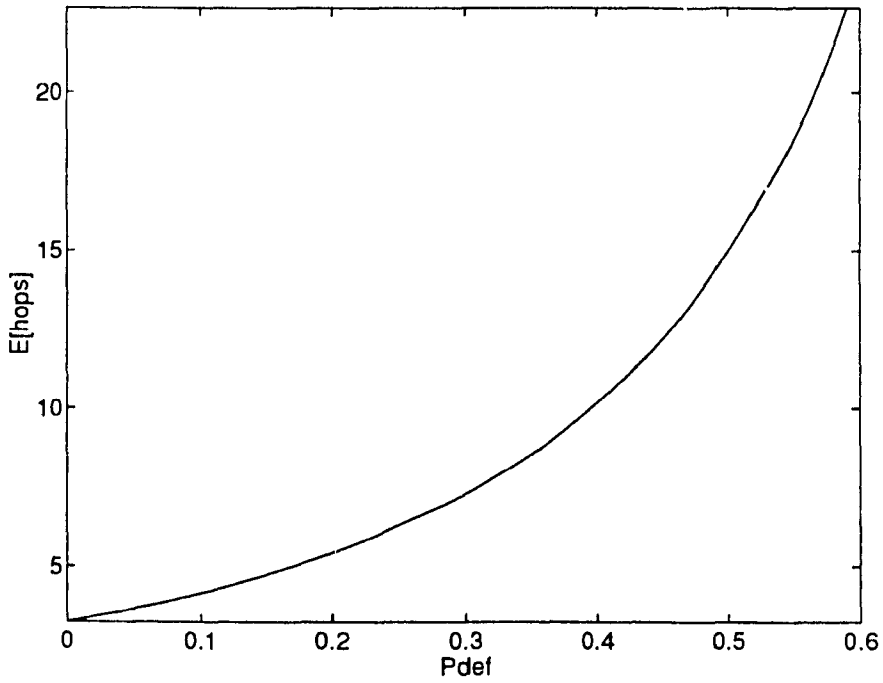

FIGURE 4.13 Average number of hops versus probability of deflection for the case of the SR_Net.

4.3 Performance Comparison and Discussion

The deflection probability is mainly due to the collision between different packets contending for the same output channel. The value of this probability (P_{def}) is function of the traffic load, P_{def} will increase by increasing the traffic load. For a light traffic load P_{def} will have a maximum value of 0.1 to 0.2. For a heavy traffic load P_{def} can reach very easily a value of 0.9. For a normal value of traffic load P_{def} can have an average value of 0.5.

Using the results obtained in the previous sections, we can compare the expected number of hops for the case of the bilayered ShuffleNet to the case of the SR_Net. Using the assumption of only using the shortest path in case of deflection for the case of the bilayered ShuffleNet (first assumption) and compared to the case of the SR_Net, we obtain the result shown in Figure 4.14. By using the more realistic model of the bilayered ShuffleNet and compared to the case of the SR_Net, the result obtained is shown in Figure 4.15.

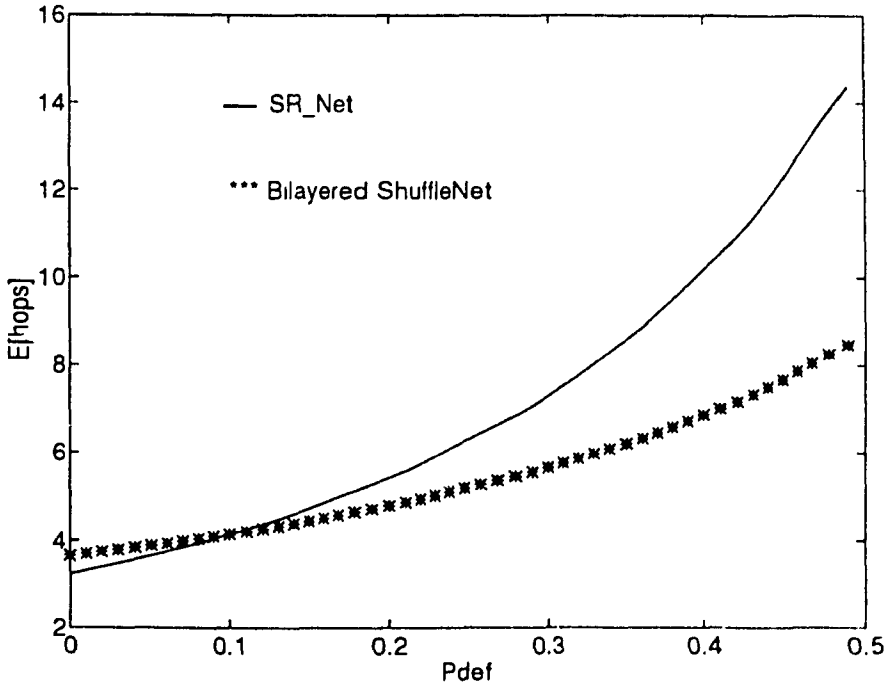

FIGURE 4.14 Average number of hops versus probability of deflection for the case of the bilayered ShuffleNet and the SR_Net for the first case.

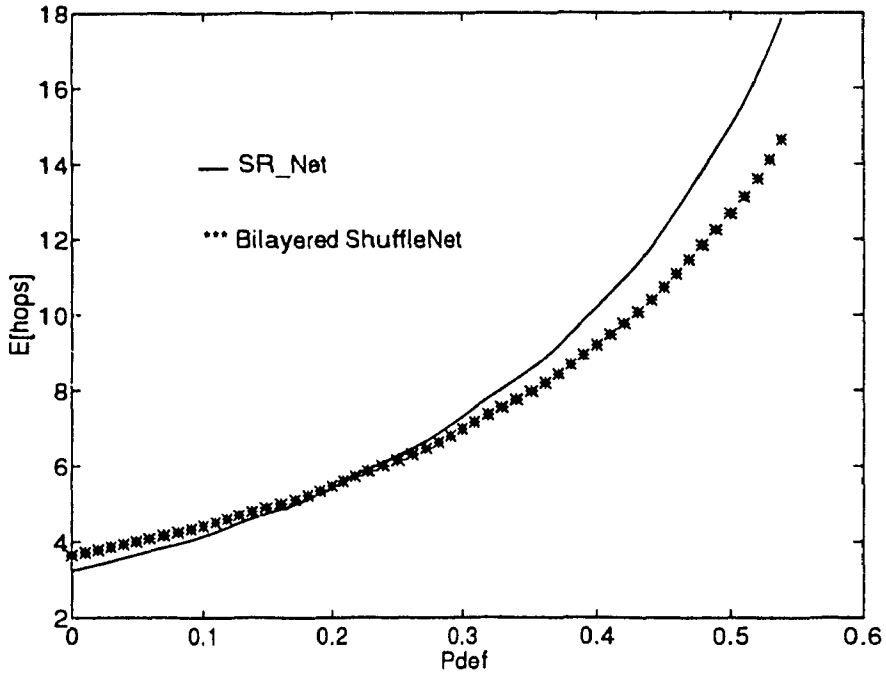

FIGURE 4.15 Average number of hops versus probability of deflection for the case of the bilayered ShuffleNet and the SR_Net for the second case.

These results show that by increasing the P_{def}, the expected number of hops increase in both cases. However, after a certain value of P_{def} which we call P_{equ}, the expected number of hops for the case of the SR_Net becomes larger than the case of the bilayered ShuffleNet in both cases. The result of this will be the following:

- For P_{def} less than P_{equ}, or under a light traffic load it is more advantageous to use the SR_Net than the bilayered ShuffleNet due to the fact that the average number of hops required for a packet to reach its destination is smaller for the SR_Net than the bilayered ShuffleNet.
- For a P_{def} greater than P_{equ}, or under normal or heavy traffic load it is more advantageous to use the bilayered ShuffleNet than the SR_Net for the same reasons as explained earlier.

P_{equ}, is much lower for the first case because a more optimistic model is used. This model can be considered as lower bound model. P_{equ}, in this case is equal to 0.1. For the

more realistic, model P_{equ} is equal to 0.2.Based on this result, an adaptive configuration using the P_{def} can be implemented. All the details of the study of this configuration and the issue of physical implementation of several multihop networks using basic topologies, such as the bus, the tree, and the star or the wavelength division multiplexing cross-connect will be discussed in the next chapter.

Chapter V

Application of WDM Cross-connects to Different Multihop Networks

WDM cross-connect is a device based on integrating a two-dimensional array of Bragg diffraction cells. This device can be used in various wavelength routing network applications and overcomes major problems related to the conventional star coupler. In this chapter, we propose a method of using this device in the implementation of different multihop topologies, such as the perfect and the bidirectional ShuffleNet, the unidirectional and bidirectional Manhattan Street Network, and the bilayered ShuffleNet.

5.1 Introduction

When multihop networks are implemented using basic topologies, such as the bus, the star, and the tree or compound configurations such us the tree-star-tree configuration using optical amplifiers [4], they introduce two major problems. First, the number of different wavelengths needed in the network is very large. Second, the network size is limited by inherent power splitting of the required passive couplers used to interconnect various nodes.

To overcome this problem, wavelength division multiplexing cross-connect plays an important role in wavelength routing in multihop networks. One way to implement such a

wavelength routing device is to use the WDM cross-connect star based on Bragg diffraction grating.

5.2 WDM cross-connected star topology

Wavelength division multiplexed (WDM) cross connects [21] are used to replace the conventional NxN passive star couplers. The device plays an important role in wavelength routing networks, where the path that the signal takes is uniquely determined by the wavelength and the port through which it enters the network. The fabric of the network consists of an array of wavelength-selective devices connected in a specific pattern in order to obtain the required interconnection between the nodes of the network. One way to implement a WDM cross-connect star topology is to use wavelength multiplexers and demultiplexers as shown in Figure 5.1. This method involves a large number of interconnections between various elements and will cause a large insertion loss. However, using the technology based on Bragg diffraction grating, all these multiplexers and demultiplexers can be integrated on a single substrate. Several techniques for fabricating integrated-optic wavelength multiplexers and demultiplexers have been reported [58]. Among these are the single tuned-Bragg-cell shown in Figure 5.2. This device has the wavelength selectivity on the entire bandwidth necessary for dense WDM. A single Bragg cell is a 2x2 wavelength selective switch. To obtain an NxN wavelength selective switch, different 2x2 Bragg cells tuned to different wavelengths can be used to construct this device. As an example, a 4x4 cross-connect network is implemented by using 16 Bragg-cells, four different Brag-cells, each re-used four times.

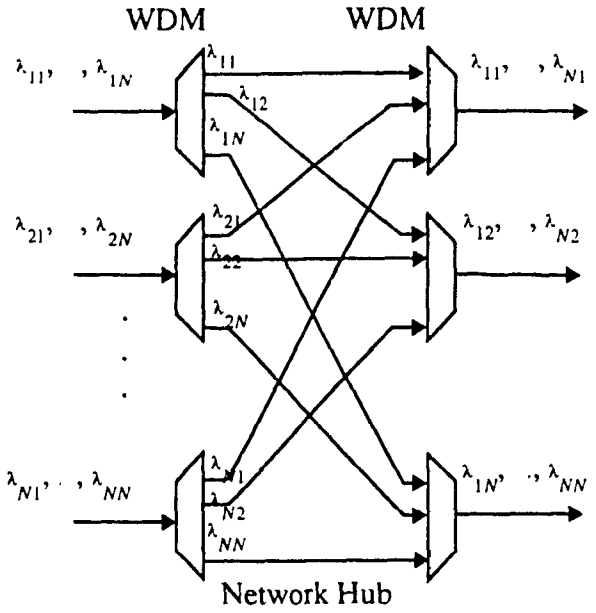

FIGURE 5.1 A WDM cross-connect.

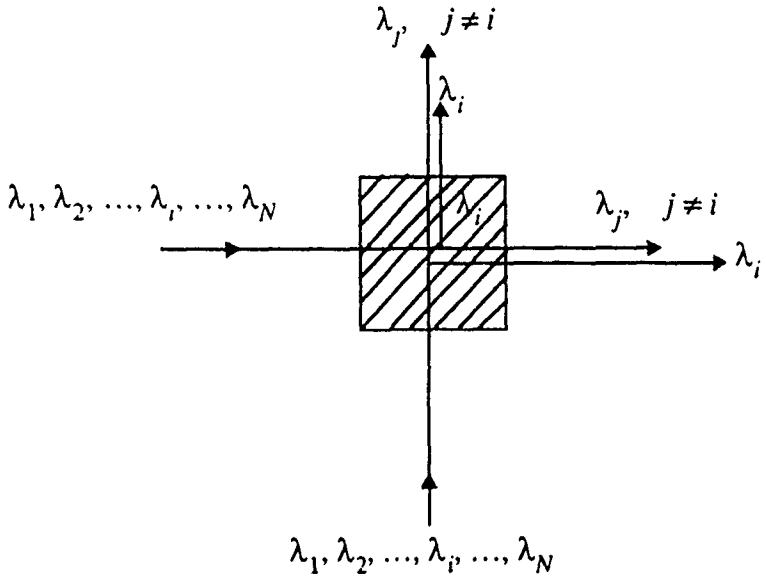

FIGURE 5.2 Single Bragg cell tuned to λ_i. From N incoming wavelengths in the x or z direction, only λ_i will be deflected by 90° and all other λ_j $(j \neq i)$ will propagate in the x or z direction.

The advantages of using this approach are the following:

1)P wavelengths instead of PN or kP^{k+1} wavelengths in the conventional topology are required, where P is the number of input/output pairs per user and N is the total number of users in the network.

2) The signal power loss due to the $1/N$ power splitting at the star coupler no longer exists.

5.3 Application of WDM Cross-connect to Multihop Networks

5.3.1 ShuffleNet Implementation using WDM Cross-Connect

Consider a (P, k) ShuffleNet with $P=2$, $k=2$ and $N=kP^k=8$. This network can be implemented by using 4 different 2x2 WDM cross-connect star couplers, but only two wavelengths are used in the whole network. Every 2x2 WDM coupler is shared by four different stations, two in the transmitting side and two in the receiving side. Using the grouping procedure described in [2], the four sets are (T_1, T_3, R_5, R_6), (T_6, T_8, R_3, R_4), (T_5, T_7, R_2, R_1), (T_2, T_4, R_7, R_8). The connection graph is shown in Figure 5.3. The members of each group are connected to each other and with no connection between the members of different groups. The same set of wavelengths can be reused for different groups. This will reduce the number of wavelengths used in the network. For each group only P wavelengths can be used. By reusing these P wavelengths in all the other groups, the number of wavelengths used in the network will be limited to only P wavelengths. For a (P, k) ShuffleNet, the total number of groups that can use the same set of wavelengths is equal to kP^{k-1}.

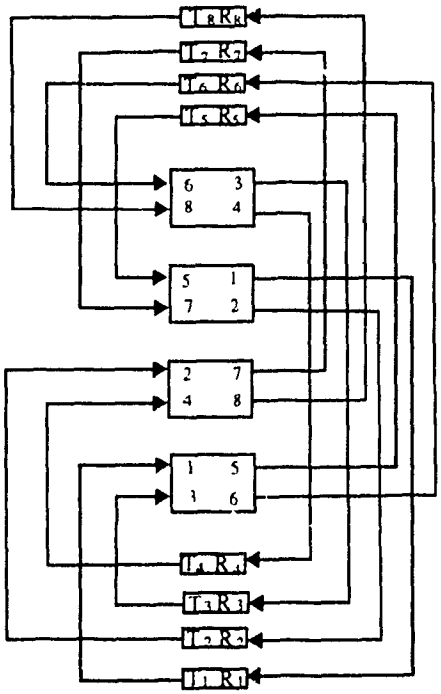

FIGURE 5.3 Implementation of an 8-users ShuffleNet using four 2x2 Bragg-cells

5.3.2 Implementation of MSN using a WDM Cross-Connect Star Coupler

The cross-connect technique can also be applied to the Manhattan street network [22]. As an example, we take the case of the one directional Manhattan street network with 16 users shown in Figure 5.4. The number of wavelengths used in the network can be reduced to two by grouping the users in sets of four as in the ShuffleNet. By examining the connection graph as shown we see, for example, that stations one and six transmit to stations two and five. If we continue checking the connections, we can have 8 sets of 4 different stations each with two on the transmission side and two on the receiving side where these sets are: (T_1, T_6, R_2, R_5), $(T_2, T_{15}, R_3, R_{14})$, (T_3, T_8, R_4, R_7), $(T_4, T_{13}, R_1, R_{16})$, (T_5, T_{12}, R_8, R_9), $(T_7, T_{10}, R_6, R_{11})$, $(T_9, T_{14}, R_{10}, R_{13})$, $(T_{11}, T_{16}, R_{12}, R_{15})$.

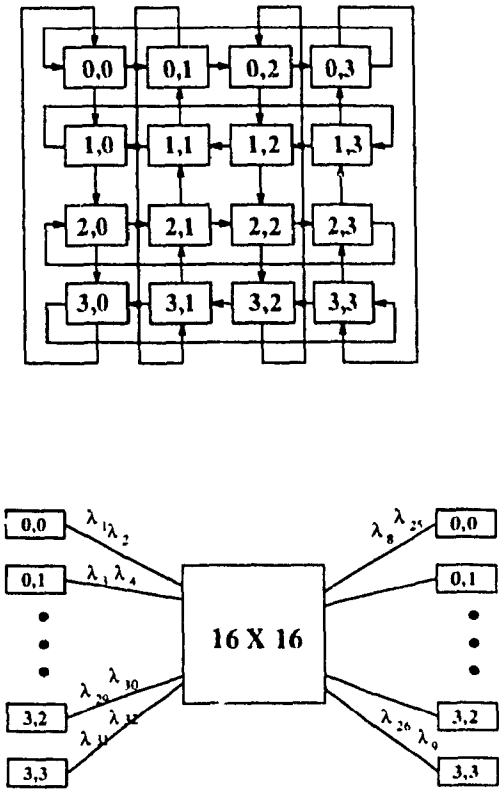

FIGURE 5.4 The logical and physical configuration for a 16-user Manhattan Street Network.

By grouping these stations and using a 2x2 WDM lapped coupler, each station will transmit on two different wavelengths and receive on the same two wavelengths because the same two wavelengths are reused by the other stations in the network on separate fibers. This network will use only two wavelengths. The connection graph is shown in Figure 5.5. The same results obtained in the case of the ShuffleNet are applied to the uni-directional Manhattan street network with different sets and different connections between stations.

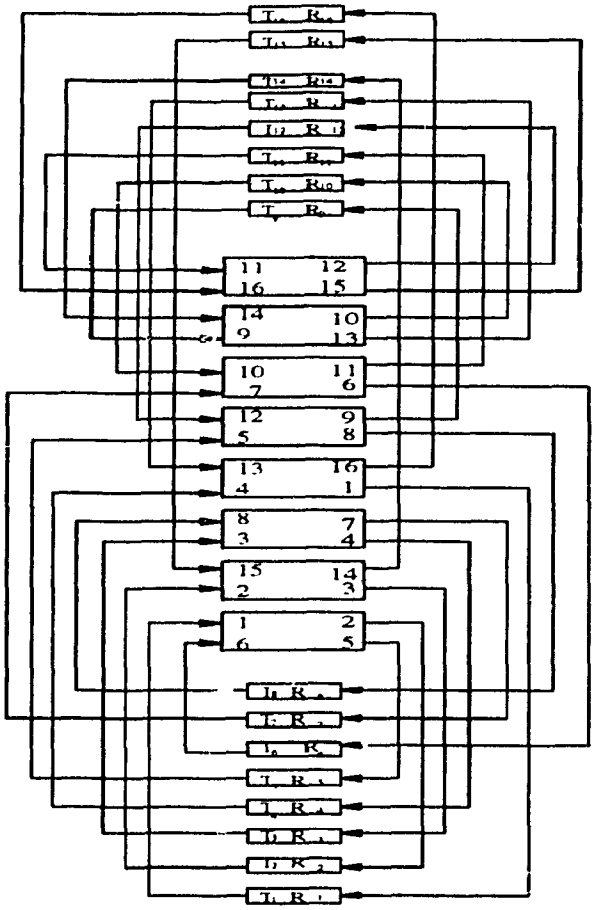

FIGURE 5.5 The implementation of a 16 users MSN using WDM cross-connected star topology.

5.3.3 Bidirectional Manhattan Street Network Implementation

For the case of the unidirectional Manhattan-Street-Network, the reduction of the number of wavelengths from 32 to two used in the conventional method can be affected. We can also apply this result to the case of the bidirectional Manhattan street network where each station can transmit to and receive from the same adjacent station, in contrast to the unidirectional Manhattan street where a station can either transmit to or receive from only one adjacent station. In the case of the bidirectional Manhattan-Street-Network, each station will transmit to four different stations and receive from the same four stations. This is an increase in the connectivity from P=2 to P=4, and this will increase the number

of wavelengths used in the conventional method from 32 wavelengths to 64 wavelengths by using a 16x16 star coupler and 4 different wavelengths for each user.

To reduce the number of wavelengths used in the bidirectional MSN the same technique used in the case of unidirectional MSN can be extended by adding the stipulation that each station can either transmit to or receive from each of the adjacent stations. For a 16 user network this will duplicate the number of 2X2 WDM lapped couplers and each user will have two inputs and two outputs. The first output is connected to a particular 2x2 coupler and the second output to a second 2x2 coupler. Since there are two different out puts coming out from each transmitter and different fibers are used, the same two wavelengths can be reused for each output fiber. In this way, we only use two wavelengths in the network instead of using only one fiber for each output and four wavelengths in the network. In this case, each user has two inputs and two output links each operating on the same two wavelengths λ_1, and λ_2, but different information is transmitted or received per link. The network terminal interface shown in Figure 5.6 is equipped with two inputs and two outputs each operating with the same two wavelengths λ_1, and λ_2.

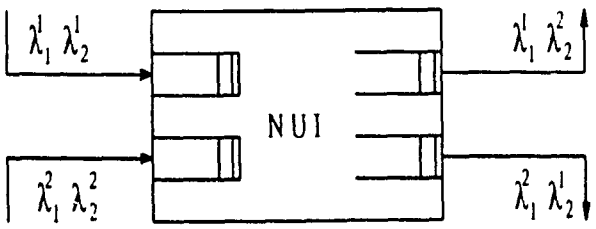

FIGURE 5.6 The network unit interface

The connectivity graph of the network using this kind of network terminal interface is similar to the case of unidirectional MSN. It uses 16 2x2 WDM cross-connect star couplers connected to the corresponding input or output. This configuration uses only two wavelengths in the entire network.

5.3.4 Bidirectional ShuffleNet implementation

The results found earlier show by going from a unidirectional Manhattan street to a bidirectional Manhattan street network, we increase the connectivity between stations. Moreover, by using a slight difference in the network unit interface, we keep the number of wavelengths in the network at two. We can extend these results to the case of ShuffleNet by proposing a bidirectional ShuffleNet. The operation is similar to the bidirectional Manhattan street network in as much as each port can both transmit and receive, simultaneously. This change will increase the connectivity of the network implying an increase in the amount of traffic that can be handled by the network. We also expect a decrease in the expected number of required hops for a message to reach its destination. At the same time, the number of wavelengths in the network can remain the same; only P wavelengths in the network.

As an example, we take the case of a (2, 2) ShuffleNet where we form 4 groups of 4 stations each, these groups are shown in Figure 5.7. Each one of the 4x4 star couplers is made by using eight Bragg-cells, four of which are tuned to λ_1 and four to λ_2. These eight Bragg-cells are arranged in order to have a directional 4x4 WDM cross-connect star coupler as shown in Figure 5.7. The connectivity graph for a (2,2) bidirectional ShuffleNet is shown in Figure 5.8 where each station is equipped with two inputs and two output links.

For the next step, we compute the tree growth for the case of bidirectional ShuffleNet. Our results for a limited set of cases show a clear gain in connectivity which affect the way of reaching a station in the network. In the case of the unidirectional (2, 2) ShuffleNet, station 0, for example, transmits to stations 4 and 5 and receives from stations 4 and 6. For the bidirectional ShuffleNet, this same station will transmit to stations 4, 5, and 6; thereby, allowing it to reach stations 1, 2, and 3 in two hops and station 7 in three hops (see Figure 5.9).

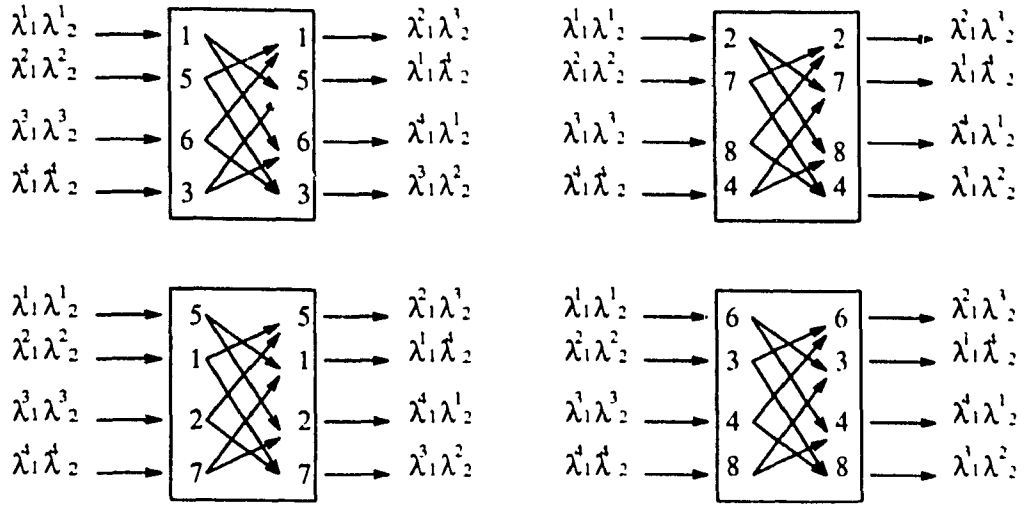

FIGURE 5.7 Bidirectional ShuffleNet connectivity graph arranged in 4 groups.

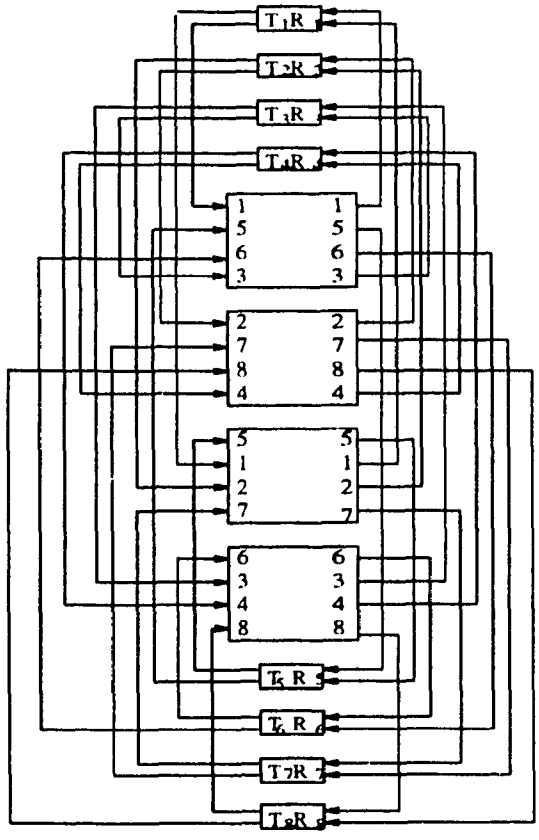

FIGURE 5.8 The connectivity of the bidirectional ShuffleNet using 4x4 WDM cross-connect star coupler.

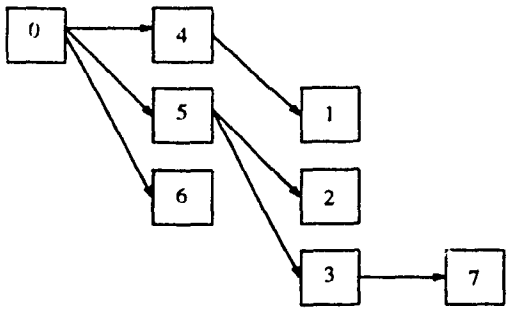

FIGURE 5.9 The tree growth of an 8-users bidirectional ShuffleNet.

This modification in the tree growth for the case of bidirectional ShuffleNet will reduce the value of the expected number of hops which is given by

$$E[hops] = \frac{3+2\times 3+1\times 3}{7} = \frac{12}{7} = 1.714 \tag{5.85}$$

compared to the unidirectional case where the expected number of hops is given by:

$$E[hops] = \frac{2+2\times 3+2\times 3}{7} = \frac{14}{7} = 2 \tag{5.86}$$

This result can be extended to a more general case, to the case of $k=2$ and $\{P=2,3,4,.....\}$. The maximum number of hops is equal to three. The number of stations reached after a certain number of hops is equal to $n(1)=3$, $n(2)=P^k-1$, and $n(3)=P^k-3$ and the expected number of hops will be equal to

$$E[hops] = \frac{5}{2} - \frac{11}{2(N-1)} \tag{5.87}$$

Compared to the normal case we get

$$E[hops] = \frac{5}{2} - \frac{5}{2(N-1)} \tag{5.88}$$

This example shows an improvement in the expected number of hops needed for a message to reach its destination leading to a better performance result in terms of delay as

a function of the throughput traffic. This result is limited to the case of k=2 but more research is under way to find similar results for any k and P.

5.4 Application of WDM Cross-connect to the Bilayered ShuffleNet

The results found for the case of ShuffleNet, in terms of the application of the cross-connect technique in the physical configuration, can be extended to the bilayered ShuffleNet. As an example, we take the case of a (2, 4) bilayered ShuffleNet (64 users). Starting with the conventional case, each station receives from two different stations located in the adjacent column. In the bilayered case, each station will also receive from two other different stations located in the next column. Using the conventional method, the 64 stations can be regrouped into 32 different groups each one with two transmitters from one column and two receivers from the next column by considering only one direction. The same can be obtained in the other direction (32 different groups). These 64 groups can be overlapped; hence, we can use the fact that each station receives from two different stations in one direction and from two other different stations in the other direction to form 16 groups each with four transmitters and four receivers (two from the previous column and two from the next column). These groups are shown in Figure 5.10 implemented in a 4x4 star coupler made by using 16 Bragg-cells, each four of which are tuned to a different wavelength for a total of four wavelengths per star coupler. The same four wavelengths can be reused by other groups for a total of four wavelengths in the entire network. The connectivity for a (2, 4) bilayered ShuffleNet is obtained by properly connecting the inputs to the corresponding outputs.

The implementation of a (2, 4) bilayered ShuffleNet using the WDM cross-connect star topology reduces the total number of noninterfering groups from 32 in the case of the conventional ShuffleNet to only 16 in the case of the bilayered ShuffleNet by using 4x4 groups instead of 2x2 groups. If we turn-off all the links transmitting in the reverse direc-

tion, we will have the same set of noninterfering groups for a conventional ShuffleNet. In terms of stability of the logical and physical topology, the bilayered ShuffleNet performs better because it is very easy to pass from the conventional ShuffleNet to the bilayered ShuffleNet since the same arrangement of the stations in the network is maintained, and by using the WDM cross-connect it is possible to reduce the number of noninterfering groups by a half compared to the conventional case. However, if we compare the case of two ShuffleNets, one with connectivity P and the other with connectivity $2P$ where the number of stations is the same (if it exists), this will require a new arrangement of the network in terms of the logical and the physical topology and the set of the noninterfering groups will not be the same. In summary, we find it is more attractive to use the bilayered ShuffleNet compared to other logical configurations with the same degree of connectivity.

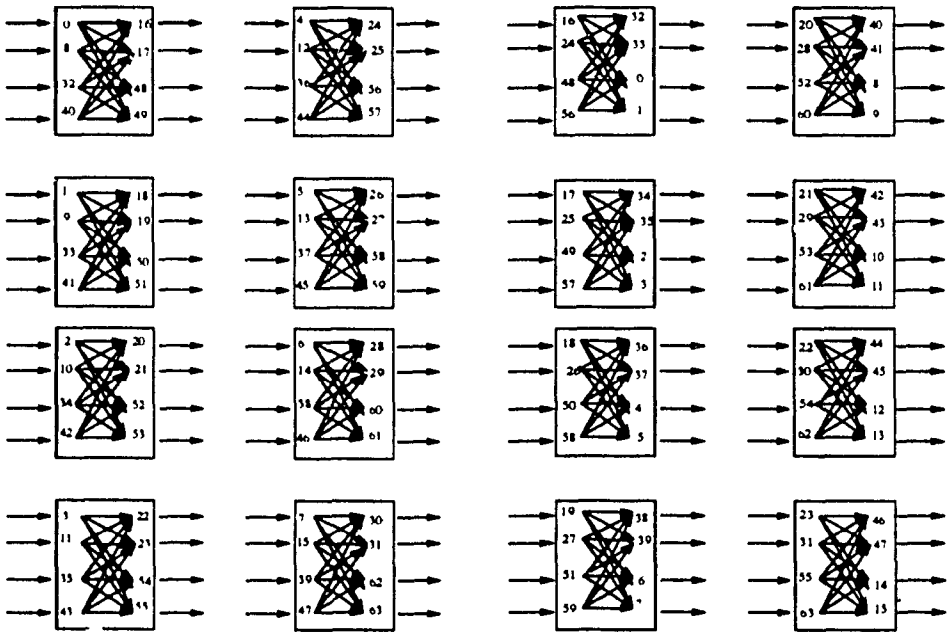

FIGURE 5.10 Bilayered ShuffleNet connectivity arranged in 16 groups.

5.4.1 Implementation of the SR_Net

In this section, we are interested in the application of the cross-connect technique in the physical configuration for the case of a (4, 2, 4) SR_Net. Using the grouping procedure

described in [21], we notice that for each column there are four different stations that transmit to the same four stations in the next column. By doing this, for all the network, the 64 stations can be arranged into 16 noninterfering sets, each set has 4 different transmitters from one column and 4 different receivers from the next column. Each set of eight stations will share a 4x4 WDM star coupler, four on the transmitting side and four on the receiving side. The members of each group connect to each other with no connection between the members of different groups. The same set of four wavelengths used by a specific set can be reused for different groups. This will reduce the number of wavelengths used by the SR_Net to four wavelengths in the whole network. All the 16 groups are shown in Figure 5.11 which are implemented in a 4x4 star coupler made by using 16 Bragg-cells, each four of which are tuned to a different wavelength for a total of four wavelengths per star coupler.

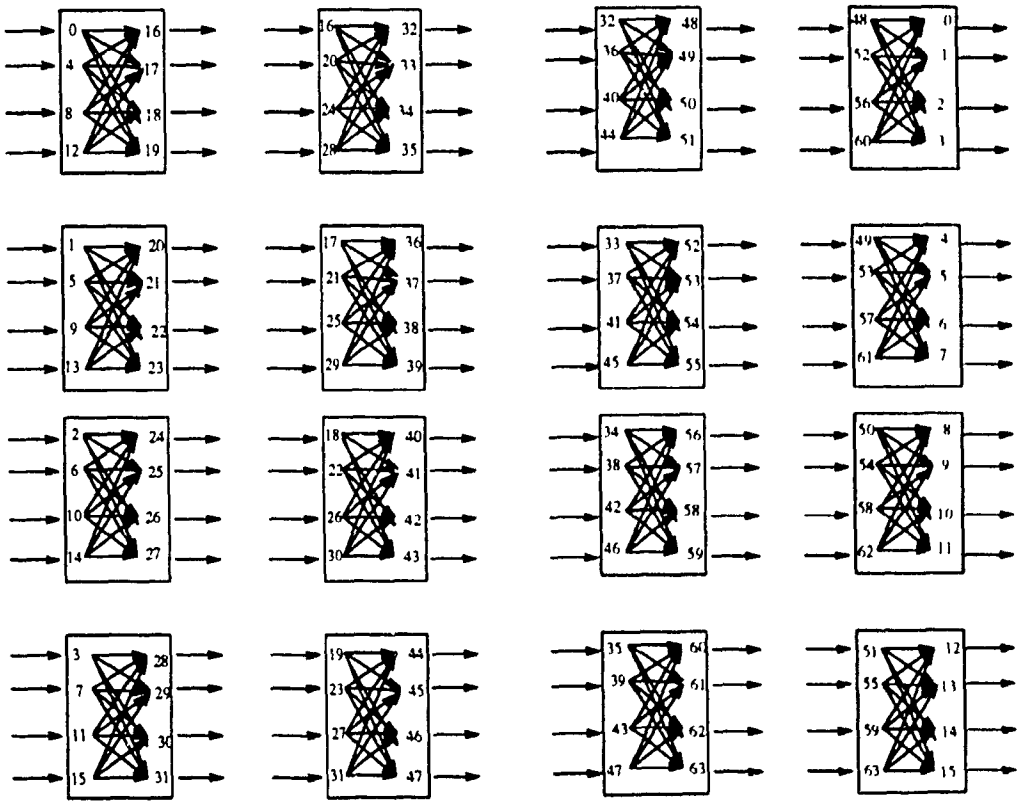

FIGURE 5.11 SR_Net connectivity arranged in 16 groups.

By observing Figures 5.10 and 5.11, we notice that the physical configuration is the same for the bilayered ShuffleNet and the SR_Net. In both cases, the 64 nodes are arranged into 16 noninterfering groups. Each group is implemented in a 4x4 WDM cross connect passive star coupler and a total of four wavelengths are used. The only difference between Figures 5.10 and 5.11 is the mapping of the logical configuration to the physical configuration. The set of noninterfering groups are not the same. For example, the first set for the case of the bilayered ShuffleNet and the SR_Net is composed of (T_0, T_8, T_{32}, T_{40}, R_{16}, R_{17}, R_{48}, R_{49}) and (T_0, T_4, T_8, T_{12}, R_{16}, R_{17}, R_{18}, R_{19}), respectively. This difference is due to the fact that when a different logical configuration is used, the logical mapping of the stations into the physical topology is not the same.

5.5 Adaptive structure based on P_{def}

In order to have improved performance in terms of average number of hops as a function of P_{def}, a new physical configuration should be found in order to accommodate both logical configurations of the bilayered ShuffleNet and the SR_Net. This adaptive configuration will take only the minimum value of the average number of hops from both cases as a function of the probability of deflection. This optimum (adaptive) configuration will be the following:

- For P_{def} less than P_{equ}, the logical configuration of the optimum structure is the same as the SR_Net logical configuration due to the fact that the average number of hops required for a packet to reach its destination in this case is less for the SR_Net than for the bilayered ShuffleNet.
- For P_{def} greater than P_{equ}, the logical configuration of the optimum structure is same as for the bilayered ShuffleNet, because the average number of hops required for a packet to reach its destination in this case is less for the bilayered ShuffleNet than for the SR_Net.

In order to accomodate this adaptivity a central control processor is required in order to measure the deflection probability or more appropriate to measure the traffic load, and to control the process of reconfigurating the network.

5.5.1 Network re-configuration

As shown in Section 2, the bilayered ShuffleNet and the SR_Net have the same physical topology which consists of 16 4x4 WDM passive star cross-connects. The only difference is the logical mapping of different stations in this physical topology. In order to verify if this physical configuration can handle both logical configurations, we map the logical configuration of the bilayered ShuffleNet into the SR_Net configuration. In this case, instead of assuming that each station will transmit to two different stations in the next column and to two other stations in the previous column, we assume each station will transmit to four different stations in the next column and follow the same set of logical connection as the SR_Net. By selecting the first eight noninterfering groups of the bilayered ShuffleNet and mapping them as an SR_Net, we form a new arrangement for the network. The first column will be formed by stations (0, 1, 2, 3, 8, 9, 10, 11, 32, 33, 34, 35, 40, 41, 42, 43), the second column by stations (16, 17, 18, 19, 20, 21, 22, 23, 48, 49, 50, 51, 52, 53, 54, 55), the third column by (4, 5, 6, 7, 12, 13, 14, 15, 36, 37, 38, 39, 44, 45, 46, 47) and finally the fourth column by (24, 25, 26, 27, 28, 29, 30, 31, 56, 57, 58, 59, 60, 61, 62, 63). This arrangement is made in order to maintain the same logical and physical arrangement of the eight groups. The mapping of the physical implementation of this eight groups into a logical SR_Net structure is shown in Figure 5.12. As an example, stations 0, 8, 32, and 40 are always transmitting to stations 16, 17, 48, and 49 for the case of bilayered ShuffleNet and SR_Net. This result is true for the first eight groups.

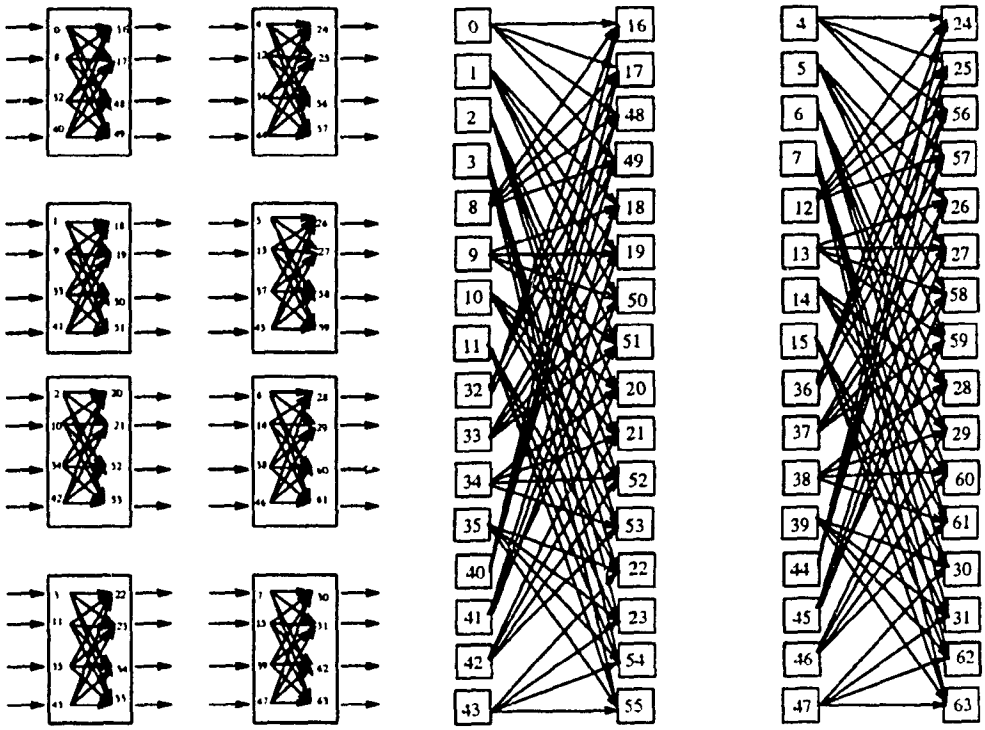

FIGURE 5.12 The mapping of the first eight groups of the bilayered ShuffleNet into SR_Net

In the next step, we try to map the logical connection between columns two and three and between columns four and one into a set of eight non-interfering group and compare them with the already existing groups (group 6-16 of the bilayered ShuffleNet). This is shown in Figure 5.13. The groups found are different from the existing ones. This means that it is impossible to keep the same physical configuration for all remaining groups (group 9-16). As an example, stations 16, 24, 48, and 65 should be connected to stations 32, 33, 0 and 1 in the bilayered ShuffleNet, but, by using the logical configuration of the SR_Net stations these connections are impossible and a new group is formed by stations 16, 18, 20 and 22 that connect to stations 4, 5, 6 and 7. The rearrangement of the last eight groups in order to accommodate the SR_Net logical configuration is shown in Figure 5.13. By making this rearrangement, the bilayered ShuffleNet will become an SR_Net.

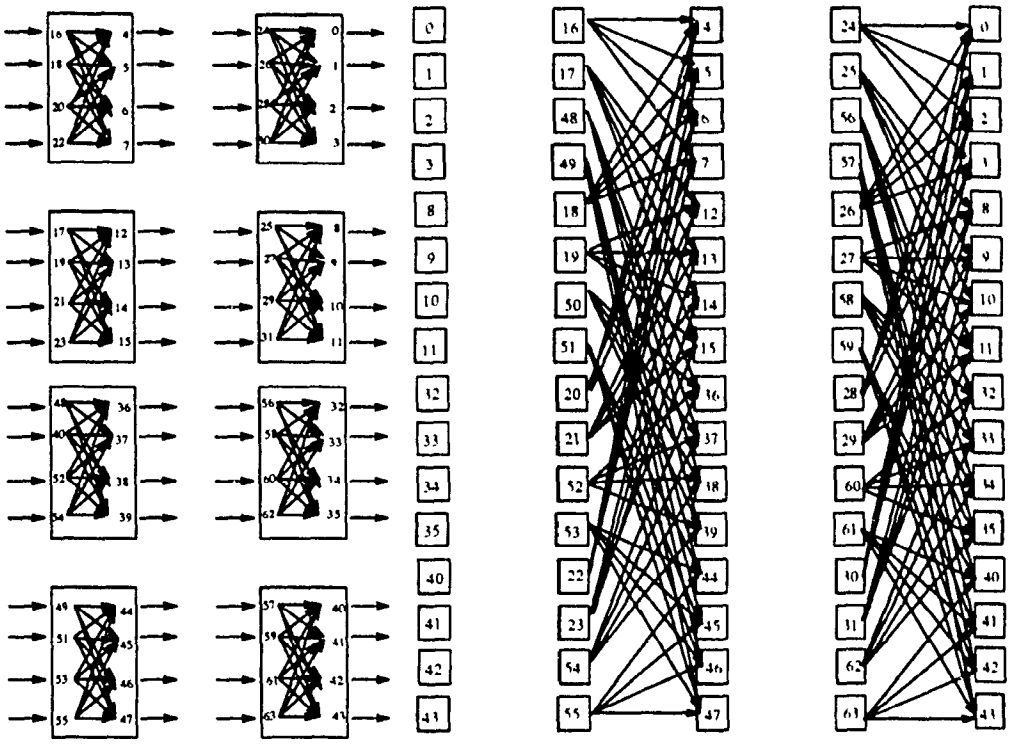

FIGURE 5.13 The mapping of the logical connection into eight noninterfering groups

5.5.2 Physical implementation

The physical implementation of this adaptive configuration will require a certain modification of the original topology formed by 16 4x4 WDM cross-connects in order to accommodate both network configurations: the bilayered ShuffleNet and the SR_Net. The results found in the previous section show that this modification will affect only half the network. The other half will remain the same. In order to accommodate this change in the network configuration, two solutions can be proposed. First, the use of a passive star coupler will accommodate any change in the logical configuration for the last eight groups. This will require a 32x32 passive star coupler and a total of 128 wavelengths. The physical topology in this is shown in Figure 5.14 and requires a total of 8 4x4 WDM cross-connects and a 32x32 passive star coupler. Second, the use of two different sets, each set with a total of 8 4x4 WDM cross-connect star couplers in addition to the existing ones, one set

is used when the bilayered ShuffleNet configuration is required and the other set for SR_Net configuration. The physical configuration is shown in Figure 5.15 requiring a total of 24 4x4 WDM cross-connect star couplers. Each user in the unchanged set will be equipped with two transmitters if it is connected to the transmitting side or with two receivers if it is connected to the receiving side. In this case, the optimum configuration will not require tunable receivers or transmitters because the same physical topology in terms of using 16 4x4 WDM cross-connect star couplers is used for each case. In this physical configuration, each user is equipped with the same four wavelengths as any other user in the network. By switching from one set to the next we pass from one configuration to another and there is no need for a new wavelength assignment. Only a logical assignment of stations that share the same set exists.

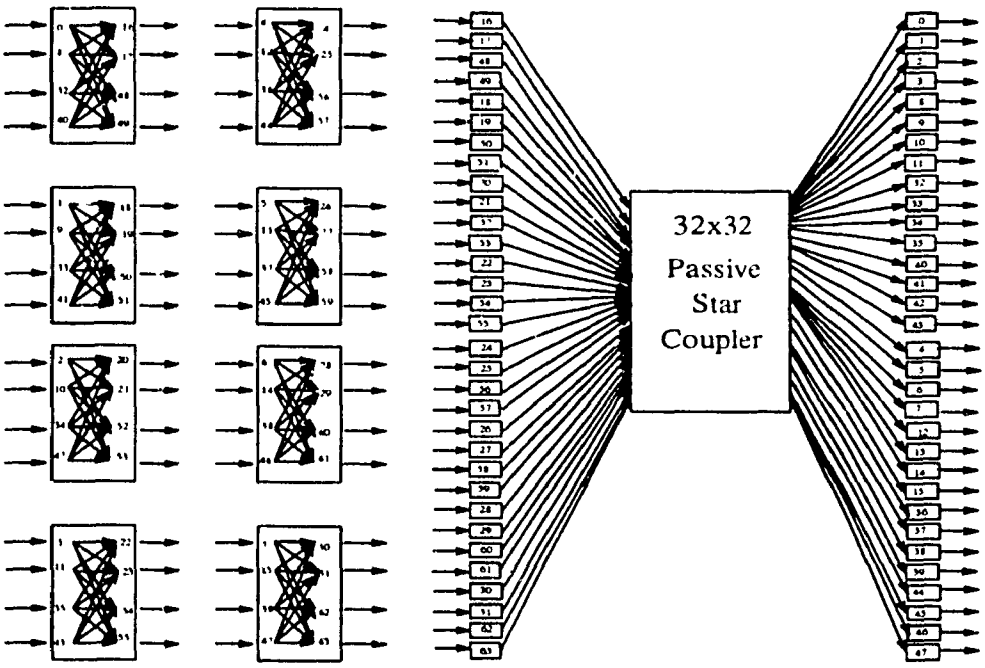

FIGURE 5.14 The first physical implementation for the optimum configuration

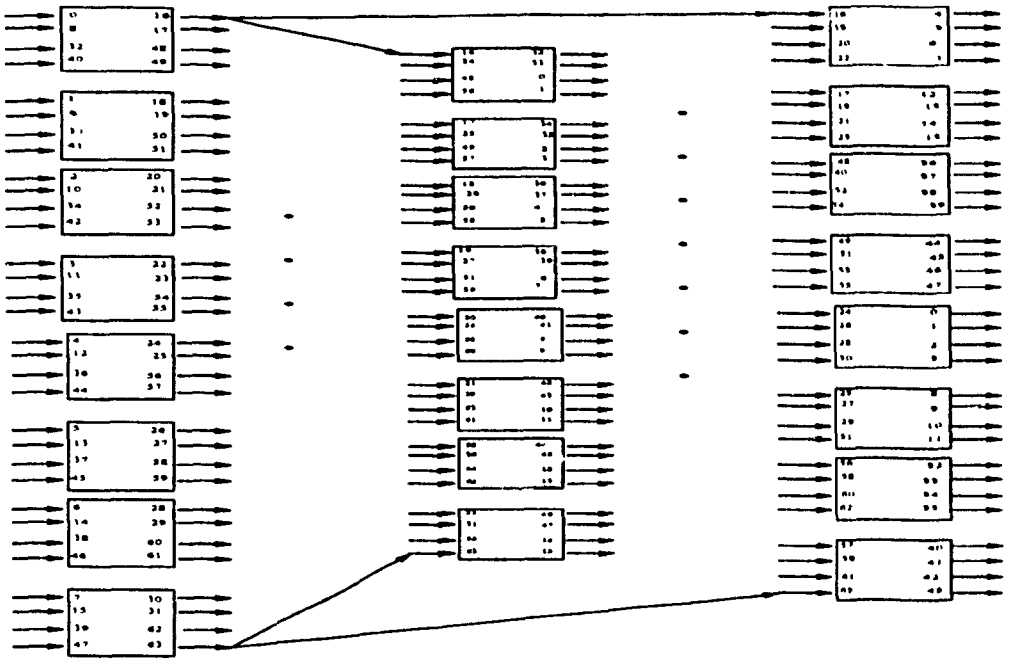

FIGURE 5.15 The second physical implementation for the optimum configuration

5.6 Discussion

The WDM cross-connect can be used in the physical implementation of different networks such as the ShuffleNet, the MSN, the bilayered ShuffleNet and the SR_Net. For the adaptive configuration this is still possible but this will require a complicated physical topology or a combination of two different physical configurations such as the star and a set of WDM cross-connects. The implementation of an adaptive configuration using only the WDM cross-connect, which maps three or more logical configurations can be very complicated. In this case, the choice of a conventional configuration such as the star, the tree or the bus will be the appropriate solution.

This will bring us to the case of systems using the basic physical configuration where all nodes can communicate with each other within a single hop, this correspond to single hop systems. In the next chapter, we will focus on the use of optical CDMA in single-hop systems.

Chapter VI

The Use of CDMA in Optical Networks

One possible application of spread spectrum techniques that has been discussed in the literature is code division multiple access (CDMA). In such a system, a group of individual signals can be multiplexed onto a common communication medium via a set of orthogonal codes. In optical networks the number of available orthogonal codes is limited, this automatically limits the number of users in such networks. One way to increase the number of users in an optical LAN using optical CDMA is to use a hybrid WDMA/ CDMA (wavelength-division multiple access/code division multiple access) system where the spread-spectrum technique allows multiple users sharing the same wavelength. In the following we propose an enhancement of this approach, which increases the number of users in the network. In this approach, known as partial CDMA, a number of users share the same spread spectrum code. This can be presented as a network where all system users are grouped into clusters and all users in the same cluster are grouped into cells assuming that all users in a given cell use the same spread spectrum code. In this case, we increase the number of users in the network without requiring the addition of more receivers. The increase in the number of users with this new scheme can be obtained at the price of a reduction in the throughput. However, with an appropriate choice of system parameters, the throughput reduction can be made insignificant compared to the increase in the number of users.

In the following, we give an introduction to spread spectrum in multiuser networks, then we show how CDMA is used in optical networks due to the requirement of new sets of optical orthogonal codes different from the conventional codes. Finally, we end this chapter by showing the performance calculation in terms of the throughput of the new proposed system configuration for overcoming the limitation in the number of users of an optical network.

6.1 Introduction to Spread Spectrum in Multiuser Networks

Spread-Spectrum techniques are used to solve a wide range of communications problems. Among these problems we mention the fact of suppressing the effect of interference related to jamming, interference arising from other users of channel, and self-interference due to multipath propagation. Spread-spectrum can be used to hide a signal by transmitting it at low power and making it difficult for an unintended listener to detect it in presence of background noise. Finally, spread-spectrum is used to achieve message privacy in presence of other listeners.

Interference from other users arises in multiple-access communications systems where a number of users share a common channel. At any given time, a group of these users may transmit information simultaneously over the common channel to corresponding receivers. Assuming that all users employ the same code for the encoding and decoding of their respective information sequences, the transmitted signals in this common spectrum may be distinguished by superimposing a different pseudo-random pattern, also called a code, on each transmitted signal. Thus, a particular receiver can recover the transmitted information intended for it by knowing the pseudo-random pattern, i.e., the key, used by the corresponding transmitter. This type of communication technique, which allows multiple users to simultaneously use a common channel for transmission of information, is called code division multiple access (CDMA).

The most common form of CDMA is Direct-Sequence Spread-Spectrum Multiple Access (DS/SSMA) in which each user is assigned a particular code sequence modulating the carrier along with the digital data. The DS/SSMA techniques are characterized by the effect of spreading the bandwidth of the data signal.

In order to understand how a spread-spectrum multiple access system operates, it is necessary to know the required properties of the direct sequence code.

6.1.1 Properties of Direct Sequence Code

Spread-spectrum communications systems require sets of signals that have the following two properties:

1. each signal in the set is easy to distinguish from a time-shifted version of itself;

2. each signal in the set is easy to distinguish from a possible time-shifted version of every other signal in the set.

The signals of interest for this particular application are periodic signals, which consist of sequences of time-limited pulses. The periodicity allows simplifications in system implementation. These pulses are all of the same shape, so that the signal can be written as

$$x(t) = \sum_{n=-\infty}^{+\infty} x_n P_{T_c}(t - nT_c) \tag{6.89}$$

where P_{T_c} is a unit amplitude rectangular pulse and T_c is the time duration of this pulse. If $x(t) = x(t+T)$ for all t, then T must be a multiple of T_c and the sequence (x_n) must be periodic with a period which is a divisor of T/T_c. Suppose $x(t)$ and $y(t)$ are periodic signals, as described above. One of the most common and most useful measures of distinguishability between two signals is the mean-square difference. In order for the two signals $x(t)$ and $y(t)$ to be very easy to distinguish, the mean-squared differences between

them should be very large. It is not only required that $x(t)$ be easy to distinguish from $y(t)$ bu· also $-x(t)$ be easy to distinguish from $y(t)$. The measure of distinguishing for this case is given by

$$T^{-1}\int_0^T [y(t) \pm x(t)]^2 dt = T^{-1}\left\{\int_0^T [y^2(t) + x^2(t)]\, dt \pm \int_0^T x(t)\, y(t)\, dt\right\} \tag{6.90}$$

The first integral on the right-hand side of the above equation is the energy in $x(t)$, $0 \le t \le T$, plus the energy in $y(t)$, $0 \le t \le T$. Thus for a fixed signal energy, $y(t)$ is easy to distinguish from both $+x(t)$ and $-x(t)$ if and only if the magnitude of the quantity

$$r = \int_0^T x(t)\, y(t)\, dt \tag{6.91}$$

is small.

For $y(t)$ given by

$$y(t) = \sum_{n=-\infty}^{+\infty} y_n P_{T_c}(t - nT_c) \tag{6.92}$$

it is easy to show that r is given by

$$r = T_c \sum_{n=0}^{N-1} x_n y_n \tag{6.93}$$

In general, according to the above equation, the inner product of the continuous time periodic signal $x(t)$ and $y(t)$ is proportional to the inner product of the corresponding vectors $(x_0, x_1, \ldots, x_{N-1})$ and $(y_0, y_1, \ldots, y_{N-1})$. Furthermore, if $\tau = lT_c$, equation (6.93) generalizes to

$$r_{x,y}(\tau) = T_c \sum_{n=0}^{N-1} x_n y_{n+l} \tag{6.94}$$

The above discussion motivates the consideration of the periodic crosscorrelation function for sequences (x_n) and (y_n), which is defined by

$$\theta_{x,y}(l) = \sum_{n=0}^{N-1} x_n y_{n+l} \tag{6.95}$$

From equation (6.94), we see that $r_{x,y}(\tau) = T_c\theta_{x,y}(l)$ whenever $\tau = lT_c$. In addition, for arbitrary values of τ, $r_{x,y}(\tau)$ can be determined from the periodic crosscorrelation function. For instance, for $0 \le \tau \le T$,

$$r_{x,y}(\tau) = T_c\theta_{x,y}(l') + (\tau - l'T_c)\,[\theta_{x,y}(l'+1) - \theta_{x,y}(l')] \tag{6.96}$$

where l' is the largest integer such that $l'T_c \le \tau$.

Since the periodic crosscorrelation parameters for the continuous-time signals $x(t)$ and $y(t)$ of equations (6.91) and (6.92) are completely determined by the crosscorrelation function, the signal requirements described at the beginning of this section reduce to the problem of having sets of periodic sequences with the following two properties:

3. for each sequence $x = x(n)$ in the set, $|\theta_{x,x}(l)|$ is small for $1 \le l \le N-1$.

4. for each pair of sequences $x = x(n)$ and $y = y(n)$, $|\theta_{x,y}(l)|$ is small for all l.

In the following, we will discuss different properties of several classes of sequences such as m-sequences and Gold sequences.

6.1.1.1 Properties of m-sequences

The sequences that have received the most attention in the literature are binary maximal-length linear feedback shift-register sequences, which we refer to as m-sequences. As the title suggests these are precisely the sequences of maximum possible period $N = 2^n - 1$ from an n-stage binary shift-register with a linear feedback. Let $h(x) = h_0x^n + h_1x^{n-1} + \ldots + h_{n-1}x + h_n$ denote a binary polynomial of degree n where

$h_0 = h_n = 1$ and the other h_i's take on values 0 and 1. A binary sequence u is said to be a sequence generated by $h(n)$ if for all integers j

$$h_0 u_j \oplus h_1 u_{j-1} \oplus \ldots \oplus h_n u_{j-n} = 0 \tag{6.97}$$

Here $\oplus$ denotes modulo 2 addition (i.e., the EXCLUSIVE-OR operation). Replacing j by $j+n$ in the above equation, and using the fact that $h_0 = 1$, we obtain

$$u_{j+n} = h_n u_j \oplus h_{n-1} u_{j+1} \oplus \ldots \oplus h_1 u_{j+n-1} \tag{6.98}$$

From this, it follows that the sequence u can be generated by an n-stage binary linear feedback shift register. For example, the shift register in Figure 6.1 corresponds to $h(x) = x^5 + x^4 + x^3 + x^2 + 1$.

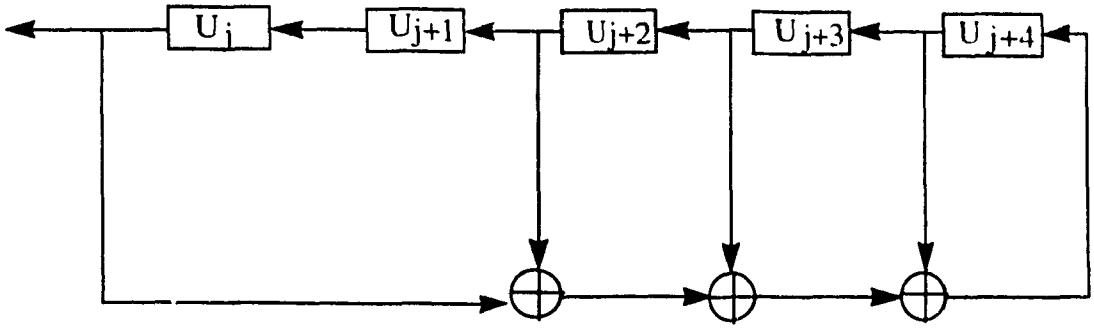

FIGURE 6.1 Maximal length sequence generator

An n^{th}-order polynomial $h(x)$ is irreducible if it is not divisible by any polynomial of degree less than n but greater than 0. The period of sequence u generated by polynomial $h(x)$ is at most $N = 2^n - 1$. If $h(x)$ is an irreducible polynomial of degree n, sequence u has a maximal period $N = 2^n - 1$ and is called an m-sequence, and $h(x)$ is called a primitive binary polynomial of degree n.

Some properties of m-sequences that are useful in their application to spread spectrum are listed below:

1. The period of an m-sequence u is $N = 2^n - 1$.

2. There are exactly N nonzero sequences generated by $h(x)$, and they are just the N different phases of u; namely $u, Tu, T^2u, \ldots, T^{N-1}u$.

3. Given distinct integers i and j, $0 \le i,\ j \le N$, there is a unique integer k, distinct from both i and j, such that $0 \le k \le N$ and $T^i u \oplus T^j u = T^k u$. This property is known as the shift-and-add property.

4. A maximal-length sequence contains an additional "one" compared to the number of "zero". The number of ones in the sequence is equal to $\frac{1}{2}(N+1)$

5. The periodic autocorrelation function $\theta_u(l)$ is two-valued and is given by:

6. $$\theta_u(l) = \begin{cases} N, & \text{if } l \bmod N = 0 \\ -1, & \text{if } l \bmod N \neq 0 \end{cases}$$

7. Let u and v denote m-sequences of period $N = 2^n - 1$. The crosscorrelation function $\theta_{u,v}(l)$ is equal to $\theta_{u,v}(l+N)$ and $|\theta_{u,v}(l)| \le N$ for all l. Moreover, $\sum_{l=0}^{N-1} \theta_{u,v}(l) = 1$ and $\sum_{l=0}^{N-1} |\theta_{u,v}(l)|^2 = N^2 + N - 1$.

6.1.1.2 Gold Sequences

One important class of periodic sequences that provides larger sets of sequences with good periodic crosscorrelation is the class of Gold sequences [38]. A set of Gold sequences of period $N = 2^n - 1$ consists of $N+2$ sequences for which the periodic autocorrelation function has the maximum value:

$$\theta_{max} = t(n) = 1 + 2^{\lfloor (n+2)/2 \rfloor} \tag{6.99}$$

where $\lfloor y \rfloor$ denotes the integer part of the real number y. Thus, for instance, each class of 129 Gold sequences of period 127 has a correlation bound of 17. In contrast, the largest possible set of m-sequences of period 127 for which this bound holds contains only 6

sequences. Gold sequences have a three-valued correlation function taking on values from $\{-1, -t(n), t(n)-2\}$. A set of Gold sequences can be constructed from appropriately selected m-sequences as described below.

Suppose a shift register polynomial $f(x)$ factors into $h(x)\,\hat{h}(x)$ where $h(x)$ and $\hat{h}(x)$ have no factors in common. Then the set generated by $f(x)$ is just the set of all sequences of the form $\alpha \oplus \beta$ where α is generated by $h(x)$ and β is generated by $\hat{h}(x)$. Now suppose, $h(x)$ and $\hat{h}(x)$ are two different primitive binary polynomials of degree n that generate the m-sequences u and v, respectively, of period $N = 2^n - 1$ respectively. If y denotes a nonzero sequence generated by $f(x) = h(x)\,\hat{h}(x)$, then, from the above and the second property of m-sequences, we get either $y = T^i u$ or $y = T^j v$ or $y = T^i u \oplus T^j v$, where $0 \le i, j \le N-1$ and $T^i u \oplus T^j v$ denotes the sequence whose k^{th} element is $u_{i+k} \oplus v_{j+k}$. From this, it follows that y is a phase of some sequence in the set $G(u, v)$ defined by

$$G(u, v) = \{u, v, u \oplus Tv, u \oplus T^2 v, \ldots, u \oplus T^{N-1} v\} \qquad (6.100)$$

Note that, $G(u, v)$ contain $N+2 = 2^n - 1$ sequences of period N. It is not difficult to show that if we have two sequences y_1 and y_2 generated by $f(x)$, then $T^i y_1 \otimes T^j y_2$ is a phase of some sequences of this set.

As we have stated earlier, each sequence with element {0, 1} represented by the sequence $\alpha = (\alpha_0, \ldots, \alpha_{N-1})$ is mapped into a sequence with element {1, -1} represented by the sequence $a = (a_0, \ldots, a_{N-1})$ where $a_i = (-1)^{\alpha_i}$ for $0 \le i \le N-1$; then, adding modulo-2 of the sequences with elements {0, 1} corresponds to multiplying of the sequences with elements {1, -1}. Therefore, from the above, product of two Gold sequence with an arbitrary shift is still another Gold sequences from the same set. This means, the shift-and-add property also holds for Gold sequences.

As an example, take n = 7, the polynomials 211 and 217 are a preferred pair of primitive polynomials. Their product is the polynomial

$$\begin{aligned} f(x) &= (x^7 + x^3 + 1)\ (x^7 + x^3 + x^2 + x + 1) \\ &= x^{14} + x^9 + x^8 + x^5 + x^4 + x^2 + x + 1 \end{aligned} \tag{6.101}$$

which is represented in octal by 41567, as illustrated in Figure 6.2.

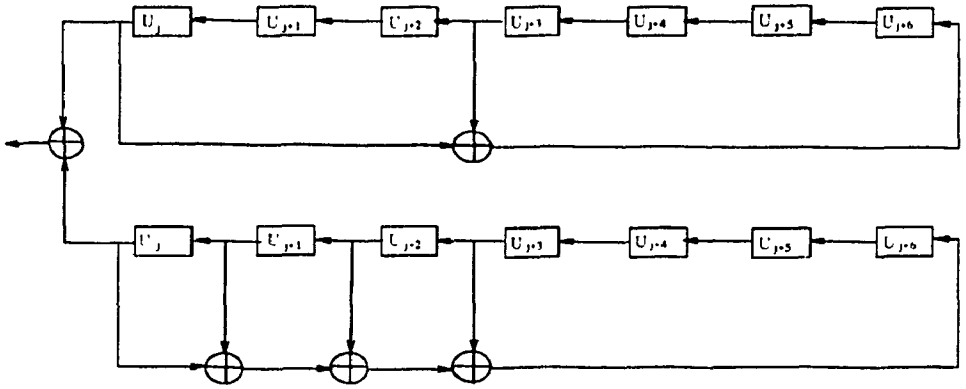

a) Double Shift-Registers Representation

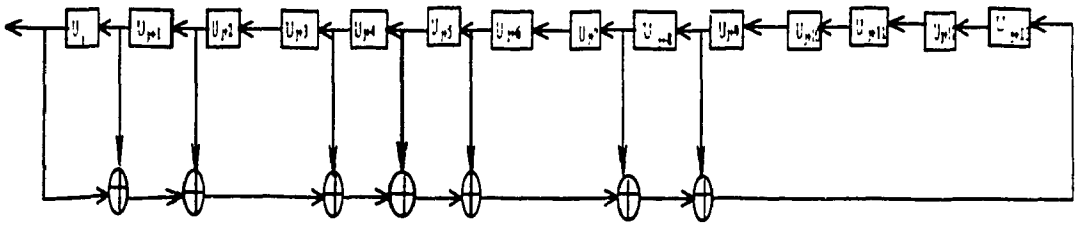

b) Single Shift-Registers Representation

FIGURE 6.2 Gold code generation

According to Gold's theorem, in this design, the corresponding shift register will generate 129, i.e., $2^7 + 1$ different linear sequences of period length 127, i.e., $2^7 - 1$. The maximum correlation valued for this set of sequences is 17. The generated codes in this

example have a three-valued autocorrelation function and a three-valued crosscorrelation taking values from the set (-1, -17, 15).

6.2 Optical CDMA

Optical code division multiple access (CDMA) has been proposed as another alternative to take advantage of large bandwidth of single-mode fiber. It maps low-information-rate electrical or optical signals into high-rate optical sequences to achieve random, asynchronous multi-access among many users [39]. In the following, we will describe the choice of such sequences for optical networks.

6.2.1 Noncoherent Optical CDMA Sequence Design

Optical processing will increase the processing speed, will allow more users in the network (large N) and will increase the capacity of the network. However, a fundamental difference exists between optical processing and conventional processing, which may use tapped delay lines, for example. Using noncoherent optical processing, the levels in the transmitted optical code sequence correspond to light pulses "ON" or "OFF" levels. This corresponds to a 1 or a 0 for the value of the taps of the optical correlator. Using conventional processing, the level of the transmitted code sequence corresponds to a positive or a negative voltage and the taps are equal to +1 or -1. The resulting difference between the conventional processing and the optical processing is shown in Figure 6.3. For this correlator, the peak of the autocorrelation function is equal to the number of 1's in the code sequence. The peak of the cross-correlation functions is equal to the maximum number of coincidences of 1's in all the shifted versions of the two code sequences. For this reason, a new set of code sequences with fewer coincidences of 1's is needed for optical processing. Codes or sequences that can be used in fiber-optic communication systems would not necessarily maintain the same properties once correlated with 0/1 sequences. Therefore, there

is a need for a new class of signature sequences with fewer coincidences of 1's. Two possible classes of optical codes can be taken into consideration.

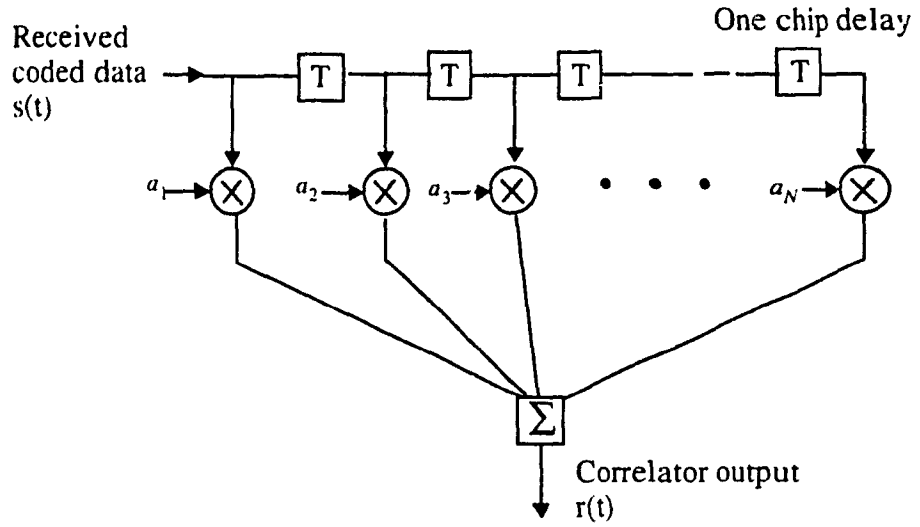

FIGURE 6.3 Block diagram of the correlation process for either conventional processing or optical processing. The coefficients a_i take the values +1 or -1 for conventional processing and the values 1 or 0 for optical processing.

The first candidate is a set of Prime codes of length $N = P^2$ derived from prime sequences of length P obtained from Galois field GF(P), where P is a prime number [27]. The performance of this code in terms of simultaneous users with N=121 and using optical processing is compared to Gold codes, which provide a larger set of orthogonal codes $N = 2^n - 1$ by using an n-stage binary linear feedback shift register and using conventional processing with N=127. The result of this is shown in Figure 6.4. The signal-to-interference ratio (SIR) (interference is from multi-user transmission), for the Gold code using conventional processing is given by [27]:

$$SIR = 4\left[\frac{N^3}{(K-1)\,(N^2+N-1)}\right] \tag{6.102}$$

and for Prime code using optical processing the SIR is given by [27]:

$$SIR = \frac{1}{0.29}\left[\frac{N}{(K-1)}\right] \tag{6.103}$$

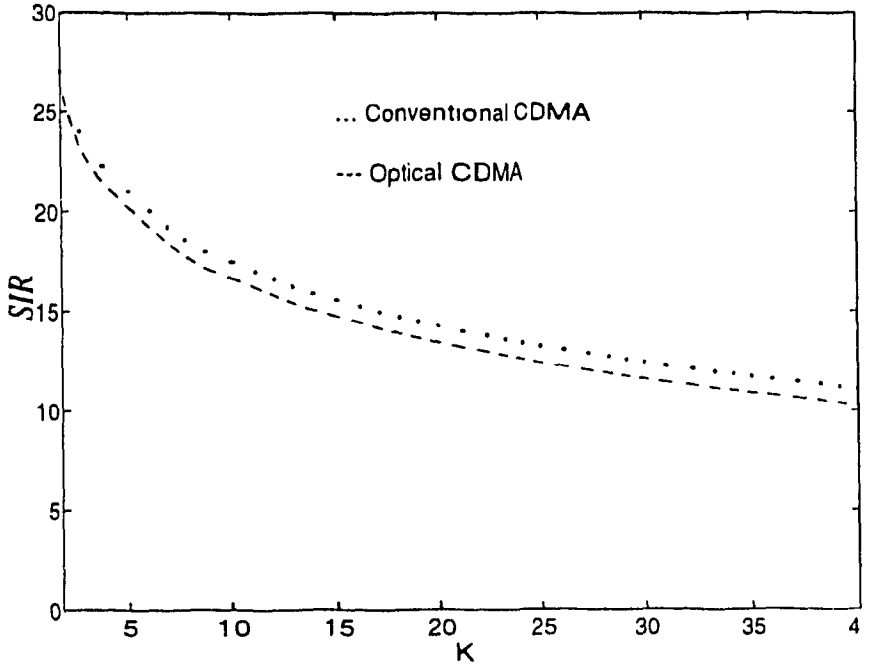

FIGURE 6.4 Signal-to-Interference ratio versus number of simultaneous users both for conventional processing using Gold sequences of length N=127 (upper curve) and for optical processing using prime code sequences of length N=121 (lower curve).

The second new class of codes is called "Optical Orthogonal Codes", or OOC's for positive systems or specially for fiber-optic CDMA systems [39]. In general, an (F, M, λ_a, λ_c) optical orthogonal code [39], [40], is a family of (0, 1) sequences of length F and weight M with auto- and cross-correlation constraints λ_a and λ_c. In this case, M is the number of 1's in the sequence. For a given integer number F (code length) and weight M where $M(M-1) \leq F-1$ and $\lambda_a = \lambda_c = 1$, one can construct at most N OOC's, where N is upper bounded by [39]

$$N \leq \left\lfloor \frac{F-1}{M(M-1)} \right\rfloor \tag{6.104}$$

where the symbol $\lfloor x \rfloor$ denotes the integer portion of the real value x. The rules for constructing families of N OOC's have been described in [39], [40]. Figure 6.5 shows two

OOC's, A and B, with a length of $F = 32$ and a weight of $M = 4$, such that $\lambda_a = \lambda_c = 1$ are constructed.The first code A as shown in Figure 6.5a is represented by placing a pulse at the 1st, 10th, 13th, and 28th chip positions. This code is designated as {1, 10, 13, 28}. The second code B shown in Figure 6.5b is represented by placing a pulse at the 1st, 5th, 12th, and 31st chip positions; the code is designated as {1, 5, 12, 31}. One bit of information T is divided into 32 equal chip times T_c, i.e., $F = T/T_c = 32$. The "fundamental rules" that ensure OOC's A and B to have periodic autocorrelation peak (K) and low periodic correlation ($\leq \lambda_a$) at any other time shift, with T_c as the unit of time shift, can best be explained from set theory (see [40]). From the above example, a maximum of two codes can be constructed by choosing $F = 32$ and $M = 4$. For a large value of F (F =1000) at most 84 OOC's can be constructed under the condition of $\lambda_a = \lambda_c = 1$ [62].

Based on the same technique, a new set of codes called the temporal codes can be constructed. These codes are based on the fact that the auto- and the cross-correlation sidelobes are bounded by 2 ($\lambda_a = \lambda_c = 2$). In this case, the constraint on the number of users becomes [62]

$$N \leq \frac{(F-1)\,(F-2)}{M\,(M-1)\,(M-2)} \tag{6.105}$$

which is considerably higher than for OOC. For the same parameters mentioned above (F = 1000, M = 4), a maximum of 41 500 codes can be constructed compared to only 84 in the first case. It is shown [62] that the temporal codes may increase the number of users in the network considerably without a significant loss in the performance.

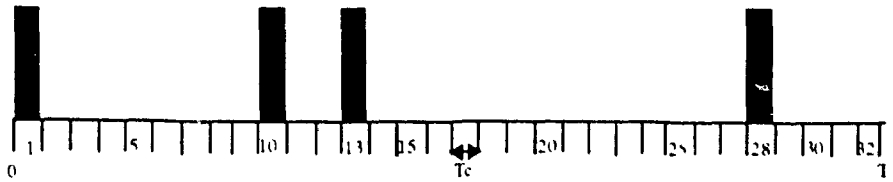

(a)

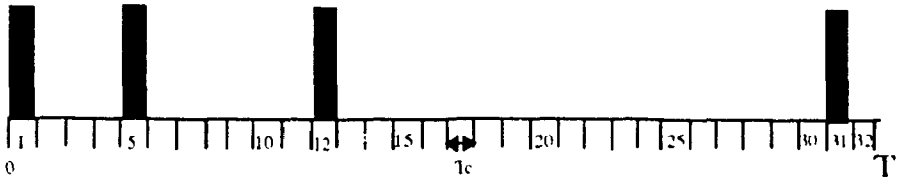

(b)

FIGURE 6.5 Two optical orthogonal codes.

6.2.2 Coherent Optical CDMA

The use of CDMA to address a multiplicity of users in a coherent optical network was proposed in [63] and the feasibility of spreading-despreading using a Mach-Zehnder electro-optic modulator was demonstrated in [64]. The modulation schemes, namely binary phase-shift keying (PSK) and on-off keying (OOK) can be used as in [65]. This coherent optical CDMA scheme employs some other orthogonal codes. These codes are well-correlated binary sequences due to using +1/-1 sequences. The correlation constraint can be made zero. Furthermore, a well-correlated +1/-1 sequence typically has about the same number of +1's and -1's while a good optical orthogonal code has many more 0's than 1's in each codeword [66] The Gold code, which uses a +1/-1 sequence and takes advantage of the well-correlated sequence provides a large set of sequences, a total of $N + 2$ sequences ($N = 2^n - 1$) for each sequence of period N. As an example, for $N = 31$ ($n = 5$) a total of 32 different sequences can be constructed using Gold codes with coherent detection compared to only 5 OOC using the same sequence length with direct detection. Using

coherent detection as in PSK, lack of "negative components" is no longer a limitation for the optical transmission technology and this will allow us to use the well-correlated +1/-1 sequences that offer a larger set of orthogonal codes with the same number of chips as the Gold codes.

6.2.3 Optical CDMA by Spectral Encoding of LEDs

An optical CDMA system based on amplitude spectral encoding of low-cost broad-band sources such as light-emitting-diodes (LED) requires only standard optical elements and simple direct-detection receivers [67], [68]. It is shown that by using a single unipolar m-sequence of period N and by assigning the N cycle shifts of this sequence to N different subscribers, a complete orthogonality between the users can be achieved provided that the spectrum is properly equalized. For $N = 511$, up to 200 users can transmit asynchronously with an average error probability equal to 10^{-9}[67]. Furthermore, since the spectral width of an LED is independent of the modulating signal, the so-called spreading gain is independent of the data rate, a major advantage in CDMA systems.

The schematic diagram of this system is shown in Figure 6.6. All users are connected through a passive star coupler. A simple unipolar m-sequence is used in order to encode the spectrum of LED's. The autocorrelation of the unipolar sequence $(x) = (x_0, x_1, ..., x_{N-1})$ of period N is equal to [67]:

$$\Theta_x(k) = \sum_{i=0}^{N-1} x_i x_{i+k} \tag{6.106}$$

resulting in a $\Theta_x(0) = (N+1)/2$ for $k = 0$ and $\Theta_x(k) = (N+1)/4$ for $k = 1$ to $N - 1$. A receiver that computes:

$$Z = \sum_{i=0}^{N-1} x_i x_{i+k} - \sum_{i=0}^{N-1} (1 - x_i) x_{i+k} = 2\Theta_x(k) - \Theta_x(0)$$
$$= 2 \times (N+1)/4 - (N+1)/2 = 0 \tag{6.107}$$

will reject the signal coming from the interfering user having sequence $(x)_k$. This is true for any k and it can be achieved by assigning the N cycle shifts of a single m-sequence to N different subscriber users without any interference. Complete orthogonality between the users is theoretically achieved [68].

Encoding of broadband sources by the well known temporally nondispersive lens and grating apparatus is shown in Figure 6.6. After direct intensity modulation of the LED according to the data, the signal is reflected from the grating where the different wavelengths are angularly dispersed and focused by the lens on the plane of the specially patterned amplitude mask. A second lens and grating recombine the unfiltered spectral components into a single optical beam, which is then sent to all the receivers via a passive star coupler.

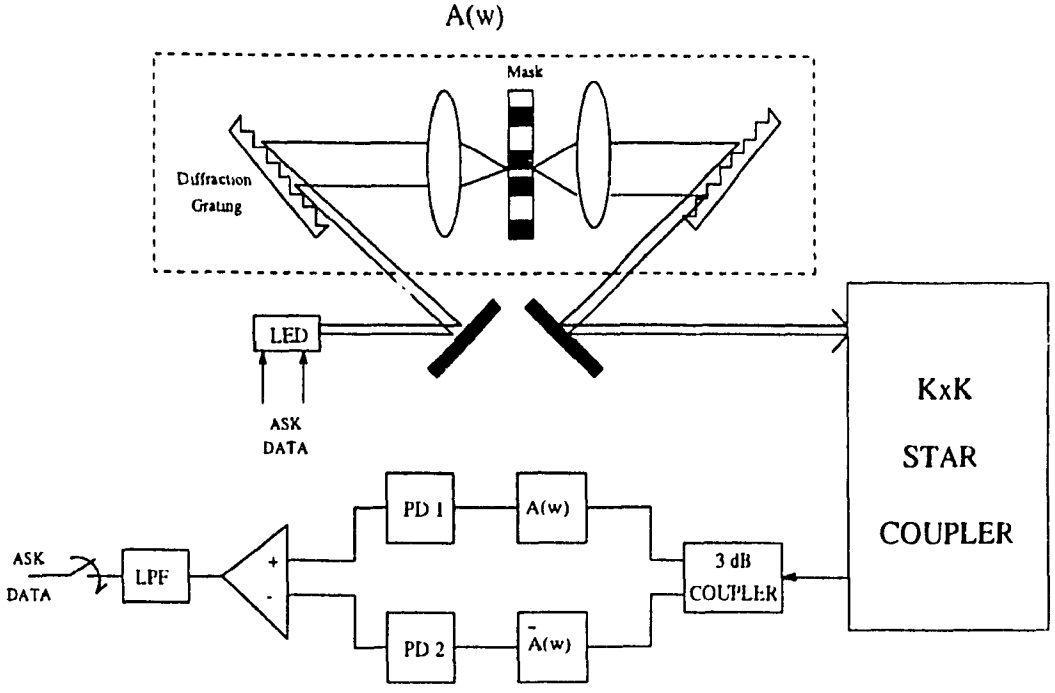

FIGURE 6.6 Schematic diagram of the proposed optical CDMA system.

The receiver needs to compute Z in (6.107). This is done by using two photodetectors, one to receive $\sum x_i x_{i+k}$ and the other to receive $\sum (1 - x_i) x_{i+k}$ and subtracting the outputs. To do that, two masks that transmit complementary frequency bands are needed [68].

6.3 Network Architecture for CDMA Optical Networks

In the following, we will present different architectures used in order to increase the capacity of an optical network in terms of the number of users.

6.3.1 A CDMA model for Optical networks

The application of CDMA protocol to an optical network may be presented by the baseband CDMA model shown in Figure 6.7 and directly applicable to a passive star network topology [70]. This model consists of U users where the u-th user's binary data sequence $B_u(t)$ is a sequence of unit amplitude unipolar rectangular pulses (bits) of duration T. The u-th user is assigned a code waveform $A_u(t)$, which consists of a periodic sequence of unit amplitude unipolar rectangular pulses (chips) of duration T_c. The u-th user's code sequence has a period $N_p = T/T_c$ chips so that there is one code period per data symbol. The modulation operator 'm' causes the transmitted signal to comprise the original sequence or its complement according to whether the current data bit is a 0 or a 1, respectively. This form of data modulation is referred to as sequence inversion keying (SIK).

The input of the correlator receiver $r(t)$ consists of the signal sequence $S_i(t)$ plus the sum of (U-1) equal power interference sequences $i_u(t)$ and the receiver Additive White Gaussian Noise (AWGN) process $n(t)$, which has a double-sided power spectral density of a height $N_o/2$. The expression for $r(t)$ is given by:

$$r(t) = n(t) + S_i(t) + \sum_{\substack{u=1 \\ u \neq i}}^{U} i_u(t) \tag{6.108}$$

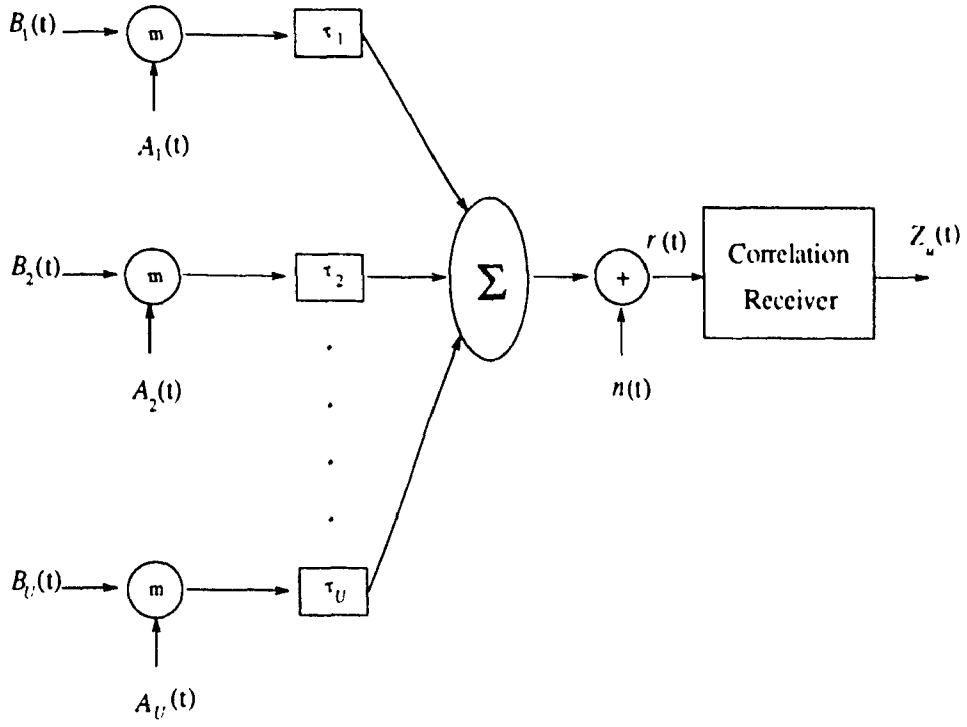

FIGURE 6.7 Optical fiber CDMA model

A general expression for the signal $Z_i(T)$ at the output of a correlator matched to the unipolar signal sequence $A_u(t)$ is given by:

$$Z_i(T) = \int_0^T r(t)\, h(t)\, dt \tag{6.109}$$

where $h(t)$ is a bipolar version of $A_u(t)$ for the optical system. In this case, the auto- and cross-correlation functions obtained in the SIK optical system with a bipolar reference have the same relative values to those obtained in a SIK bipolar baseband CDMA system [70].

6.3.2 The hybrid WDMA/CDMA system.

One way to increase the number of users in an optical CDMA network is to use a hybrid WDMA/CDMA (wavelength-division multiple access/code division multiple access) system where the spread-spectrum technique allows multiple users to share the

same wavelength. This system can be presented as a network where all the users are grouped into clusters and each of the users in a given cluster uses a different code. Figure 6.8 illustrates a block diagram of this architecture.

In this architecture, multiple groups of users would typically be wavelength multiplexed on the network with a wavelength spacing larger than 1 nm. Multiple users can then share a single-carrier wavelength by using their own unique code sequence. If there are N users per cluster, this means that the network capacity compared to a WDMA system using M different wavelengths would then simply be multiplied by N for a total of $N.M$ users in the network.

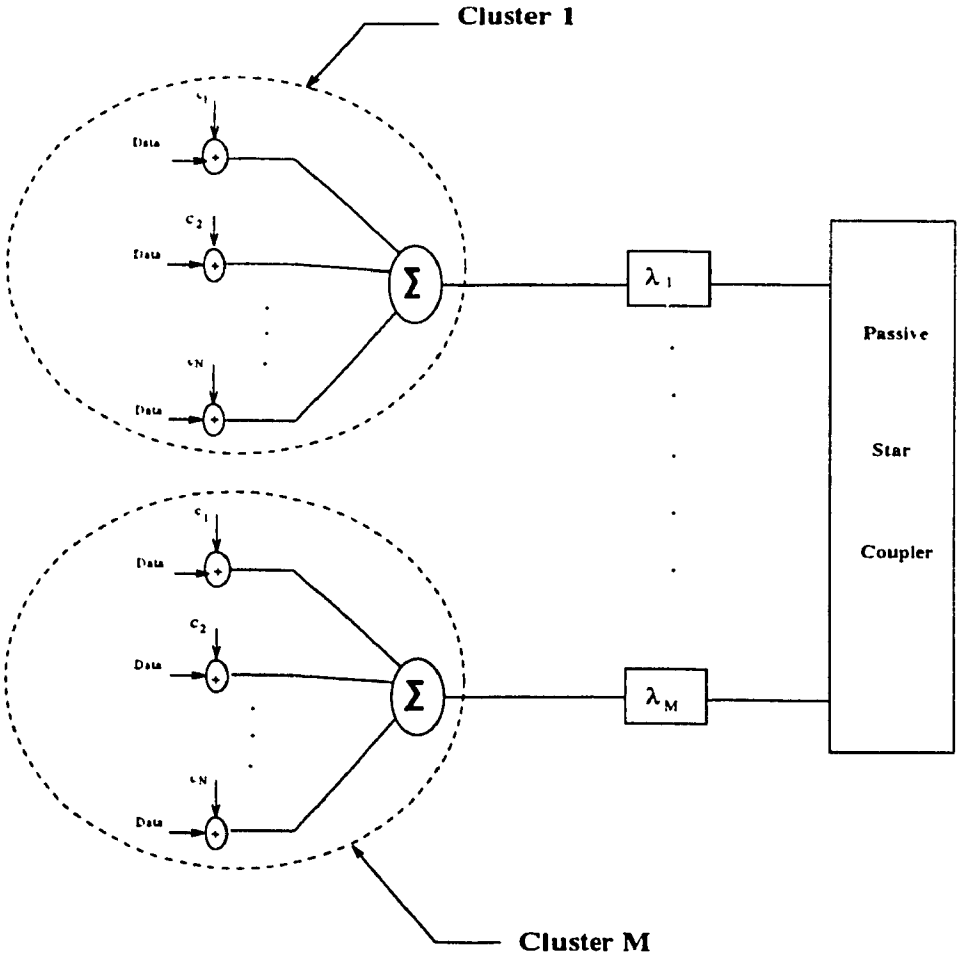

FIGURE 6.8 The hybrid WDMA/CDMA system

6.3.3 The Partial CDMA System

Another way to increase the number of users in an optical network, by only using optical CDMA, is to allow many users to use the same spread spectrum code. The network configuration was first introduced for personal communications in order to increase the number of users in such an environment. This configuration can be adapted to LANs using optical fiber with the use of a passive star coupler as the broadcast medium. In order to show the idea of using the same code for different users and to simplify the study of this new configuration, we assume that all system users, N_1, are grouped into M cells, with m users in each cell [72]. All users within a particular cell transmit their data using a common code in a contention mode of operation. Two users from different cells use different codes. Since all the users in a given cell use the same code to communicate with a particular receiver corresponding to that cell, intra-cell collisions occur. In this case, the receiver is able to capture only the first arriving packet with a certain probability and all the remaining packets are treated as interference. This phenomenon is called the delay capture [74]. Figure 6.9 illustrates a block diagram of this architecture. For M codes and m users per cell, this means the network capacity will increase by m for a total of $m.M$ users in the network.

6.3.4 The New System Configuration

The combination of these two techniques allows us to considerably increase the total number of users in the network. The methodology can be used in a MAN. This system can be presented as a network where all the users are grouped into clusters and all the users in the same cluster are grouped into cells and within the same cell all the users use the same code. Figure 6.10 illustrates the block diagram of this architecture. The total number of users in this network will be equal to the number of clusters N multiplied by the number of cells per cluster M multiplied by the number of users per cell m for a total of $m.M.N$ users. As an example, if $N = 20$ and $M = 100$, m should be equal to 5 in order to have a total of

10,000 users in the network. The determination of all these parameters is related to many other considerations such as the bit rate, the code length, the chips rate and the required total number of users. The characterization of all of these is shown in the following.

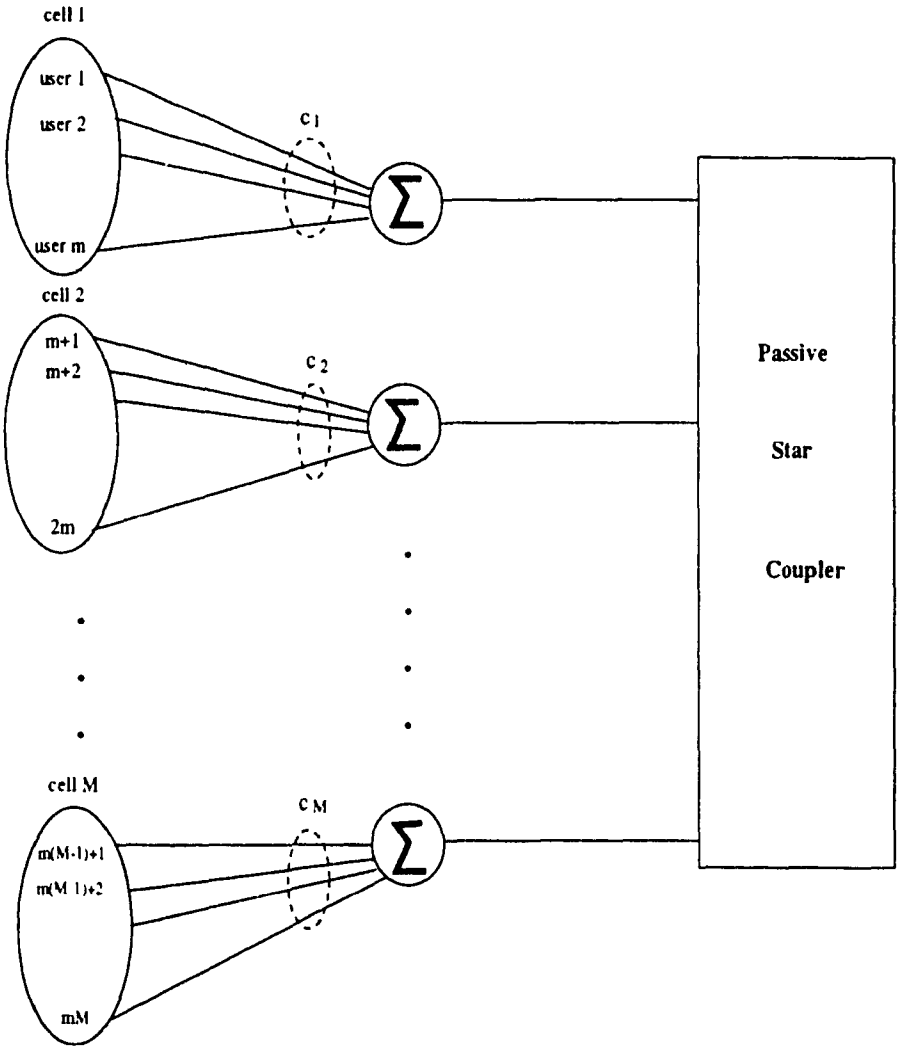

FIGURE 6.9 The partial CDMA system.

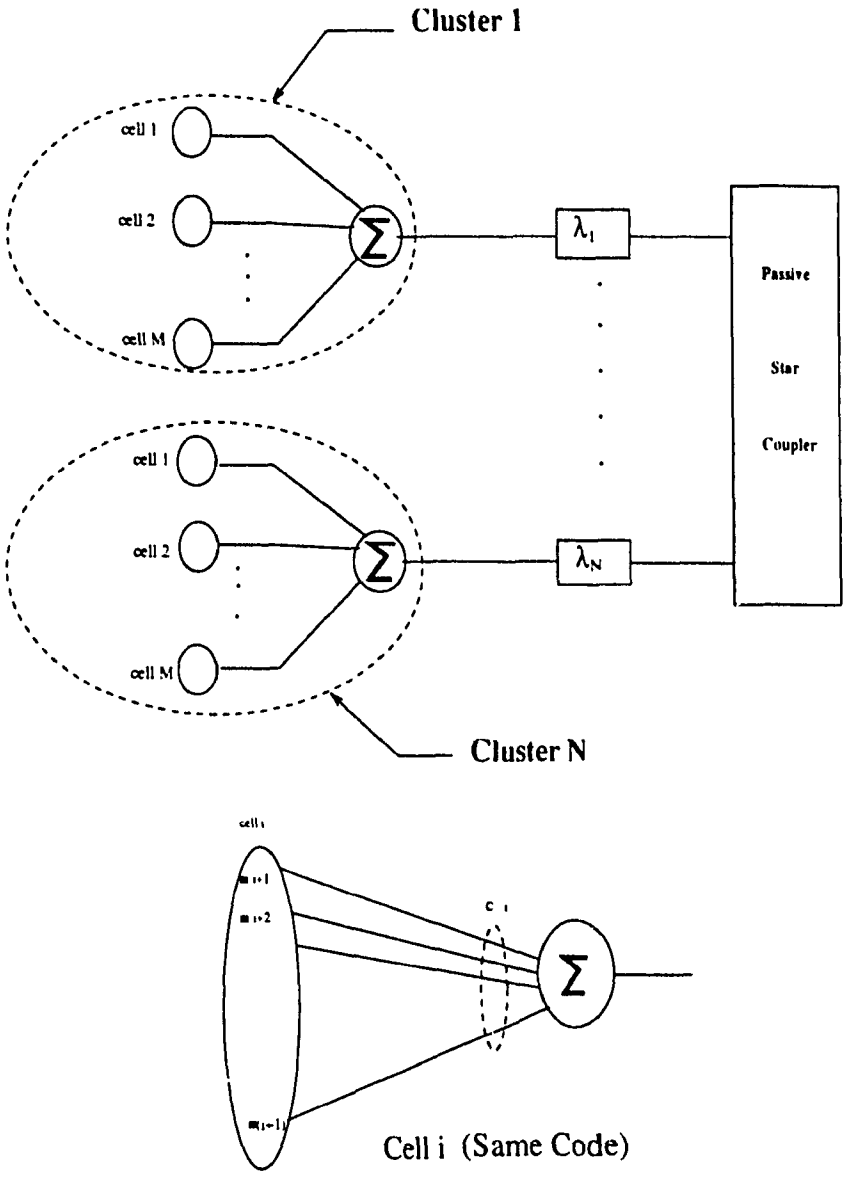

FIGURE 6.10 The new system configuration.

6.4 The Characterization of Different Parameters of the Proposed System

In order to characterize the new system, different parameters should be determined. These parameters are: the number of clusters, the number of cells and finally the number of users per cell. The first parameter can be determined by knowing the maximum rate of

the sequences generated. Generally, the maximum sequence rate is limited to 10 Gchips/s due to the use of an electro-optic modulator as well as other electronic components. At this sequence rate, multiple clusters would typically be wavelength multiplexed on the network with a wavelength spacing larger than 1 nm. Based on this, a maximum of 100 different wavelengths can be used to cover all the useful bandwidth of the optical fiber, which allows us to use a maximum of 100 different clusters. In the following, we assume the number of clusters in the network will be equal to 20, which is a reasonable and a realistic choice for such a system architecture. At a sequence rate of 10 Gchp/s and with a spreading gain between 100 and 250, we obtain a bit rate ranging from 40 to 100 Mbit/s. However, different techniques can be used in order to increase the chip rate without decreasing the bit rate. The simplest one is probably to cascade G phase modulators as done to obtain an optical AND gate [79]. For example, by using three cascaded phase modulators each driven by a sequence of length equal to 85 at 10 GHz, a sequence length of 255 is obtained for an individual bit rate of 117.6 Mbit/s [76]. This will be quite sufficient for a MAN. The choice of the sequence length depends on the modulation scheme; which determines the number of simultaneous users for a given probability of error. By using the sequence inversion keying (SIK) modulation scheme, the optical system using a pseudorandom sequence of length 127 can allow up to 7 simultaneous users for a 10^{-6} probability of bit error [69]. For the same probability of bit error and using a sequence of length 255 and by using ASK modulation, only 11 simultaneous users are allowed [76]. In the following, we assume the sequence length of 127 will be used and up to 7 simultaneous users are allowed. By using 20 clusters, each one will accommodate 500 users, by using 100 different codes. The 500 users will be divided into 100 different cells, each cell will accommodate 5 users. Other combinations can be used in order to accommodate those 500 users. A complete analysis of the throughput of the partial CDMA system (one cluster in the complete system) will determine the number of users that can use the same code within one cell for a certain degradation of the throughput.

6.4.1 Throughput Analysis

In the following, we will analyze and compare the partial CDMA system to the conventional system using different codes for different users. The analysis is based on a slotted Direct-Sequence Spread-Spectrum Multiple Access (DS/SSMA) [70]. For a given slot, many packets can be transmitted without any collision if the number of simultaneous users (number of packets) is less than a certain value. Otherwise, no packet is successfully transmitted and a retransmission is required.

6.4.1.1 Throughput of the Conventional System

The CDMA channel traffic can be modeled as a Poisson process with (ΛT) packets per slot (newly generated as well as retransmitted packets) for an infinite number of users, but for a finite number of system users U, the CDMA channel traffic can be modeled as a binomial process with $\rho = \lambda T$ packets per slot per user, where λ is the packet arrival rate (number of newly generated as well as retransmitted packets per second) per user. For a large U, both the Poisson and the binomial model give very similar results [72]. However, for our study we will consider the binomial model. In this case, the occurrence probability of K packets in a slot is [78]:

$$P(K) = \binom{U}{K} \rho^K (1-\rho)^{U-K} \tag{6.110}$$

The channel throughput for the conventional system using a different code for each user is given by [78]:

$$S = \sum_{K=1}^{U} K \cdot P(K) \cdot P_{nc}(K) \tag{6.111}$$

where $P(K)$ is given by (6.110) and $P_{nc}(K)$ is the probability of no collision (probability of correctly receiving a packet from a user, given that there are K simultaneous transmissions). The probability of no collision, which is known as the probability of packet success, depends basically on the CDMA channel model considered. In order to facilitate the

analysis, we first assume a simple CDMA channel model in order to compare the performance of the two different proposed systems. In this CDMA channel model, no transmission error occurs if the number of simultaneous transmissions does not exceed a certain threshold, denoted by K_m. If more than K_m packets are transmitted during a slot, all packets suffer from collision and are thus destroyed. This is known as the step function CDMA channel model, as the conditional probability of packet success versus the number of interfering transmissions is a step function. Mathematically, this channel model can be represented by:

$$P_{nc}(K) = \begin{cases} 1 & \text{for } K \le K_m \\ 0 & \text{otherwise} \end{cases} \tag{6.112}$$

Second, we propose a practical system based on the results given in [69], where the probability of a successfully transmitted packet is given by

$$P_{nc}(K) = \left[1 - Q\left[\left(\frac{2}{3}\frac{(K-1)}{U} + \frac{N_0}{E_b}\right)^{-1/2}\right]\right]^L \tag{6.113}$$

where $U = 127$, $E_b/N_O = 20$dB, L=1024 data bits and $Q(x) = \int_x^\infty \frac{exp(-t^2/2)}{\sqrt{2\pi}} dt$. In Figure 6.11, P_{nc} is plotted as a function of K showing that as K increases, $P_{nc}(K)$ decreases to zero.

One way to choose K_m is to evaluate the probability of bit error as a function of the number of simultaneous users. For a probability of bit error less than 10^{-6}, the model proposed here can accommodate up to 7 simultaneous users, so K_m can be determined. Figure 6.12 shows the probability of error as a function of the number of simultaneous users. Also, we can evaluate the system throughput using the real model but with different values of K_m. The result of this comparison (see Figure 6.13) shows that the choice of $K_m = 25$ is

enough to model the system, there is no need to continue the computations up to U. The throughput is given by:

$$S = \sum_{K=1}^{U} K \binom{U}{K} \rho^K (1-\rho)^{U-K} \left[1 - Q\left[\left(\frac{2}{3} \frac{(K-1)}{U} + \frac{N_0}{E_b} \right)^{-1/2} \right] \right]^L \tag{6.114}$$

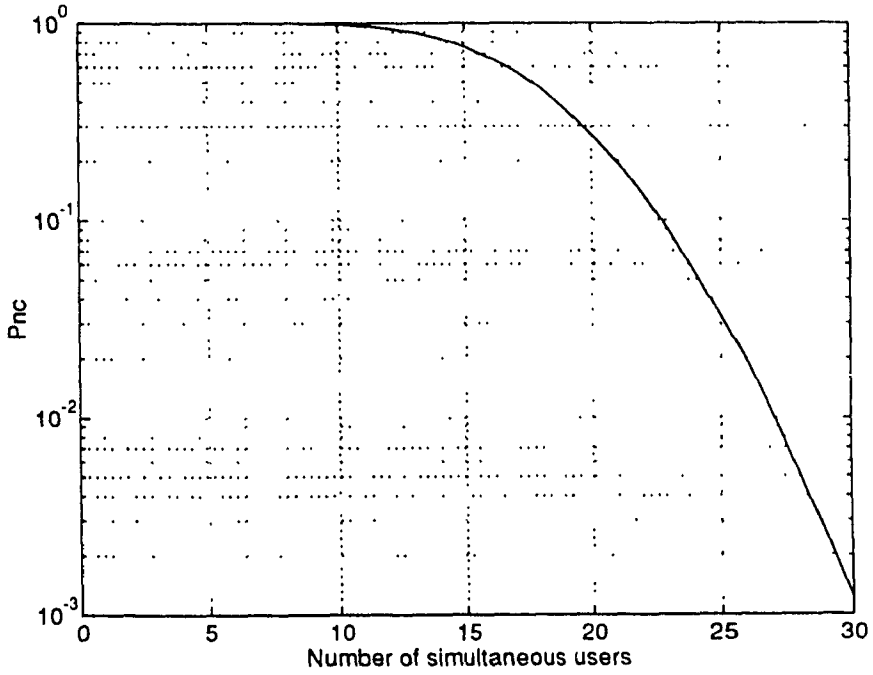

FIGURE 6.11 Probability of receiving a correct packet as a function of the number of simultaneous users.

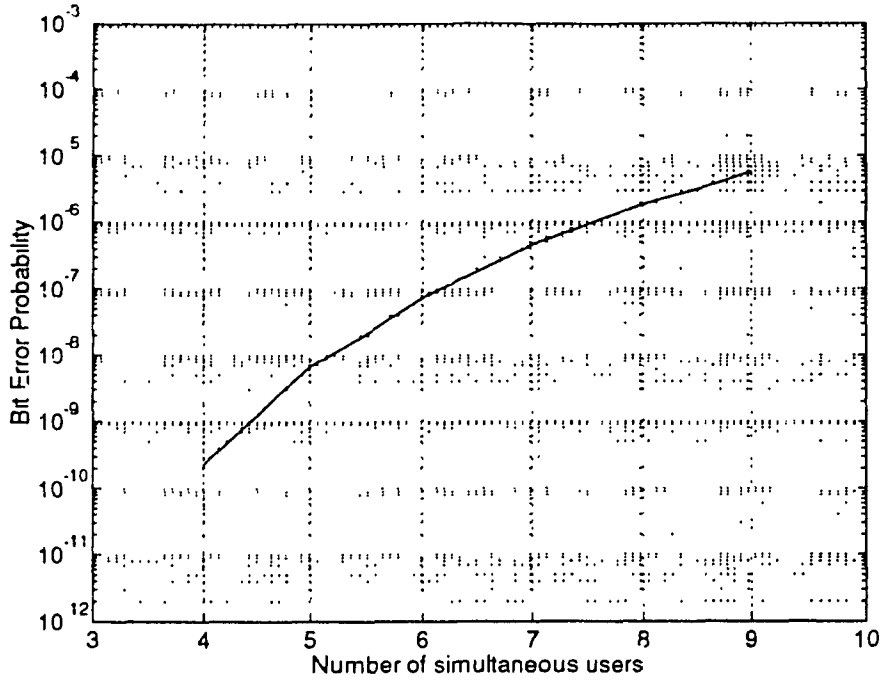

FIGURE 6.12 Probability of Bit error as a function of the number of simultaneous users.

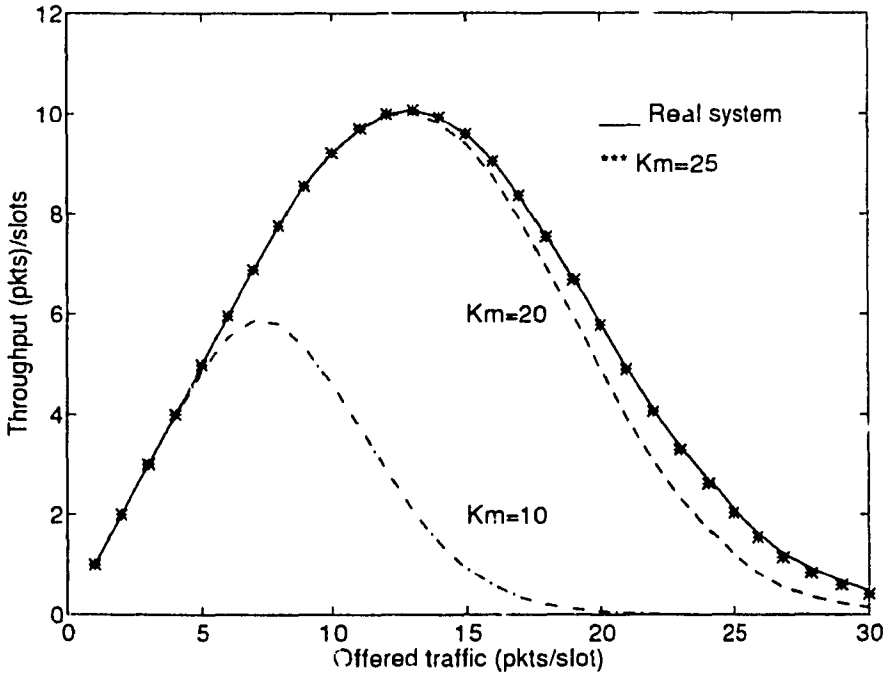

FIGURE 6.13 System throughput for different values of K_m and using the real model

Finally, we propose another way to do this by modeling the system using the set function model. In this case, we vary K and at the same time we compare the system throughput using the step function model and the system throughput using a real model, which uses the general form of the probability of correctly receiving a packet from a user, given that there are K simultaneous transmissions. For the same parameters mentioned above, a choice of K_m= 17 offers a similar system throughput with the use of a very simplified model, which is the step function model. Figure 6.14 shows the system throughput using the real model and compared to the system throughput using the step function model for different values of K_m. In this case, the system throughput is given by:

$$S = \sum_{K=1}^{K_m} KP(K) = \sum_{K=1}^{K_m} K\binom{U}{K}\rho^K(1-\rho)^{U-K} \tag{6.115}$$

In the following, we assume K_m = 17 and a step function model will be used in order to simplify our calculations without any loss of accuracy.

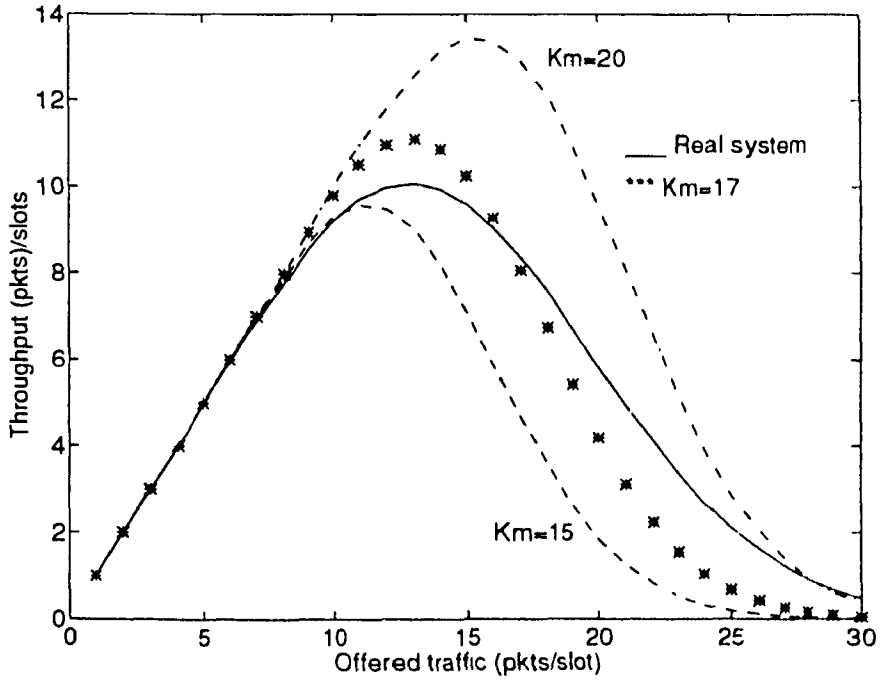

FIGURE 6.14 System throughput using the step function model

6.4.1.2 Throughput of the partial CDMA system

For a finite population of users, if we assume $m = U/M > K_m$, which is the case in reality, the throughput using the step function model is given by [72]:

$$S_P = \sum_{K=1}^{K_m} \bar{C}_K P(K) \tag{6.116}$$

where $P(K)$ is given by (6.110) and $\bar{C}_K$ is the average number of captured packets for a given number of simultaneous users K. The computation of this is given in the following:

Evaluation of $\bar{C}_K$

We first define the following:

$$\zeta^1 = \{l_1^1, l_2^1, \ldots, l_m^1\} \rightarrow \text{cell 1}$$

$$\zeta^2 = \{l_1^2, l_2^2, \ldots, l_m^2\} \rightarrow \text{cell 2}$$

$$\vdots$$

$$\zeta^M = \{l_1^M, l_2^M, \ldots, l_m^M\} \rightarrow \text{cell M}$$

where l_j^i is the j'th user of the i'th cell. There is one code per cell, and there is a receiver associated with each ζ^i. Suppose that K packets come from C different cells, then

$$K = \sum_{i=1}^{M} K_i \tag{6.117}$$

where K_i is equal to the number of packets that come from cell i. If $C=M$, then all K_i's are greater than zero. If $C < M$, then we have C non-zero K_i's and $(M-C)$ zero K_i's. The probability that K packets come from C different cells with K_1 packets from cell 1, K_2 packets from cell 2, etc... is given by:

$$p(K_1, K_2, \ldots, K_M) = \frac{K!}{K_1!K_2!\ldots K_M!} p_1^{K_1} p_2^{K_2} \ldots p_M^{K_M} \tag{6.118}$$

where p_i is the probability that a packet comes from cell i. Assuming that p_i is equal to $1/M$ for all i, equation (6.118) will be equal to:

$$p(K_1, K_2, \ldots, K_M) = \frac{K!}{K_1!K_2!\ldots K_M!} M^{-K} \tag{6.119}$$

where $K = K_1 + K_2 + \ldots + K_M$.

Once we find the combinations, then the probability of k packets coming from C different cells can be computed as:

$$P_K^{(C)} = \begin{cases} \sum_J Pr\{I_{j/C,K}\} & \text{for } 1 \le C \le \min(M, K) \\ 0 & \text{otherwise,} \end{cases} \tag{6.120}$$

where $I_{j/C,K}$ is the j'th possible combination for a given C and K and is represented as $I_{j/C,K} = (I_j^1, I_j^2, \ldots, I_j^C)$ where $\sum_{s=1}^{C} I_j^s = K$. The probability of a given combination is given by:

$$Pr\{I_{j/C,K}\} = \sum_{i_1}^{M}\sum_{i_2}^{M}\ldots\sum_{i_C}^{M} p(K_{i_1} = I_j^1, K_{i_2} = I_j^2, \ldots, K_{i_C} = I_j^C) \tag{6.121}$$

All the possible combinations and the calculation of the $P_K^{(C)}$ for $1 \le C \le K$ and $1 \le K \le K_m$ could be found by a computer program. The flowchart of the program we used is shown in Figure 6.15. To illustrate the main idea of this algorithm, we give a simple example to better understand the computation of the $P_K^{(C)}$ for different C given K and M. Suppose we want to compute $P_K^{(C)}$ for K = 4, thus we need to compute $P_4^{(1)}$, $P_4^{(2)}$, $P_4^{(3)}$ and $P_4^{(4)}$. In the computation of the probability that four packets come from one cell, $P_4^{(1)}$, the only possibility is all four packets come from a given cell. Then

$$P_4^{(1)} = \sum_{i_1=1}^{M} p(K_{i_1} = 4) = \sum_{i_1=1}^{M} \frac{1}{M^4} = \frac{1}{M^3} \tag{6.122}$$

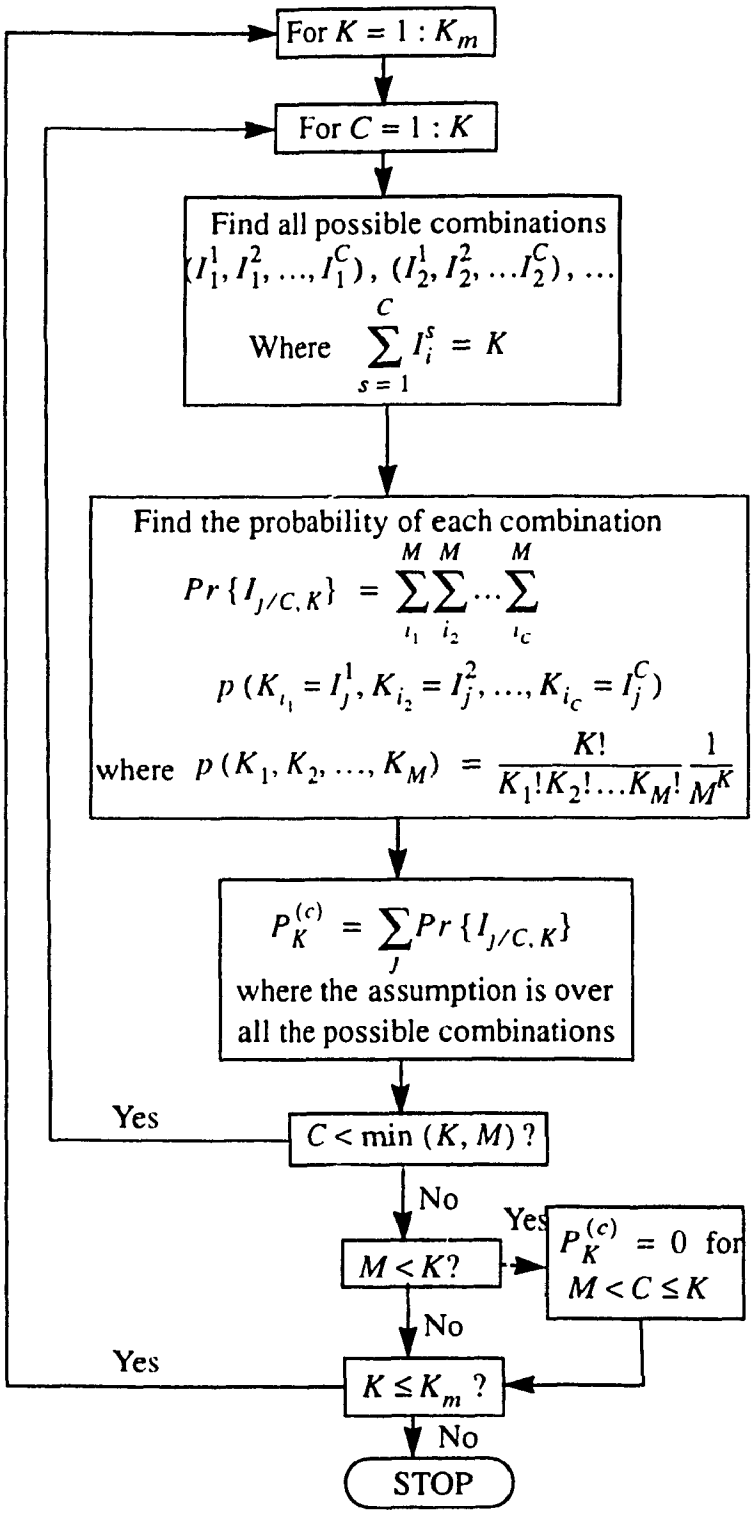

FIGURE 6.15 Algorithm for finding the values of $P_K^{(C)}$ [72].

In the computation of the probability that four packets come from two different cells, $P_4^{(2)}$, there are two possibilities. 1) One packet come from one cell and three packets comes from another cell. 2) Two packets come from one cell and two other from another cell. Then

$$P_4^{(2)} = \sum_{\substack{i_1=1 \\ i_2 \neq i_1}}^{M} \sum_{i_2=1}^{M} p\left(K_{i_1}=1, K_{i_2}=3\right) + \sum_{i_1=1}^{M} \sum_{i_2=i_1+1}^{M} p\left(K_{i_1}=2, K_{i_2}=2\right) \tag{6.123}$$

In the computation of the probability that four packets come from three different cells, $P_4^{(3)}$, the only possibility is one packet comes from a given cell, one packet comes from a second cell and two others come from a third cell. Then

$$P_4^{(3)} = \sum_{i_1=1}^{M} \sum_{i_2=i_1+1}^{M} \sum_{\substack{i_3=1 \\ i_3 \neq i_1 \\ i_3 \neq i_2}}^{M} p\left(K_{i_1}=1, K_{i_2}=1, K_{i_3}=2\right) \tag{6.124}$$

Finally, in the computation of the probability that four packets come from four different cells, $P_4^{(4)}$, the only possibility is all four packets come from four different cells. Then

$$P_4^{(4)} = \sum_{i_1=1} \sum_{i_2=i_1+1} \sum_{i_3=i_2+1} \sum_{i_4=i_3+1} p\left(K_{i_1}=1, K_{i_2}=1, K_{i_3}=1, K_{i_4}=1\right) \tag{6.125}$$

After the evaluation of $P_K^{(C)}$ for all possible combinations, the average number of captured packets for a given number of simultaneous users K is given by:

$$\overline{C}_K = \sum_{C=1}^{K} C P_K^{(C)} \tag{6.126}$$

Figure 6.16 shows the results obtained for the case of K_m = 15 and M = 15, 30, and 45. The result obtained for each case is compared to the conventional case of using one code per user. As M increases, the performance of the new system improves and becomes closer to the conventional case.

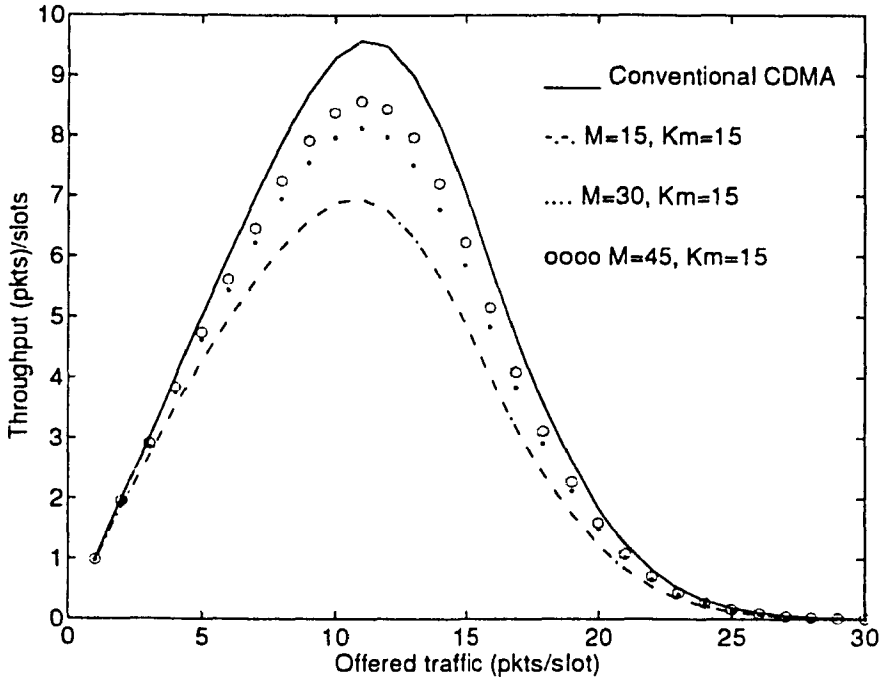

FIGURE 6.16 System throughput for K_m=15

6.4.2 Throughput per Cluster

Calculation of the throughput per cluster is based on: First, the number of users per cluster is equal to 500. Second, a real model with K_m = 15 and a sequence length of 127 is used in order to evaluate the throughput. Finally, we use several combinations between the number of cells and the number of users per cell, and for each case we evaluate the total throughput. The result obtained is shown in Figure 6.17. First, we compare the results obtained for the case of using the configuration (M = 100 and m = 5) to the ideal case of using one code per user, we see that we obtain a reduction of the maximum throughput by almost 5%, which is not too much compared to the reduction by 5 of the number of differ-

ent receivers. In the second configuration, we reduce the number of receivers by 2 for the price of another reduction of 5% in the throughput. Finally, by using the third configuration ($M = 25$, $m = 20$) and compared to the first configuration, a reduction of only 14% in the throughput but with using 25 different receivers compared to 100.

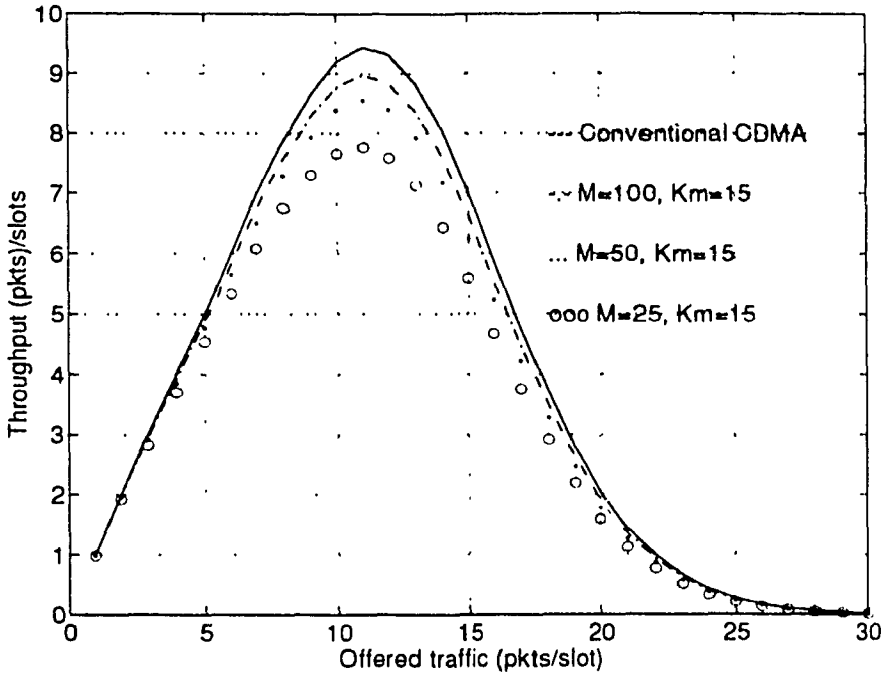

FIGURE 6.17 Throughput per cluster for different configurations.

6.4.3 Network Throughput

The calculation of network throughput uses the same parameters as for the case of the calculation of the throughput per cluster, with the addition of using a total of 20 clusters in the network. The result is shown in Figure 6.18. Network throughput is shown for many different combinations of the number of users per cell and the number of cells per cluster. From this result, we see that with a small reduction of the network throughput we can accommodate more users in the network by allowing several users to use the same code. We also can allow another reduction in order to reduce the complexity of the network in

terms of using a smaller number of different receivers at the receiving side. In this case, we reduce the number of cells and we increase the number of users per cell.

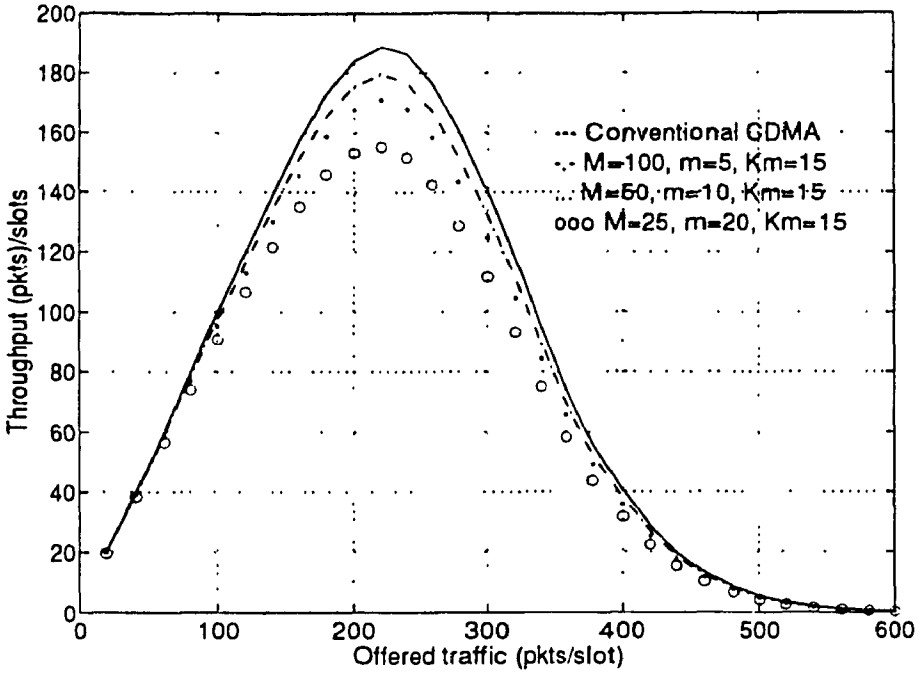

FIGURE 6.18 Network throughput

6.5 Summary

In this chapter, we have studied different optical CDMA schemes that can be used for optical CDMA networks. We have also proposed a new configuration, which uses one of the proposed schemes in order to increase the number of users in optical networks. This configuration uses a hybrid WDMA/CDMA system with the addition of allowing different users to use the same code. The throughput performance of this new configuration known as partial CDMA has been analyzed and compared to the conventional configuration. The analysis shows that the number of users in this new configuration can be increased considerably without a loss in the performance compared to the conventional configuration. With an appropriate choice of system parameters, the throughput reduction can be made insignificant compared to the increase in the number of users in the new configuration.

Chapter VII

Conclusions and Suggestion for Further Research

7.1 Conclusions

The use of the optical technology in the implementation of networks leads to the design of several network architectures in order to exploit the 30 THz bandwidth of a single mode fiber. Two general classes of optical networks can be identified: the single hop network and the multihop network. In the single hop network, a message, once transmitted, reaches its destination directly without being routed through tandem nodes in the network or being converted to its electronic form on the way. In multihop network, a message has to go through one or several hop to reach its destination, in this case WDM is used mainly. Different architectures are presented such as the ShuffleNet, the MSN and so on. The choice of architecture is mainly related to the application of the network.

In Chapter 3, we introduced a new property that can be added to the conventional ShuffleNet, which is the addition of a second layer of physical connectivity in order to improve the performance of multihop networks in terms of maximum number of hops and channel efficiency. The results show that by using this new configuration, called the bilayered ShuffleNet, we decrease the maximum number of hops required for a message to reach its destination from $2k$-1 to k for an odd k and to k+1 when k is even. This will affect the general form of the number of stations reached as a function of the number of hops for the case of the bilayered ShuffleNet. This reduction will also decrease the expected num-

ber of hops, and increase the channel efficiency compared to the conventional ShuffleNet. The numerical results in terms of message delay show what we had expected which is a reduction in the total delay and the increase of the total traffic generated by each station for two different sets of (P, k) for the case of bilayered ShuffleNet compared to the conventional case. The study of this new network under the nonuniform traffic shows that the effect of load imbalance due to traffic intensity variability is to reduce throughput per user by a certain factor relative to the balanced-load situation. The results are similar to the case of the conventional ShuffleNet but with a certain improvement in terms of mean intensity on worst link, the probability that the traffic intensity on the worst channel is greater than the channel capacity, and the amount of throughput reduction (relative to balanced load).

In chapter 4, the signal flow graphs for path enumeration analysis are applied to different networks such as the ShuffleNet, the bilayered ShuffleNet and the SR_Net. The above analysis shows that the number of paths of a given length between source and destination is larger for the case of the bilayered ShuffleNet compared to the case of conventional ShuffleNet. This implies that the routing strategies in the case of the bilayered ShuffleNet can provide alternate paths to reach a node in a case of congestion or link failure, with increased reliability, recoverability, and reduced delay. The same performance can be obtained by using a conventional ShuffleNet with higher connectivity. However, often it is not possible to find the correct configuration with the same number of nodes and with a higher connectivity. By comparing the bilayered ShuffleNet to the SR_Net, we found that the former offers alternative shorter paths in the case of message deflection than the latter. This implies that the routing strategies in the case of the bilayered ShuffleNet can provide alternative shorter paths to reach a node in case of congestion or link failure, with increased reliability, recoverability, and reduced delay due to the fact that the message is free to go forward or backward in the case of the bilayered ShuffleNet. The analysis of these networks under deflection routing shows the advantage of the bilayered ShuffleNet in terms of expected number of hops as a function of the deflection probability compared to the SR_Net which has the same connectivity. An adaptive configuration could be used to minimize the expected number of hops as function of the P_{def}. This con-

figuration will use the combination of both structure of the bilayered ShuffleNet and the SR_Net.

In chapter 5, the WDM cross-connect is used in the physical implementation of different networks such as the ShuffleNet, the Manhattan street network and for all different modified versions of these two networks. The advantage of this method is to reduce the total number of wavelengths required to just two or four wavelengths instead of *PN* in the conventional case without restricting the maximum number of users in the network. We also show how an adaptive configuration can be implemented using either WDM cross-connect or the combination of WDM cross-connect and the usual passive star coupler.

In chapter 6 we proposed a new configuration in order to increase the number of users in optical networks and using optical CDMA. This configuration uses a hybrid WDMA/ CDMA system with the addition of allowing different users to use the same code. The throughput performance of this new configuration, known as partial CDMA, has been analyzed and compared to the conventional configuration. The analysis shows that the number of users in this new configuration can be increased considerably without a loss in the performance compared to the conventional configuration. With an appropriate choice of system parameters, the throughput reduction can be made insignificant compared to increasing the number of users in the new configuration.

7.2 Suggestion for further research

The implementation and the design of new multihop architectures involves the development of several optical components in order to overcome all the problems related to the multihop implementation, such as the total number of wavelengths for each configuration, which can be solved using the WDM cross-connect. For the implementation of an adaptive distribution, the use of the WDM cross-connect leads to a complicated physical structure. The direction of further research will involve the incorporation of new advances in technology into this kind of network.

In our study of the single-hop network, the performance calculation of fiber-optic CDMA packet networks in terms of throughput calculation is limited to the case of using Gold codes and ASK modulation. The analysis of our new system architecture using other optical CDMA schemes such as OCC or spectral encoding can be suggested as part of further research in the area.

References

[1] S. E. Miller and I. P. Kaminow, "Optical Fiber Telecommunication II," New York: Academic Press, 1988, chap.2.

[2] M. I. Irshid and M. Kavehrad, "A WDM Cross-Connected Star Multihop Optical Network," *ICC' 92 Conf.Proc.*, pp.1451-1455.

[3] M. G. Hluchyj and M. Karol, "ShuffleNet: An Application of Generalized Perfect Shuffles to Multihop Lightwave Networks," *INFOCOM'88 Conf.Proc.*, pp. 379-390, March 1988.

[4] J. F. Hayes and F. Ayadi, "Local Optical Distribution," *INFOCOM'92 Conf.Proc*, pp. 68-74, May 1992.

[5] J. M. Senior, "Optical Fiber Communications Principles and Practice," Prentice Hall, 1985.

[6] Technical Staff of CSELT, "Optical Fiber Communications," McGraw Hill Book Company, 1980.

[7] C. H. L. Goodman, "Solid-State Electron. Dev.," vol. 2, pp.129, 1978.

[8] G. Keiser, "Optical Fiber Communications," McGraw Hill Book Company, 1983.

[9] J. C. Palais, "Fiber Optic Communications," Prentice Hall, 1984.

[10] I. P Kaminow, "Non-Coherent Photonic Frequency-Multiplexed Access Networks," IEEE Network Magazine, pp. 4-10, March 1989.

[11] P. S. Henry, "High-Capacity Lightwave Local Area Networks," IEEE Commun. Mag., Vol. 27, No. 10, October 1989.

[12] H. Kressel, "Semiconductor Devices for Optical Communication," Springer Series in Solid-State Sciences, Springler Verlag, Vol. 39, 1980.

[13] J. Salz, "Modulation and Detection for Coherent Lightwave Communications," *IEEE Commun. Mag.*, vol.24, no.6, June 1986.

[14] R. A. Linke, "Frequency Division Multiplexed Optical Networks Using Heterodyne Detection," *IEEE Network Mag.*, March 1989.

[15] S. T. Personick, "Fiber Optics Technology and Applications," *AT&T Technical Journal*, vol. 66, Jan./Feb. 1987.

[16] P. E. Green, Jr., "Fiber Optic Networks," Prentice Hall, 1993.

[17] M.Gerla and L. Fratta, "Tree Structure Fiber Optic MAN's," *IEEE J.Select.Areas Commun.*, vol.6, no.6, July 1988.

[18] A. M. Saleh and H. Kogelnik, "Reflective Single-Mode Fiber-Optic Passive Star Couplers," *J.Lightwave Technol.*, March 1988.

[19] J. F. Hayes and F. Ayadi, "Performance Calculation for an Optical Metropolitan Area Network", *Computer Communications*, Vol. 17, No. 1, pp. 17-24, January 1994.

[20] M. I. Irshid and M. Kavehrad, "A WDM Cross-Connect Star Topology for Multihop Lightwave Networks," *J.Lightwave Technology*, vol. 10, no.6, June 1992.

[21] M. Tabiani, M. Kavehrad and M. I. Irshid, "A Novel Integrated-Optic WDM Cross-Connect for Wavelength Routing Networks," *GLOBCOM'92 Conf.Proc.*, December 1992.

[22] F. Ayadi, J. F. Hayes and M. Kavehrad, "WDM Cross-Connect Star Topology for the Bilayered ShuffleNet," *The Canadian Conference on Electrical and Computer Engineering*, Vancouver, September 1993.

[23] F. Ayadi, J. F. Hayes and M. Kavehrad, "Bilayered ShuffleNet a New Logical Configuration for Multihop Networks," *GLOBCOM'93 Conf.Proc.*, November 1993.

[24] F. Ayadi, J. F. Hayes and M. Kavehrad, "A WDM Cross-Connect Star Topology for the Bilayered ShuffleNet," *J.Lightwave Technology*, vol. 12, no. 9 September 1994.

[25] R. Ramaswami, "Multiwavelength Lightwave Networks for Computer Communication," *IEEE Comun.Mag.*, vol. 31, no. 2 1993.

[26] F. Ayadi, J. F. Hayes and M. Kavehrad, "Optical Fiber Networks: Single-Hop and Multihop System", to published in *the Canadian Journal of Electrical and Computer Engineering*.

[27] P. R. Prucnal, M. A. Santoro, and T.R. Fan. "Spread Spectrum Fiber-Optical Area Network Using Optical Processing," *J.Lightwave Technology*, vol. LT-4, no. 5, May 1986.

[28] C. A. Brackett, "Dense Wavelength Division Multiplexing Networks: Principles and Applications," *IEEE J.Select.Areas Commun.*, vol.8, no.8, August 1990.

[29] G. Coquin, K. W. Cheung, and M. Choy, "Single and Multiple Wavelength Operation of Acousto-Optically Tuned Lasers at 1.3 microns," *Proc. 11th IEEE Int'l. Semiconductor Laser Conf.*, Boston, MA, pp. 130-131, 1988.

[30] I. M. Habbab, M. Kavehrad, and C. -E. W. Sundberg, "Protocols for Very High-Speed Optical Fiber Local Area Networks Using a Passive Star Topology," *J.Lightwave Technology*, vol. LT-S, December 1987.

[31] B. Mukherjee, "WDM-Based Local Lightwave Networks Part I: Single-Hop Systems," *IEEE Network Mag.*,May 1992.

[32] M. S. Goodman et al., "The LAMBDANET Multiwavelength Network: Architecture, Applications, and Demonstrations," *IEEE J.Select.Areas Commun.*, vol.8, no.8, August 1990.

[33] N. R. Dono et al., "A Wavelength Division Multiple Access Network for Computer Communication," *IEEE J. Sel. Areas in Commun.*, vol. 8, pp. 983-994. Aug. 1990.

[34] E. Arthurs et al., "Multiwavelength Optical Crossconnect for Parallel Processing Computers," *Elect. Lett.*, vol. 24, pp. 119-120, 1986.

[35] P. W. Down and K. Bogineni, "Simulation Analysis of a Collisionless Multiple Access Protocol for a Wavelength Division Multiplexed Star-Coupled Configuration," 25th Annual Simulation Symp., Orlando, Fla., April 1992.

[36] I. Chlamtac and A. Ganz, "Channel Allocation Protocols in Frequency-Time Controlled High Speed Networks," *IEEE Trans.Commun.* vol.COM-36, pp. 430-440, April 1987.

[37] A. Ganz and Z. Koren, "WDM Passive Star Protocols and Performance Analysis," *INFOCOM'91 Conf.Proc*, pp. 991-1000, April 1991.

[38] R. E Ziemer and R. L. Peterson, "Digital Comminications and Spread Spectrum Systems," Macmillan, New York, 1995.

[39] J. A. Salehi, "Emerging Optical Code-Division Multiple Access Communications Systems," *IEEE Network Magazine*, pp,31-39. March 1989.

[40] J. A. Salehi, "Code Division Multiple-Access Techniques in Optical Fiber Networks - Part I: Fundamental Principles," *IEEE Trans.com*, vol. 37, no. 8, August 1989.

[41] M. G. Hluchyj and M. Karol, "ShuffleNet: An Application of Generalized Perfect Shuffles to Multihop Lightwave Networks," *INFOCOM'88 Conf.Proc.*, pp. 379-390, March 1988.

[42] N. F Maxemchuk, "Routing in the Manhattan Street Network," *IEEE Trans.Commun.* vol.COM-35, pp. 503-512, May 1987.

[43] B. Mukherjee, "WDM-Based Local Lightwave Networks Part II: Multihop Systems," *IEEE Network Mag.*, July 1992.

[44] D. Towsley, "The Analysis of a Statistical Multiplexer with Nonindependent Arrivals and Errors", *IEEE Trans.Com* , vol.COM-28, no.1, January 1980.

[45] J. F. Hayes and F. Ayadi, "Local Optical Distribution", *INFOCOM'92 Conf.Proc*, pp. 68-74, May 1992.

[46] J. F. Hayes, "Modeling and Analysis of Computer Communications Networks", New York: Plenum Press, 1984, chp.5.

[47] T. Y. Chung and D. P. Agrawal, "On Network Characterization of and Optimal Broadcasting in the Manhattan Street Network," *INFOCOM'90 Conf.Proc*, pp. 465-472, June 1990.

[48] A. K. Choudhury, "A Comparative Study of Architectures for Deflection Routing," *GLOBCOM'92 Conf.Proc.*, pp. 1911-1920, December 1992.

[49] F. Ayadi, J. F. Hayes and M. Kavehrad, "Performance of the Bilayered ShuffleNet Under Nonuniform Traffic", *17th Biennial Symposium on Communications*, Queen's University, May 1994.

[50] M. Eisenberg, and N. Mehravari, "Performance of the Multichannel Multihop Lightwave Network Under Nonuniform Traffic," *J. Selected Areas in Comm* vol. 6, no. 7, August 1988.

[51] A. Papoulis, Probability, Random Variables, and Stochastic Processes," Third Edition, McGraw-Hill Series in Electrical Engineering, 1991.

[52] A. Krishna and B. Hajek. "Performance of Shuffle-Like Networks with Deflection," *INFOCOM'90 Conf.Proc*, pp. 473-480, June 1990.

[53] E. Ayanoglu, "Signal Flow Graphs for Path Enumeration and Deflection Routing Analysis in Multihop Networks," *GLOBCOM'89 Conf.Proc.*, pp. 1022-1029, December 1989.

[54] L. A. Zadeh and C. A. Desoer, "Linear System Theory: The State Space Approach," McGraw-Hill, New York, 1963.

[55] F. Ayadi, J. F. Hayes and M. Kavehrad, "WDM Cross-Connect Star Topology for the Bilayered ShuffleNet", *The Canadian Conference on Electrical and Computer Engineering*, Vancouver, September 1993.

[56] S. G. Chan and H. Kobayashi, "Performance Analysis of ShuffleNet with Deflection Routing," *GLOBCOM'93 Conf.Proc.*, December 1993.

[57] A. K. Choudhury, "A Comparative Study of Architectures for Deflection Routing," *GLOBCOM'92 Conf.Proc.*, pp. 1911-1920, December 1992

[58] K. Wagatsuma, H. Sakaki and S. Saito, "Mode Conversion and Optical Filtering of Obliquely Incident Wave in Corrugated Optical Waveguide Filters," *IEEE J. Quantum Electronics*, Vol QE-15, pp. 632-637, 1979.

[59] A. Krishna and B. Hajek. "Performance of Shuffle-Like Networks with Deflection," *INFOCOM'90 Conf.Proc*, pp. 473-480, June 1990.

[60] L. A. Zadeh and C. A. Desoer, "Linear System Theory: The State Space Approach," McGraw-Hill, New York, 1963.

[61] J. A. Salehi, "Emerging Optical Code-Division Multiple Access Communications Systems," *IEEE Network Magazine*, pp,31-39, March 1989.

[62] M. Azizoglu, J. A. Salehi and Y. Li, "Optical CDMA via Temporal Codes," *IEEE Trans. Commun.* vol.COM-40, mo. 7, July 1992

[63] G. Foschini and G. Vannucci, "Using spread spectrum in high capacity fiber optical network," *J.Lightwave Technol.*, pp. 370-379, March 1988.

[64] G. Vannucci and S. Yang, "Experimental spreading and despreading of the optical spectrum," *IEEE Trans.com*, vol. 37, no. 7, July 1989.

[65] S. Benedetto and G. Olmo, "Performance evaluation of coherent optical code division multiple access," *Electron. Lett.*, 12th August 1991.

[66] F. R. K. Chung, J. A. Salehi and V. K. Wei, "Optical Orthogonal Codes: Design, Analysis, and Applications," *IEEE Trans. on Inf. Theory*, vol. 35, no. 3, May 1989.

[67] D. Zaccarin and M. Kavehrad, "An Optical CDMA System Based on Spectral Encoding of LED," *IEEE Photonic Technology Lett.*, vol. 4, no. 4, pp. 479-482, April 1993.

[68] D. Zaccarin and M. Kavehrad, "Optical CDMA by Spectral Encoding of LED for Ultrafast ATM Switching," *ICC'94 Conf.Proc*, May 1994.

[69] T. O'Farrell, "Throughput analysis of CDMA protocol with channel sensing and overload detection for fiber optic LANs," *Electronics Letters*, 14 June 1993.

[70] T. O'Farrel and M. Beale, "Code-division Multiple-access (CDMA) techniques in optical fiber LANs," *Proc. 2nd IEE National Conf. on Telecomm.*, 1989 (York, United Kingdom).

[71] R. Rom and M. Sidi, "Multiple access protocol: Performance and analysis," Springer-Verlag, 1990.

[72] C. Trabelsi and A. Yongaçoglu, "A reduced Complexity DS-CDMA System for Personal Communication Networks," *Journal of Vehicle Technology.*

[73] M. Kavehrad, F. Khaleghi and G. Bodeep, "An Experiment on a CDMA Subcarrier Multiplexed Optical Fiber Local Area Network," *IEEE/LEOS Photonic Technology Letters*, July 1992.

[74] M. Soroushnejad and E. Geraniotis, "Probability of Capture and Rejection of Primary Multiple Access Interference in Spread-Spectrum Networks," *IEEE Trans Commun.*, Vol. Com-39, No.6, pp. 986-994, June 1991.

[75] L. Kleinrock and F. A. Tobagi, "Packet switching in Radio channels: Part 1-carrier sense multiple access modes and their throughput-delay characteristics," *IEEE Trans. Commun.*, Vol. Com-23, pp. 1400-1416, 1975.

[76] D. Zaccarin and M. Kavehrad, "Performance Evaluation of Optical CDMA Systems Using Non-Coherent Detection and Bipolar Codes," *J. Lightwave Tech* , Vol. 12, No. 1, January 1994.

[77] G. Vanucci, "Combining Frequency-Division and Code-Division Multiplexing in a high-Capacity Optical Network," *IEEE Network Mag.*, vol. 3, pp. 21-30, March 1989.

[78] D. Raychaudhuri, "Performance Analysis of Random Access Packet-Switched Code Division Multiple Access System," *IEEE Trans. Commun.*, Vol. Com-29, no.6, pp.895-901, June 1981.

[79] M. Jinno, "49.6 Gb/s Electro-optic Demultiplexing Using Cascaded ON/OFF Gates," *IEEE Photon. Technol. Lett.*, vol. 4, pp. 641-644, June 1992.